AD

USAAVLABS TECHNICAL REPORT 66-72

INVESTIGATION OF CIRCULATION CONTROL AIRFOILS BY MEANS OF JETS

By

S. W. Yuan

J. C. Westkaemper

L. D. Kemp

W. L. Richter, Jr.

November 1966

U. S. ARMY AVIATION MATERIEL LABORATORIES
FORT EUSTIS, VIRGINIA

CONTRACT DA 44-177-AMC-200(T)
THE UNIVERSITY OF TEXAS
AUSTIN, TEXAS

Disclaimers

The findings in this report are not to be construed as an official Department of the Army position unless so designated by other authorized documents.

When Government drawings, specifications, or other data are used for any purpose other than in connection with a definitely related Government procurement operation, the United States Government thereby incurs no responsibility nor any obligation whatsoever; and the fact that the Government may have formulated, furnished, or in any way supplied the said drawings, specifications, or other data is not to be regarded by implication or otherwise as in any manner licensing the holder or any other person or corporation, or conveying any rights or permission, to manufacture, use, or sell any patented invention that may in any way be related thereto.

Trade names cited in this report do not constitute an official endorsement or approval of the use of such commercial hardware or software.

Disposition Instructions

Destroy this report when no longer needed. Do not return it to originator.

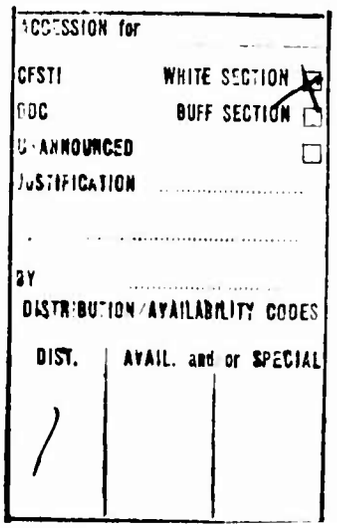

DEPARTMENT OF THE ARMY
U. S. ARMY AVIATION MATERIEL LABORATORIES
FORT EUSTIS, VIRGINIA 23604

The investigation described in this report is concerned with the performance aspects of a rotor system to achieve increased efficiency at high advance ratios through control of circulation about the airfoil.

The report has been reviewed by the U. S. Army Aviation Materiel Laboratories, and is considered to be technically sound.

The report is published for the exchange of information and the stimulation of ideas.

TASK 1D121401A14203

CONTRACT NO. DA 44-177-AMC-200 (T)

USAAVLABS Technical Report 66-72

November 1966

INVESTIGATION OF CIRCULATION CONTROL AIRFOILS BY MEANS OF JETS

by

S. W. Yuan
J. C. Westkaemper
L. D. Kemp
W. L. Richter, Jr.

Prepared by
Department of Aerospace Engineering
The University of Texas
Austin, Texas

for
U. S. ARMY AVIATION MATERIEL LABORATORIES
FORT EUSTIS, VIRGINIA

SUMMARY

Based on the potential flow theory calculation, the capacity of the air supply, the limitation of the internal pressure of the model and the limitation due to the compressibility effect of the jet stream at high velocities, the elliptical airfoils of 18- and 12-percent-thickness ratios were designed and constructed. Experimental investigations for both models with trailing edge jets include force (lift and drag) and pitching moment measurements. In addition, static pressure measurements were made in both spanwise and chordwise directions. These results were used to compare with available theories.

Circulation control with dual jets for the elliptical airfoil of 18-percent-thickness ratio was tested with very satisfactory results. Tests were also made to determine the practicality of circulation control using a jet issuing from the leading edge region of the airfoil.

The determination of the aerodynamic response of the airfoil model to cyclic changes in jet mass flow was also made. The cyclic results were very satisfactory and are presented in the form of pulsating lift coefficient, drag coefficient, and pressure coefficient as a function of pulsating jet coefficient.

FOREWORD

This report was prepared by The University of Texas under Department of the Army Task 1D121401A14203 and Contract No. DA 44-177-AMC-200 (T), entitled "Helicopter Rotor Research," during the contract periods 1 July 1964 to 15 August 1965 and 1 February 1966 to 30 June 1966. The contract was administered under the direction of U. S. Army Aviation Materiel Laboratories, Fort Eustis, Virginia.

Thanks are expressed to Professor P. H. Miller for his invaluable help in the experimental work, for his constructive comments and for his careful reading of the manuscript. Mr. Robert White assisted in performing the experiments on response of chordwise pressure of the airfoil model to cyclic change of jet.

CONTENTS

		Page
	SUMMARY	iii
	FOREWORD	v
	LIST OF ILLUSTRATIONS	viii
	LIST OF SYMBOLS	xv
1.	INTRODUCTION	1
2.	THEORETICAL CONSIDERATIONS	
	2.1 Theoretical Pressure Distribution About an Elliptical Airfoil Without Trailing Edge Jet	3
	2.2 Elliptical Airfoil With Trailing Edge Jet	5
	2.3 Separation Prediction For the Elliptical Airfoil With and Without Trailing Edge Jet	7
3.	APPARATUS AND TESTS	
	3.1 The Model	11
	3.2 Auxiliary Air Supply	12
	3.3 Wind Tunnel	13
	3.4 Instrumentation	13
4.	EXPERIMENTAL RESULTS	
	4.1 The Jet Efflux Calibration	15
	4.2 Shape of the Jet	15
	4.3 Elliptical Airfoil with Trailing Edge Jet	16
	4.4 Elliptical Airfoil with Both Dual Jets and Single Leading Edge Jet	19
	4.5 Aerodynamic Response of the Model to Cyclic Changes of Jet	20
	4.6 Response of Chordwise Pressure of the Model to Cyclic Change of Jet	21
	CONCLUSIONS	23
	RECOMMENDATIONS	24
	BIBLIOGRAPHY	25
	DISTRIBUTION	87

ILLUSTRATIONS

Figure		Page
1	Elliptic Coordinates	27
2	Length of the Arc of Ellipse	27
3	Dividing Streamline and Jet Path for Elliptical Airfoil of 18-Percent-Thickness Ratio	28
4	Dividing Streamline and Jet Path for Elliptical Airfoil of 12-Percent-Thickness Ratio	28
5	Velocity Distribution for Elliptical Airfoil of 18-Percent-Thickness Ratio Without Trailing Edge Jet (C_L = 1.0, $\theta = 30^{\circ}$)	29
6	Velocity Distribution for Elliptical Airfoil of 12-Percent-Thickness Ratio Without Trailing Edge Jet (C_L = 0.75, $\theta = 40^{\circ}$)	30
7	Pressure Distribution for Elliptical Airfoil of 18-Percent-Thickness Ratio Without Trailing Edge Jet (C_L = 1.0, $\theta = 30^{\circ}$)	31
8	Pressure Distribution for Elliptical Airfoil of 12-Percent-Thickness Ratio Without Trailing Edge Jet (C_L = 0.75, $\theta = 40^{\circ}$)	32
9	Pressure Distribution of Elliptical Airfoil of 18-Percent-Thickness Ratio With Trailing Edge Jet (C_L = 1.1, C_J = 0.154, $\theta = 30^{\circ}$)	33
10	Pressure Distribution of Elliptical Airfoil of 12-Percent-Thickness Ratio With Trailing Edge Jet (C_L = 0.70, C_J = 0.084, $\theta = 40^{\circ}$)	34
11	Flat Plate Asymmetrical Loading (α = 0)	35
12	Location of Points of Separation for Elliptical Airfoil of 18-Percent-Thickness Ratio With and Without Trailing Edge Jet	36

Figure		Page
13	Location of Points of Separation for Elliptical Airfoil of 12-Percent-Thickness Ratio With and Without Trailing Edge Jet	36
14	General View of the 18-Percent Model Arrangement	37
15	Jet Slot Configuration for the 18-Percent Model	37
16	Section of Model Showing Locations of the Static Pressure Taps (18-Percent-Thickness Ratio)	38
17	Model Mounting in the Test Section	39
18	Multiple-Gate Type Valve for Controlling the Front Jet of 18-Percent Model	39
19	The Model Exterior Showing the Pressure Taps	40
20	Section of Model Showing Locations of the Static Pressure Taps (12-Percent-Thickness Ratio)	41
21	Air Supply System	42
22	Force and Moment Strain Gages	42
23	Volume Flow Rate Versus the Plenum Pressure of the Model (18-Percent Model)	43
24	Volume Flow Rate Versus the Plenum Pressure of the Model (12-Percent Model)	43
25	Jet Path for the Elliptical Airfoil of 18-Percent-Thickness Ratio ($\theta = 30^{\circ}$, $\alpha = 0$)	44
26	Jet Path for the Elliptical Airfoil of 12-Percent-Thickness Ratio ($\theta = 40^{\circ}$, $\alpha = 0$)	44
27	Lift Coefficient Versus Jet Coefficient for Elliptical Airfoil of 18-Percent-Thickness Ratio ($\theta = 30^{\circ}$, $\alpha = 0$)	45
28	Lift Coefficient Versus Jet Coefficient for Elliptical Airfoil of 12-Percent-Thickness Ratio ($\theta = 40^{\circ}$, $\alpha = 0$)	46

Figure		Page
29	Total Lift Coefficient Versus the Jet Coefficient at Various Angles of Attack ($\frac{b}{a}$ = 18%)	47
30	Total Lift Coefficient Versus Angle of Attack at Various Values of C_J ($\frac{b}{a}$ = 18%)	48
31	Pressure Distribution in the Spanwise Direction for the Elliptical Airfoil of 18-Percent-Thickness Ratio (C_J = 0.154)	49
32	Pressure Distribution in the Spanwise Direction for the Elliptical Airfoil of 12-Percent-Thickness Ratio (C_J = 0.461)	49
33(a)	Pressure Distribution in the Chordwise Direction for the Elliptical Airfoil of 18-Percent-Thickness Ratio (C_J = 0.0738)	50
33(b)	Pressure Distribution in the Chordwise Direction for the Elliptical Airfoil of 18-Percent-Thickness Ratio (C_J = 0.0952)	50
33(c)	Pressure Distribution in the Chordwise Direction for the Elliptical Airfoil of 18-Percent-Thickness Ratio (C_J = 0.119)	51
33(d)	Pressure Distribution in the Chordwise Direction for the Elliptical Airfoil of 18-Percent Thickness Ratio (C_J = 0.154)	51
33(e)	Pressure Distribution in the Chordwise Direction for the Elliptical Airfoil of 18-Percent-Thickness Ratio (C_J = 0.1874)	52
33(f)	Pressure Distribution in the Chordwise Direction for the Elliptical Airfoil of 18-Percent-Thickness Ratio (C_J = 0.202)	52
33(g)	Pressure Distribution in the Chordwise Direction for the Elliptical Airfoil of 18-Percent-Thickness Ratio (C_J = 0.233)	53

Figure | Page

33(h) Pressure Distribution in the Chordwise Direction for the Elliptical Airfoil of 18-Percent-Thickness Ratio (C_J = 0.301) 53

33(i) Pressure Distribution in the Chordwise Direction for the Elliptical Airfoil of 18-Percent-Thickness Ratio (C_J = 0.330) 54

33(j) Pressure Distribution in the Chordwise Direction for the Elliptical Airfoil of 18-Percent-Thickness Ratio (C_J = 0.389) 54

33(k) Pressure Distribution in the Chordwise Direction for the Elliptical Airfoil of 18-Percent-Thickness Ratio (C_J = 0.490) 55

33(ℓ) Pressure Distribution in the Chordwise Direction for the Elliptical Airfoil of 18-Percent-Thickness Ratio (C_J = 0.559) 55

34(a) Pressure Distribution in the Chordwise Direction for the Elliptical Airfoil of 12-Percent-Thickness Ratio (C_J = 0.084) 56

34(b) Pressure Distribution in the Chordwise Direction for the Elliptical Airfoil of 12-Percent-Thickness Ratio (C_J = 0.095) 56

34(c) Pressure Distribution in the Chordwise Direction for the Elliptical Airfoil of 12-Percent-Thickness Ratio (C_J = 0.352) 57

34(d) Pressure Distribution in the Chordwise Direction for the Elliptical Airfoil of 12-Percent-Thickness Ratio (C_J = 0.370) 57

34(e) Pressure Distribution in the Chordwise Direction for the Elliptical Airfoil of 12-Percent-Thickness Ratio (C_J = 0.461) 58

Figure		Page
34(f)	Pressure Distribution in the Chordwise Direction for the Elliptical Airfoil of 12-Percent-Thickness Ratio (C_J = 0.647)	58
34(g)	Pressure Distribution in the Chordwise Direction for the Elliptical Airfoil of 12-Percent-Thickness Ratio (C_J = 0.727)	59
35	Measured Thrust for the Elliptical Airfoil of 18-Percent-Thickness Ratio ($\theta = 30^o$, $\alpha = 0$)	60
36	Measured Thrust for the Elliptical Airfoil of 12-Percent-Thickness Ratio ($\theta = 40^o$, $\alpha = 0$)	61
37	Pitching Moment Coefficient Versus Lift Coefficient (Relative to Mid-Chord Point) for Model of 18-Percent-Thickness Ratio	62
38	Pitching Moment Coefficient Versus Lift Coefficient (Relative to Mid-Chord Point) for Model of 12-Percent-Thickness Ratio	63
39	Elliptical Airfoil Model of 18 Percent with Dual Jets	64
40	The Total Lift Coefficient Versus the Ratio of Leading Edge Jet Coefficient to Trailing Edge Jet Coefficient (18-Percent-Thickness Ratio)	65
41	C_L Versus C_J for Single Leading Edge Jet (18-Percent Model)	66
42	Pulsating Lift and Model Pressure for Elliptical Airfoil of 18-Percent-Thickness Ratio at Valve Speed 360 r. p. m. . . .	67
43	Pulsating Lift Coefficient Ratio Versus Pulsating Jet Coefficient Ratio for 18-Percent Model	68
44	Pulsating Lift Coefficient Versus Pulsating Jet Coefficient for 18-Percent Model at Valve Speed 386 r. p. m. .	69
45	Pulsating Lift Coefficient Versus Pulsating Jet Coefficient for 18-Percent Model at Valve Speed 360 r. p. m. .	70

Figure		Page
46	Pulsating Lift Coefficient Versus Pulsating Jet Coefficient for 18-Percent Model at Valve Speed 210 r. p. m. .	71
47	Pulsating Lift Coefficient Versus Pulsating Jet Coefficient for 18-Percent Model at Valve Speed 150 r. p. m. .	72
48	Pulsating Drag and Model Pressure for Elliptical Airfoil of 18-Percent Thickness Ratio at Valve Speed 215 r. p. m. . . .	73
49	Pulsating Drag Coefficient Ratio Versus Pulsating Jet Coefficient Ratio for 18-Percent Model	74
50	Pulsating Drag Coefficient Versus Pulsating Jet Coefficient for 18-Percent Model at Valve Speed 215 r. p. m.	75
51	Pulsating Static Pressure and Model Pressure for Elliptical Airfoil of 12-Percent-Thickness Ratio at Valve Speed 300 r. p. m.	76
52	Pulsating Static Pressure and Model Pressure for Elliptical Airfoil of 12-Percent-Thickness Ratio at Valve Speed 150 r. p. m.	77
53	Pulsating Pressure Coefficient Versus Pulsating Jet Coefficient For 12-Percent Model at Valve Speed 300 r. p. m.	78
54	Pulsating Pressure Coefficient Versus Pulsating Jet Coefficient For 12-Percent Model at Valve Speed 300 r. p. m.	79
55	Pulsating Pressure Coefficient Versus Pulsating Jet Coefficient For 12-Percent Model at Valve Speed 300 r. p. m.	80
56	Pulsating Pressure Coefficient Versus Pulsating Jet Coefficient For 12-Percent Model at Valve Speed 150 r. p. m.	81
57	Pulsating Pressure Coefficient Versus Pulsating Jet Coefficient For 12-Percent Model at Valve Speed 300 r. p. m.	82
58	Pulsating Pressure Coefficient Versus Pulsating Jet Coefficient For 12-Percent Model at Valve Speed 300 r. p. m.	83
59	Pulsating Pressure Coefficient Versus Pulsating Jet Coefficient For 12-Percent Model at Valve Speed 300 r. p. m.	84

Figure		Page
60	Pulsating Pressure Coefficient Versus Pulsating Jet Coefficient For 12-Percent Model at Valve Speed 300 r.p.m.	85
61	Pulsating Pressure Coefficient Versus Pulsating Jet Coefficient For 12-Percent Model at Valve Speed 150 r.p.m.	86

SYMBOLS

Fluid and Flow Properties

$F(Z)$	Complex potential [see Eq. (1)]
p	Pressure
p_∞	Free stream pressure
Q	$A_j V_j$, volume flow rate of jet (ft^3/sec)
u	Local velocity relative to airfoil
U_{max}	Maximum potential flow velocity (at minimum pressure point)
U_∞	Free stream velocity
V_J	Jet fluid velocity relative to airfoil
V_{xJ}	Jet induced velocity component in the x-direction
ν	Kinematic viscosity of air
ρ	Free stream air density
ρ_J	Jet air density
Γ	Circulation
Φ	Velocity potential
ψ	Stream function

Geometrical Properties

a, b	Semi-axes of elliptical airfoil
$2a$	Airfoil chord
A_J	Jet slot area

ℓ	Span of the airfoil
s	Distance along wall in direction of flow measured from the front stagnation point
S'	Distance along the wall in direction of flow measured from the rear minimum pressure point
x, y	Rectangular coordinates of the ellipse (see Figs. 1 and 2)
$\bar{x}$	$\frac{x}{2a}$ measured from the leading edge of the airfoil
z	Complex plane ($z = x + iy$)
Z	Transformation between a circle and an ellipse [see Eq. (2)]
α	Angle of attack
ζ	Complex plane ($\zeta = \xi + i\eta$)
θ	Jet deflection angle with respect to the chord line
ξ, η	Elliptical coordinates
ξ_0	Value of ξ on the ellipse
σ	Jet slot width

Forces

D	Total drag
J	Total jet reaction or momentum flux at the slot $J = \rho_J A_J V_J^2$
L	Total lift

Nondimensional Coefficient

C_D	Total drag coefficient or thrust coefficient

C_J Jet coefficient $C_J = J/\frac{\rho U_\infty^2}{2}(2a\ell) = \frac{\rho_J}{\rho}\frac{1}{A_J a \ell}\left(\frac{Q}{U_\infty}\right)^2$

C_L Total lift coefficient $C_L = C_{Lp} + C_J \sin\theta$

C_m Pitching moment coefficient (relative to the mid-chord point)

C_{Lp} Pressure lift coefficient

C_p Pressure coefficient [see Eq. (11)]

C_p' Nondimensional pressure [see Eq. (15)]

R_e Reynolds number ($R_e = \frac{U_\infty 2a}{\nu}$)

Miscellaneous

k The practical jet shape factor ($k = 1.0$ is assumed in this report)

γ A constant [see Eq. (32)]

I. INTRODUCTION

For two-dimensional flow of a uniform stream past an airfoil, the Kutta-Joukowski hypothesis states that the strength of circulation about an airfoil will always adjust itself so that the velocity is finite at the trailing edge. Based on this hypothesis, airfoils are designed with sharp trailing edges so that the increase of lift depends entirely on the increase of the angle of attack.

If an airfoil is designed with a trailing edge of finite curvature, the rear stagnation point in the potential flow is not situated at a fixed point. Futhermore, the production of lift is independent of the angle of attack of the airfoil but depends on the position of the rear stagnation point, which can be artifically fixed. The production of lift for an airfoil with a round trailing edge can be achieved by placing a thin flap along the calculated rear dividing streamline extending from the airfoil's surface to a certain point downstream while continuous suction is applied around the trailing edge (Reference 9). An elliptical wing section of 35-percent-thickness ratio with trailing edge flap was tested at California Institute of Technology during 1950-51; the results show that a high lift coefficient of 7.3 was obtained (Reference 4).

On the basis of the above-mentioned favorable features and results, the late Dr. Theordore von Kármán and S. W. Yuan conceived and filed a patent in 1953 on the idea of adapting this type of airfoil to helicopter rotors. A comparison of performance of the XH-16 rotor and the Kármán-Yuan rotor was made (Reference 14); the results indicate that in forward flight, at 160 miles per hour, the Kármán-Yuan rotor requires 20 percent less horsepower than the XH-16 rotor, and that in hovering there is a saving of 10 percent horsepower by the Kármán-Yuan rotor. This power saving, although only 10 percent, would result in an 80 percent increase in the vertical rate of climb.

Furthermore, the Kármán-Yuan rotor allows the elimination of the usual cyclic variation of angle of attack of the blades by substituting a cyclic flap control, thereby allowing a saving in weight reduction of mechanical complexity, reduction of vibration, and hence improvement in the fatigue characteristics. It appears that the use of an airfoil of oval profile can result in lift regardless of forward or rearward flow relative to the airfoil, so that there is no loss of lift in the reverse flow region experienced at higher forward speeds. As a consequence, the helicopter equipped with oval airfoils would not suffer as great a limitation in forward speed as

does an orthodox helicopter.

Due to the mechanical complexity of the flap and boundary layer control system of the Kármán-Yuan rotor system, it was decided that jet flaps should be introduced to the blades to replace the mechanical flap. In this way all the features and advantages of the original Kármán-Yuan rotor system can be retained without suffering the penalty of the mechanical complexity of the solid flaps. Furthermore, the jet may produce a "supercirculation" above the natural circulation level on the airfoil, provided the jet momentum is sufficiently large and flow separation does not occur. Hence, additional lift on the rotor may actually be obtained.

A rotor system utilizing blade circulation control by means of jets has been evaluated experimentally for the hovering condition at the Aerospace Engineering Laboratory of the University of Texas. The experiment was initiated by S. W. Yuan and performed by J. S. Kishi during the period 1960-61. The blade of this experimental rotor model was 52 inches in length and had an elliptical cross section with a 30-percent-thickness ratio and a chord of 2.9 inches. The results of Kishi's tests show that for a given torque the thrust coefficient for the Kármán-Yuan rotor system is about 15 percent higher than that for the conventional type rotor with a NACA 0012 airfoil. Furthermore, at an angular velocity of 30 radians per second, the lift coefficient for the Kármán-Yuan rotor blade was about twice as great as that of the NACA 0015 airfoil rotor.

The purpose of this experimental investigation is to study the basic aerodynamic characteristics of an elliptical airfoil with jet flap. Furthermore, exploratory investigations were conducted in order to gain knowledge in the area of a dual-jet system and the aerodynamic response of the elliptical airfoil to rapid cyclic change in jet momentum. It is hoped that the results of this study presented here will provide adequate information to justify further investigation toward the application of this type of airfoil to helicopter rotors.

2. THEORETICAL CONSIDERATIONS

2.1 THEORETICAL PRESSURE DISTRIBUTION ABOUT AN ELLIPTICAL AIRFOIL WITHOUT TRAILING EDGE JET

The general theory for determining the velocity distribution for two-dimensional flow of an inviscid incompressible fluid around an arbitrary airfoil has been discussed in detail by Theodorsen and Garrick (Reference 10). The basic principle of the theory is known as Riemann's Theorem; this theorem shows that the potential field around any closed contour can always be transformed into the potential field around a circle. In airfoil theory, application of the theorem consists of the transformation of an airfoil into a curve differing slightly from a circle, and then going from the near-circle to a circle. Since the flow about the circle can easily be found, the flow characteristics about the airfoil section can be determined by means of the same transformations.

For an ellipse, the velocity distribution for the potential flow can be calculated from the known complex potential for a circle

$$F(Z) = \phi + i\psi = U_\infty \left[Z e^{-i\alpha} + \frac{(a+b)^2 e^{i\alpha}}{4Z} \right] + \frac{i\Gamma}{2\pi} \ln \frac{Z}{a+b} \tag{1}$$

with the aid of the following transformation between a circle and an ellipse (Reference 7)

$$Z = \frac{1}{2}\left(z + \sqrt{z^2 - c^2} \right) \tag{2}$$

where $c^2 = a^2 - b^2$ and the expression $z = c \cosh \zeta$ represents elliptical coordinates (Figs. 1 and 2)

$$\zeta = \xi + i\eta \tag{3}$$

and

$$x = c \cosh \xi \cos \eta \quad , \qquad y = c \sinh \xi \sin \eta \, . \tag{4}$$

If the potential flow about the circle consists of a parallel and a circulatory flow, the velocity at any point on the elliptical airfoil, as determined by the above transformation, can be written as

$$\frac{u}{U_\infty} = \frac{1}{U_\infty} \left| \frac{dF}{dz} \right| = \frac{\left(1 + \frac{b}{a}\right) \sin(\eta - \alpha) + \frac{C_L}{2\pi}}{\left[\sin^2 \eta + \left(\frac{b}{a}\right)^2 \cos^2 \eta \right]^{\frac{1}{2}}} \, . \tag{5}$$

According to Eq. (1), the stream function for an elliptical airfoil with circulation is obtained as

$$\psi = U_\infty (a+b) \operatorname{Sinh}(\xi - \xi_0) \operatorname{Sin}(\eta - \alpha) + \frac{U_\infty}{2\pi} a C_L (\xi - \xi_0) \quad (6)$$

where ξ_0 is the value of ξ on the ellipse.

For any given C_L, the dividing streamline is obtained by putting $\psi = 0$ in Eq. (6); hence,

$$\operatorname{Sin}(\eta - \alpha) = - \frac{(\xi - \xi_0)\, C_L}{2\pi \left(1 + \frac{b}{a}\right) \operatorname{Sinh}(\xi - \xi_0)} \quad (7a)$$

and

$$\operatorname{Cos}(\eta - \alpha) = \left[1 - \left\{ \frac{(\xi - \xi_0)\, C_L}{2\pi \left(1 + \frac{b}{a}\right) \operatorname{Sinh}(\xi - \xi_0)} \right\}^2 \right]^{\frac{1}{2}} \quad (7b)$$

Solving Eqs. (7a) and (7b),

$$\operatorname{Sin}\eta = -F(\xi) \operatorname{Cos}\alpha + \operatorname{Sin}\alpha \sqrt{1 - [F(\xi)]^2} \quad (8a)$$

and

$$\operatorname{Cos}\eta = F(\xi) \operatorname{Sin}\alpha + \operatorname{Cos}\alpha \sqrt{1 - [F(\xi)]^2} \quad (8b)$$

where

$$F(\xi) = \frac{(\xi - \xi_0)\, C_L}{2\pi \left(1 + \frac{b}{a}\right) \operatorname{Sinh}(\xi - \xi_0)}.$$

Substituting Eqs. (8a) and (8b) into Eq. (4), the coordinates for the dividing streamlines are obtained as follows:

$$\frac{x}{a} = \left[\operatorname{Cosh}(\xi - \xi_0) + \frac{b}{a} \operatorname{Sinh}(\xi - \xi_0) \right] \left[F(\xi) \operatorname{Sin}\alpha + \operatorname{Cos}\alpha \sqrt{1 - [F(\xi)]^2} \right]$$

$$\frac{y}{a} = \left[\operatorname{Cosh}(\xi - \xi_0) + \frac{a}{b} \operatorname{Sinh}(\xi - \xi_0) \right] \left[-F(\xi) \operatorname{Cos}\alpha + \operatorname{Sin}\alpha \sqrt{1 - [F(\xi)]^2} \right]; \quad (9)$$

the coordinates of the stagnation points are

$$\frac{x}{a} = \frac{C_L \sin\alpha}{2\pi\left(1+\frac{b}{a}\right)} + \cos\alpha\left[1 - \frac{C_L^2}{4\pi^2\left(1+\frac{b}{a}\right)^2}\right]^{\frac{1}{2}}$$

$$\frac{y}{b} = \frac{C_L \cos\alpha}{2\pi\left(1+\frac{b}{a}\right)} + \sin\alpha\left[1 - \frac{C_L^2}{4\pi^2\left(1+\frac{b}{a}\right)^2}\right]^{\frac{1}{2}} \qquad (10)$$

The calculated values of the rear dividing streamlines for elliptical airfoils of 18-percent-thickness ratio ($C_L = 1.0, \alpha = 0$) and 12-percent-thickness ratio ($C_L = 0.75, \alpha = 0$) are shown in Figs. 3 and 4, respectively. The corresponding experimental data for airfoils with trailing edge jet are also shown. The agreement between the calculated values and the measured data is considered to be good.

Equation (5) gives the velocity distribution in the potential flow of an elliptical airfoil with a thin flap placed along the calculated rear dividing streamline extending from the elliptical airfoil's surface to a certain point downstream. It is assumed that there is no separation of flow in the boundary layer. These velocity distributions are shown in Fig. 5 for an elliptical airfoil of 18-percent-thickness ratio ($C_L = 1.0, \alpha = 0$) and in Fig. 6 for an ellipse of 12-percent-thickness ratio ($C_L = 0.75, \alpha = 0$).

The pressure coefficient for an incompressible flow is given by

$$C_p = 1 - \left(\frac{u}{U_\infty}\right)^2 \qquad (11)$$

The calculated values of C_p for elliptical airfoils of thickness ratios 18 percent ($C_L = 1.0$) and 12 percent ($C_L = 0.75$) without trailing edge jets are shown in Figs. 7 and 8, respectively.

2.2 ELLIPTICAL AIRFOIL WITH TRAILING EDGE JET

In order to achieve the desired lift coefficient for the elliptical airfoil discussed in Section 2.1, it is important that flow separation does not occur in the boundary layer. Hence some means such as continuous suction around the trailing edge of the elliptical airfoil must be applied so that the airstream can flow around the trailing edge and flow smoothly off the end of the thin flap. In this way the circulation necessary to create lift can be achieved with the airfoil at zero angle of attack.

If a jet is established at the rear stagnation point and ejected at high velocity along the rear dividing streamline, the additional energy imparted to the boundary layer may overcome the wall friction and prevent flow separation. Furthermore, the jet may produce a "supercirculation" above the

circulation necessary to keep the flow attached if the momentum of the jet is sufficiently large and separations of flow do not occur.

In Reference 6, an approximate method for calculating the pressure distribution of a two-dimensional airfoil in inviscid incompressible flow with jet issuing from the lower surface near the trailing edge is considered. This method assumes first a symmetrical chordwise loading fore and aft of the mid-chord point, and then a third chordwise loading is added in order to satisfy the jet-induced pressure thrust condition. The symmetrical chordwise loading consists of two flat-plate loadings $l_1(\bar{x})$ and $l_2(\bar{x})$, one producing a uniform upwash and the other a uniform downwash. The third flat-plate loading $l_3(\bar{x})$ produces a uniform downwash which compensates for the upwash induced on the surface of the plate by the jet. This asymmetric chordwise loading of a flat plate is illustrated in Fig. 11.

If the above-mentioned flat-plate solution is extended to an airfoil of nonzero thickness, then the pressure distribution along the surface of the thick airfoil can be determined. According to the method given in Reference 12, the pressure coefficient of elliptical airfoils is calculated in the form

$$C_p = 1 - \frac{1}{1+\left(\frac{b}{a}\right)^2 \frac{(1-2\bar{x})^2}{1-(1-2\bar{x})^2}} \left[\left(1 + \frac{b}{a} + \frac{V_{xJ}}{U_\infty}\right) \cos\alpha \right.$$

$$\left. \pm \left\{ \left(\frac{C_{Lp} + C_{L3}}{4\pi} + \sin\alpha \right) \sqrt{\frac{1-\bar{x}}{\bar{x}}} + \frac{C_{Lp} - C_{L3}}{4\pi} \sqrt{\frac{\bar{x}}{1-\bar{x}}} \right\} \left(1 + \frac{b}{a}\right) \right]^2 \tag{12}$$

where the jet-induced velocity component parallel to the chord

$$\frac{V_{xJ}}{U_\infty} = 0.005 \left(\sqrt{\frac{a C_J}{\sigma}} - 1 \right)$$

and

$$C_{L3} = 2\pi \frac{C_J}{C_{Lp}} (1 - \cos\theta).$$

Equation (12) may be used to calculate the pressure distribution for an elliptical airfoil with trailing edge jet at any given C_{Lp}, provided the C_{Lp} and C_J relation is known. For a thin airfoil (12.5-percent-thickness ratio and less), the relation between C_{Lp} and C_J is given by (Reference 9)

$$\frac{C_{Lp}}{\theta} = 3.54 C_J^{\frac{1}{2}} - 0.675 C_J + 0.156 C_J^{\frac{3}{2}}. \tag{13}$$

However, for the elliptical airfoil of 18-percent-thickness ratio, the above expression does not give accurate results and approximate estimation of C_{Lp} and C_J must be made.

The calculated values of the pressure distributions for the elliptical airfoil of 18-percent-thickness ratio ($C_L = 1.0$, $\alpha = 0$, $\theta = 30^\circ$) and of 12-percent-thickness ratio ($C_L = 0.75$, $\alpha = 0$, $\theta = 40^\circ$) are shown in Figs. 9 and 10, respectively. The corresponding values of the measured data are also indicated in the respective figures. The agreement between the calculated pressure distributions and the test data is fairly good.

2.3 SEPARATION PREDICTION FOR THE ELLIPTICAL AIRFOIL WITH AND WITHOUT TRAILING EDGE JET

The main difficulty in predicting the separation point of the laminar boundary layer lies in the determination of the pressure distribution for a body. This pressure is not known a priori and is different from the calculated value based on potential flow theory. The discrepancy is evidenced by a comparison of the measured and the calculated point of separation of a circular cylinder. Measurements indicated that a laminar boundary layer on a circular cylinder separates at 81° from the front stagnation point, whereas the von Kármán-Pohlhausen method (Reference 13) using measured pressure data predicts separation at 82°. However, if the potential pressure distribution is used, calculations give separation at 110° from the front stagnation point.

Although the von Kármán-Pohlhausen method using the measured pressure distribution data predicts the separation on a cylinder, it fails to give the point of separation on an elliptical cylinder. It appears that the von Kármán-Pohlhausen approximate method is satisfactory for flows with decreasing pressure or with gradually increasing pressure so that separation is not approached. The theory breaks down in the neighborhood of a separation point and fails completely to give the correct location of separation unless the pressure rise of the body is very rapid, as in the case of flow past a circular cylinder. In order to predict the separation point more accurately, several exact solutions of the boundary layer equations have been proposed (Reference 5). The analysis based either on series solutions or on finite-difference solutions of the boundary layer equations is too cumbersome for practical applications.

Recently Curle and Skan (Reference 1) developed a new, approximate technique for separation-point prediction depending heavily on empirically determined coefficients. This simplified expression for separation-point prediction for the two-dimensional laminar boundary layer is given by

$$\left(\frac{S'}{2a}\right) C_p' \frac{dC_p'}{d\left(\frac{S'}{2a}\right)} = 1.04 \times 10^{-2} \qquad (14)$$

where $\frac{S'}{2a}$ is the nondimensional distance along the wall measured from the minimum pressure point and

$$C_p' = 1 - \left(\frac{u}{U_{max}}\right)^2 \qquad (15)$$

where u = potential flow velocity around the body
U_{max} = maximum potential flow velocity (at minimum pressure point).

The calculated location of the separation point on an elliptical cylinder of thickness ratio 0.388 from Eq. (14) is $\frac{S}{a} = 2.01$, whereas the measured location by Schubauer (Reference 8) is $\frac{S}{2a} = 1.99$. Hence, for engineering purposes, separation in two-dimensional flow can be predicted with great ease and accuracy by Eq. (14).

a. Separation Prediction for the Elliptical Airfoil Without Trailing Edge Jet.

As mentioned in Section 2.1, a desired lift can be produced by an elliptical airfoil at zero angle of attack relative to the incoming flow if a thin flap is placed along the calculated rear dividing streamline extending from the elliptical airfoil's surface to a certain point downstream. The above phenomenon is true only if there is no separation of flow in the boundary layer. Hence, it is important to predict the location of separation points of this airfoil.

Based on the velocity distribution (Fig. 5) calculated from Eq. (5) for the elliptical airfoil of 18-percent-thickness ratio ($C_L = 1.0$, $\alpha = 0$, $\theta = 30^\circ$), the expression for C_p' is calculated from Eq. (15) as follows:

$$C_p' = C_1\left(\frac{S'}{2a}\right) + C_2\left(\frac{S'}{2a}\right)^2 + C_3\left(\frac{S'}{2a}\right)^3 + C_4\left(\frac{S'}{2a}\right)^4 \qquad (16)$$

where

$$C_1 = 5.09645 \quad , \quad C_2 = -7.36754 \times 10^2$$
$$C_3 = 5.33436 \times 10^4 , \quad C_4 = -5.405827 \times 10^5 .$$

Substituting the expression for C_p' [Eq. (16)] and the derivative of C_p' into Eq. (14), an algebraic equation is obtained in the form

$$A_{12}\left(\frac{S'}{2a}\right)^{12} + A_{11}\left(\frac{S'}{2a}\right)^{11} + \cdots\cdots A_3\left(\frac{S'}{2a}\right)^3 = 1.04 \times 10^{-2}. \quad (17)$$

The solution of physical significance is found to be

$$\left(\frac{S'}{2a}\right) = 0.0179. \quad (18)$$

Hence, the point of separation for the elliptical airfoil of 18 percent ($C_L = 1.0$, $\alpha = 0$) is

$$\left(\frac{S}{2a}\right) = 1.047 \quad (19)$$

measured from the front stagnation point, whereas the rear stagnation point is

$$\left(\frac{S}{2a}\right) = 1.074 \quad (20)$$

measured from the front stagnation point.

Similarly, the expression for C_p' as calculated from the velocity distribution (Fig. 6) for the elliptical airfoil of 12 percent ($C_L = 0.75$, $\alpha = 0$, $\theta = 40^\circ$) is obtained as

$$C_p' = b_1\left(\frac{S'}{2a}\right) + b_2\left(\frac{S'}{2a}\right)^2 + b_3\left(\frac{S'}{2a}\right)^3 + b_4\left(\frac{S'}{2a}\right)^4 \quad (21)$$

where

$$b_1 = 1.69665 \times 10^2, \qquad b_2 = -2.74809 \times 10^5$$

$$b_3 = 1.58277 \times 10^8, \qquad b_4 = -2.59204 \times 10^{10}.$$

With this expression for C_p' and the derivation of C_p', Eq. (14) yields a twelfth degree algebraic equation with a root

$$\left(\frac{S'}{2a}\right) = 0.0021. \quad (22)$$

Hence, the point of separation for the 12-percent ellipse ($C_L = 0.75$, $\alpha = 0$) is

$$\left(\frac{S}{2a}\right) = 1.0313 \quad (23)$$

measured from the front stagnation point , whereas the rear stagnation point is

$$\left(\frac{S}{2a}\right) = 1.043 \tag{24}$$

measured from the front stagnation point. The locations of the separation points for the elliptical airfoils of 18-percent- and 12-percent-thickness ratios are shown in Figs. 12 and 13, respectively.

b. Separation Prediction for the Elliptical Airfoil With Trailing Edge Jet.

If a jet is ejected at high velocity along the rear dividing streamline, an additional energy will be supplied to the boundary layer; hence, separation of the flow beyond the minimum pressure point may be prevented. From Fig. 9, it is seen that the minimum pressure point of the elliptical airfoil of 18-percent-thickness ratio ($C_L = 1.0$, $\alpha = 0$, $\theta = 30^o$) is indeed very close to the rear stagnation point from which the jet is issued. For this reason it is unlikely that separation of flow would occur in this case. Using a linear approximation of the C_p' function, it is found that the point of separation for the elliptical airfoil of 18 percent ($C_L = 1.0$, $\theta = 30^o$) occurs at

$$\left(\frac{S}{2a}\right) = 1.066 \tag{25}$$

measured from the front stagnation point. Since the location of the jet measured from the front stagnation point is

$$\left(\frac{S}{2a}\right) = 1.074 , \tag{20}$$

the flow separation in this case can hardly influence the flow pattern.

A similar conclusion can be drawn for the 12-percent elliptical airfoil ($C_L = 0.75$, $\alpha = 0$, $\theta = 40^o$), where the point of separation is $\frac{S}{2a} = 1.035$ measured from the front stagnation point. The corresponding location of the jet measured from the front stagnation point is $\frac{S}{2a} = 1.043$.

The locations of the separation points for elliptical airfoils of 18-percent- and 12-percent-thickness ratio with trailing jets are shown in Figs. 12 and 13, respectively.

3. APPARATUS AND TESTS

3.1 THE MODEL

Based on the theoretical results obtained in Section 2, the capacity of the air supply, the limitation of the internal pressure of the model, and the limitation due to the compressibility effect of the jet stream at high velocities, the elliptical airfoil of 18-percent-thickness ratio was designed first and subsequently the 12-percent model. According to the model geometrical configuration, the expression for C_J is

$$C_J = 135.7 \left(\frac{Q}{U_\infty} \right)^2 \tag{26}$$

for the 18-percent model and

$$C_J = 121.6 \left(\frac{Q}{U_\infty} \right)^2 \tag{27}$$

for the 12-percent model. The average value of Q corresponding to 6-inch pressure inside the model is 2.5 cubic feet per second for 18-percent elliptical airfoil and 3.37 cubic feet per second for 12-percent airfoil.

According to Reference 9, the total lift coefficient at $\alpha = 0$ is

$$C_L = 2k \sin\theta \sqrt{2\pi}\, C_J^{\frac{1}{2}} \left[1 + \frac{\pi}{48} \frac{C_J}{k^2} + O\left(C_J^2\right) \right]. \tag{28}$$

Based on the C_J values calculated from Eqs. (26) and (27), the values of C_L can be approximately estimated for both models. For example, $C_J = 0.5$, $k = 1.0$ for the 18-percent model, the estimated total lift coefficient is $C_L = 1.83$, and the corresponding test result gives $C_L = 2.05$ (Fig. 27).

The first model tested had a 12-inch chord and a 36.5-inch span. The cross section was elliptical, with a maximum thickness of 18 percent of the chord length. As seen in Fig. 14, the main structural member was a 1-3/8-inch outside diameter, round steel tube which also supplied the air for the jet. The leading and trailing edges were machined from cast-aluminum bar stock using a milling cutter ground to the elliptical contour. This model was first tested with a solid leading edge and a jet blowing in the trailing edge. The trailing edge was constructed of two pieces (Fig. 15). The jet slot configuration was machined into the mating surfaces, after which the two parts were joined by screws and then machined to the final external contour. This trailing edge jet slot width was 0.019 ± 0.001 inch wide, at

an angle of 30° to the model chord plane. Aluminum ribs and skin were employed. Seventy-six static pressure taps were installed spanwise along the top and bottom surfaces at the 50-percent chord line and, similarly, 47 taps in the chordwise direction in the mid-span plane. The location of these taps is given in Fig. 16.

The blowing air entered the interior of the model through 11 pairs of diametrically opposed slots in the steel support tube. The slots were 1/2-inch wide and 1/8-inch high, exhausting in the chordwise direction. The support tube was clamped on one end to a stand outside the tunnel; thus the model was mounted horizontally in the test section, cantilevered from one end (Fig. 17). A flexible rubber hose was used to connect the support tube to the air supply piping. The connection was made outboard of the cantilever support clamps, so that forces caused by piping misalignment were not transmitted to the model itself.

After the first model was tested with the trailing edge jet only, it was dismantled and a new leading edge installed having a slot 0.030±0.001 inch wide, also at an angle of 30° to the chord plane. A multiple-gate type valve (Fig. 18) was also installed to control the flow to the forward jet.

The second model (Fig. 19) had a thickness of 12 percent of the chord length and was 34-1/2-inches long. Construction was essentially the same as described above excpet that space limitations required the use of a 1-inch-by-2-inch rectangular steel support tube. This model had a jet slot at the trailing edge only. The jet was 0.023±0.001 inch wide and at an angle of 40° to the chord plane. The location of the pressure orifices is given in Fig. 20.

3.2 AUXILIARY AIR SUPPLY

An auxiliary air supply was used to provide jet blowing of the model. The main compressed air supply system has a capability of furnishing approximately 0.5 pound per second, at 100 psig. This capability was supplemented by the installation of storage tanks having a total volume of 200 cubic feet (Fig. 21). At 100 psig, these contained approximately 100 pounds of air which could be used over any desired time interval. The air was routed to the tunnel test section through 2-1/2-inch pipe containing two manually controlled valves and an orifice-plate flowmeter. A thermometer mounted in a mercury-filled well was used to measure the auxiliary air temperature as it entered the model. Since the tunnel static pressure was constant for all tests, the mass flow rate for the jet blowing of the model was determined by the static pressure inside the model. The orifice meter was used to obtain a correlation between mass flow rate and model internal pressure for each jet

slot configuration. This permitted the determination of flow rates from the measured model pressure, rather than using the more cumbersome orifice meter.

In order to determine the aerodynamic response of the model to cyclic changes in blowing, a series of dynamic tests were made. A butterfly-type valve was installed in the air supply tube of the 18-percent-thick model. The butterfly diameter was made smaller than the tube inside diameter so that, when the butterfly was perpendicular to the tube axis, the flow rate was approximately 60 percent of the equivalent rate without the valve. When the butterfly was parallel to the tube axis, the flow reduction was negligible. The valve was designed so that it could be continuously rotated at any desired rate by means of a motor connected to the valve shaft. The rotating valve produced a pulsating pressure in the model which in turn resulted in cyclic flow of the jet. The flow cycle was that of a sinusoidal wave.

3.3 WIND TUNNEL

The tests were conducted in the subsonic wind tunnel of the Department of Aerospace Engineering. The tunnel is of the continuous-flow, closed-circuit type, capable of a maximum velocity of 175 feet per second. The closed test section is 38 inches long, and all four walls diverge to compensate for boundary layer thickening. The entrance is approximately 22 inches high and 36 inches wide; the exit is 16 inches by 39 inches. The test section static pressure is essentially atmospheric for all tests.

3.4 INSTRUMENTATION

a. Force Measurements.

The model was mounted as a cantilevered beam by clamping the support tube to a stand fixed to the building floor. Strain gages were mounted on the tube between the clamps and the tunnel wall; three bridges were installed, oriented to measure lift, drag and pitching moment (Fig. 22). The outputs were manually recorded using SR-4 strain indicators. The pitching moments proved to be too small to measure with reasonable accuracy.

A 14-channel Midwestern Instrument 621 oscillograph was used to record the model forces for the dynamic tests during which the blowing rate was varied. The output of the strain gage bridges was too low to permit recording on the oscillograph; hence, linear variable differential transformers were mounted at the free end of the model to measure the deflections due to

lift and drag. A calibration between the forces and resulting deflections was made using dead weights and pulleys.

b. Pressure Measurements.

The steady-state pressure measurements were made using multiple-tube manometer boards filled with oil at 0.9 specific gravity. The manometer readings were manually recorded.

The measurement of the model surface static pressures during the dynamic tests was made using five Pace Model P7D-±1.0 psig variable-reluctance type pressure transducers. These were mounted outside the wind-tunnel wall and connected to various chordwise pressure orifices using plastic tubing installed inside the 12-percent-thickness ratio model. One transducer was connected to measure the model internal (blowing) pressure. The transducer output was rectified and recorded on an oscillograph. The transducers were selected because of their low internal volume and high natural frequency.

4. EXPERIMENTAL RESULTS

4.1 THE JET EFFLUX CALIBRATION

In Section 3.2 the air supply system has been described in detail. The air was taken from supply tanks to the model through a 2-1/2-inch pipe. The mass flow rate across the trailing edge slot was determined by an orifice meter installed inside the supply pipe. Simultaneously, the model plenum pressure was recorded corresponding to the inches of mercury pressure across the orifice plate of the flow meter. The volume flow rates, cubic feet per second (mass flow for incompressible fluid), across the trailing edge slot were calibrated for the complete range of wind tunnel velocities ($1.53 \times 10^5 \leq R_e \leq 9.2 \times 10^5$), and the results are plotted versus the model plenum pressure (inches of mercury absolute). These calibration curves are given in Fig. 23 for the elliptical airfoil of 18-percent-thickness ratio and in Fig. 24 for the elliptical airfoil of 12-percent-thickness ratio. It is seen from the above figures that the volume flow rate (or jet velocity) across the slot versus the model plenum pressure is independent of the wind tunnel velocity.

4.2 SHAPE OF THE JET

The angles of the jet deflection for both of the elliptical airfoil models (18-percent- and 12-percent-thickness ratios) were first checked by setting the models at inclination angles of -30° and -40°, respectively. The ejection stream of the jets in each case was surveyed with Pitot tube, and the jet stream for each model was found to be very nearly horizontal.

Measurements of the shape of the jet were made at six stations behind the trailing edge jet slot. The location of the first station is 1/3 inch behind the slot and the last station is 20-1/3 inches behind the slot. Pitot tubes were carefully aligned in order to locate the position of maximum total pressure in any one plane. Experiments were made using both models at three different wind tunnel velocities and three different mass-flow rates of the jet.

The results of the above described data were reduced to the single parameter C_J, jet coefficient. Figure 25 illustrates the path of the jet for the elliptical airfoil of 18-percent-thickness ratio at three values of C_J, and the corresponding results for the elliptical airfoil of 12 percent are shown in Fig. 26. The measured path of the jet is compared with the corresponding calculated values of the dividing streamline. The theoretical and experimental results for both models are shown in Fig. 3 for the elliptical airfoil of 18-percent-thickness ratio and in Fig. 4 for the 12-percent-thickness ratio.

In each case the agreement is reasonably good.

4.3 ELLIPTICAL AIRFOIL WITH TRAILING EDGE JET

a. Lift at Zero Angle of Attack

The lift forces (forces in a direction perpendicular to the air stream) were measured for both models at various wind tunnel velocities ($1.5 \times 10^5 \leq R_e \leq 9 \times 10^5$) and trailing edge jet velocities. The data were reduced to coefficient forms and plotted as total lift coefficient versus jet coefficient. In Fig. 27 the total lift coefficient C_L is shown as a function of the jet coefficient C_J for the elliptical airfoil of 18-percent-thickness ratio. It is seen that maximum $C_L = 3.45$ was obtained at $C_J = 1.32$.

The pressure lift coefficient C_{Lp} is defined as

$$C_L = C_{Lp} + C_J \sin\theta, \tag{29}$$

and the curve of C_{Lp} against C_J as calculated from Eq. (29) is also shown in Fig. 27. The values of the pressure lift coefficient C_{Lp} are also calculated from the measured static pressure on the surface of the model (see Section 4.3c), and these values are shown in Fig. 27. These measured values of C_{Lp} agree very well with those obtained from Eq. (29).

Similarly, the total lift coefficient versus the jet coefficient for the elliptical airfoil of 12-percent-thickness ratio is shown in Fig. 28. The values of the pressure lift coefficient are obtained both from Eq. (29) and from the measured static pressure; they are also shown in Fig. 28 with very good agreement.

b. Lift at Small Angles of Attack

The total lift coefficient for the elliptical airfoil of 18-percent-thickness ratio was measured at several angles of attack. The total lift coefficient versus the jet coefficient at various angles of attack is shown in Fig. 29. Curves of the total lift coefficient versus the angle of attack with jet coefficient as a parameter are shown in Fig. 30.

With the jet coefficient $C_J < 1.0$, the total lift coefficient at small angles of attack ($\alpha < 5^\circ$) can be expressed by the following equation (see Reference 9)*

$$C_L = C_{L_{\alpha=0}} + \alpha \left(\frac{\partial C_L}{\partial \alpha} \right)_{\alpha=0} \tag{30}$$

where

$$\left(\frac{\partial C_L}{\partial \alpha} \right)_{\alpha=0} = 2\pi \left[1 + \frac{k}{\sqrt{2\pi}} C_J^{\frac{1}{2}} + \frac{\pi}{24k} C_J + \frac{1}{24\pi k} \left(\frac{\pi C_J}{2} \right)^{\frac{3}{2}} + \cdots \right]. \tag{31}$$

As a typical example, when $C_J = 0.4$ and $\alpha = 4^\circ$, the calculated value of C_L from Eq. (30) is $C_L = 2.57$ and the corresponding measured value is $C_L = 2.45$. The difference between the calculated and experimental values is within 5 percent.

From Fig. 30 it may be seen that the stalling point, $\frac{\partial C_L}{\partial \alpha} = 0$, occurs at an angle of attack of 5° for $C_J = 1.2$; however, it may also be noted that the stalling point occurs at higher angles of attack as the value of C_J decreases. The decrease of C_L after the stalling point for the elliptical airfoil with trailing edge jet is rather gradual in contrast to the sharp drop of C_L for the conventional airfoil.

c. Pressure Distributions

In Section 3.1 it was mentioned that 47 flush orifices in the chordwise direction along the mid-span plane and 76 orifices in spanwise direction along the top and bottom surfaces at the mid-chord line were installed for both models. The results of the tests show that the spanwise pressure distribution for each of the models is very nearly constant, which can be seen from Figs. 31 and 32 for the elliptical airfoils of 18-percent-thickness ratio and 12-percent-thickness ratio, respectively.

A series of typical pressure distribution curves in the chordwise direction for the elliptical airfoil of 18-percent-thickness ratio is given in Figs. 33 (a) through 33 (l). In Figs. 33 (d), (f), (j) and (k), the calculated pressure distributions from Eq. (12) are shown to be in good agreement with the measured values. The integration of the static pressures over the chord gives the pressure lift force per unit span. The results of the integration of the pressure distribution curves, after reducing to pressure lift coefficient, C_{Lp}, are shown in Fig. 27. The agreement between the results of C_{Lp} from the pressure measurement and those from direct total lift measurement [see Eq. (29)] is considered to be good.

Similarily, a selection of pressure distribution curves in the chordwise direction for the elliptical airfoil of 12-percent-thickness ratio is given in Figs. 34 (a) through 34 (g). Two measured pressure distributions are com-

pared with the corresponding theoretically calculated values. The comparisons of these two sets of values for pressure distributions are shown in Figs. 34 (a) and 10, and they are considered to be in reasonably good agreement.

The pressure lift coefficient C_{Lp} reduced from the pressure measurements is shown in Fig. 28; it agrees reasonably well with the corresponding values obtained from the measurements of total lift force.

d. The Drag

According to thrust hypotheses (Reference 2) for an idealized jet flap system, the total thrust experienced by the airfoil model is equal to the total jet reaction disregarding the angle of deflection of the jet. This hypothesis is based on the assumptions that no mixing occurs between the main stream and the jet and that no separations of flow appear.

Actually, however, the measured thrust (negative drag) is less than the ideal system predicted. This discrepancy occurs since there is a loss in the mixing process between the main stream and the jet sheet as well as the existence of frictional drag. The measured thrust reduced to the form C_D/C_J is plotted against C_J, and these results are shown in Fig. 35 for the elliptical airfoil of 18-percent-thickness ratio and in Fig. 36 for the 12-percent model. Since in actual practice the hot jet may be used, further careful investigation of this problem will be required.

e. The Pitching Moment

The pitching moment on the elliptical airfoil was found by the combination of the results of a graphical integration of the moment of area of the pressure distribution curve about the mid-chord point with the moment due to the jet reaction. The position of the center of lift can be obtained from the pitching moment and lift coefficient data. Figures 37 and 38 show the variation of the pitching moment coefficient C_m with total lift coefficient C_L for the models of 18-percent- and 12-percent-thickness ratios, respectively.

According to the experimental data (Figs. 37 and 38) the pitching moment coefficient can be expressed as a function of C_L and C_J in the following form (Reference 3):

$$C_m = \frac{C_L}{4} - \gamma C_J^{\frac{1}{2}} \left(C_L + 2\pi \right) \qquad (32)$$

where γ is a constant depending on the airfoil geometry and the jet angle. For the elliptical airfoil of 18-percent-thickness ratio ($\theta = 30^\circ$), the values of γ are in the range of 0.08 to 0.107 for $0.06 \leq C_J \leq 0.65$; and for the 12-

percent model ($\theta = 40^{\circ}$), the values of γ are between 0.105 to 0.12 for $0.05 \leqslant C_J \leqslant 0.40$.

4.4 ELLIPTICAL AIRFOIL WITH BOTH DUAL JETS AND SINGLE LEADING EDGE JET

a. Dual Jets

In Section 2.1, an elliptical airfoil moving through a stationary fluid at a zero angle of attack was discussed. If the potential flow is calculated about an elliptical airfoil corresponding to an arbitrary circulation, the two symmetrical dividing streamlines (or zero streamline) are known and a certain lift is obtained. If either a thin flap of short length or a jet stream should be placed along the calculated rear dividing streamline corresponding to a specified circulation, approximately the same lift would be produced on the elliptical airfoil.

If a second thin flap of short length should be placed along the calculated leading edge dividing streamline (zero streamline), theoretically the flow would not be altered and the same lift would be produced as in the case of a rear thin flap. This occurs because there is no flow across the thin flaps located at the front and the rear of the elliptical airfoil.

Let us now suppose that the two thin flaps be replaced by two jet streams ejecting outward along the two dividing streamlines and let us examine the results. This exploratory experiment was performed on the elliptical airfoil of 18-percent-thickness ratio with dual symmetrical jets (Fig. 39). However, the leading edge slot is 0.010 inch larger than the trailing edge slot. The tests were made ($R_e = 5.5 \times 10^5$) by varying the mass flow of the leading edge jet while the mass flow of the trailing edge jet was maintained constant. The results of this test are presented in Fig. 40 and show the variation of the total lift coefficient as a function of the ratio of the leading edge C_J to the trailing edge C_J, $(C_J)_F/(C_J)_R$. For $(C_J)_F/(C_J)_R = 0$, the total lift coefficient is equal to the case of airfoil with trailing edge jet only. As the mass flow of the leading edge jet increases from the zero value, the total lift increases gradually. This increase of total lift is equivalent to the reaction resulting from the front jet. It is very interesting to note that even though the mass flow of the leading edge jet exceeds that of the rear jet by 50 percent, the total lift still remains above its original value when $(C_J)_F = 0$.

The important application of the elliptical airfoil (or any oval airfoil) with dual jets to the retreating blade of a rotor is evident. At high transverse speeds of a rotor, a sizable portion of the retreating blade experiences a reversal of relative airflow. This produces a condition of no lift or even

a negative lift on a conventional airfoil with positive angle of attack. If the elliptical airfoil with dual jets is used for the blade, the loss of lift in the reverse flow region which is experienced in present-day rotor systems can be completely eliminated. It is well to note that this condition for the conventional rotor system is aggravated with an increase in helicopter speed.

b. Leading Edge Jet

According to the discussion presented in the early part of Section 4.4 (a), a desired lift can also be maintained if the front dividing streamline is established. With this in mind, a single leading jet was spaced along the front dividing streamline. The results of this test show that separation of flow occurs near the trailing edg of the airfoil. This evidently was the cause of the sharp drop of the value of lift in comparison with that of the trailing edge jet results. These results are presented by the C_L versus C_J curve shown in Fig. 41.

It is believed that one of the least difficult means of preventing separation of flow is the blowing of air through a slot. This scheme has suggested that an elliptical airfoil with dual jets would be the simplest means of maintaining a desired lift regardless of whether the flow initially passes the leading edge or the trailing edge of an airfoil.

4.5 AERODYNAMIC RESPONSE OF THE MODEL TO CYCLIC CHANGE OF JET

In a conventional type of helicopter rotor, the control of the lift coefficient, C_L, must be effected by a change in incidence or angle of attack of the airfoil. The circulation created in this case is the result of the Kutta flow condition at the sharp trailing edge. In the present study, it is indicated that the value of C_L can be controlled by simply varying mass flow of the jet. Hence, experiments were made to examine the aerodynamic response of the elliptical airfoil model of 18-percent-thickness ratio to a cyclic change in the jet mass flow.

In the experiments, the cyclic change in mass flow was accomplished by the use of a rotating butterfly valve which partially interrupted the flow into the model proper. The cycling of the jet at any specified frequency was achieved by controlling the rotational speed of the valve. During the test, the cyclic pressure inside the model and the corresponding cyclically varying normal and axial forces were measured. The instrumentation for these measurements was discussed in Section 3.4.

During the tests, three rotational speeds of the valve were made,

namely, 360 r. p. m, 210 r. p. m., and 150 r. p. m. These valve speeds correspond to jet mass flow variations of 12, 7, and 5 cycles per second, respectively. A typical four cycles of pulsating lift and the pressure inside the model were obtained from the testing results for valve speed at 360 r. p. m. These results are plotted in Fig. 42 as a function of time. It is very interesting to note that the pulsating lift is almost completely in phase with the pulsating pressure inside the model; hence, there exists a negligible delay in the system of pulsating supply pressure, pulsating jet mass flow, and lift.

Figure 43 is a plot of the pulsating lift coefficient ratio versus the pulsating jet coefficient ratio for two different Reynolds numbers. The typical two cycles of pulsating lift coefficient (measured at two different Reynolds numbers) shown are very close.

Finally, the results of the lift response of the airfoil model to cyclic changes in jet mass flow are reudced to the form of nondimensional coefficients, C_L versus C_J. The pulsating C_L versus the pulsating C_J is shown in Figs. 44 through 47 for valve speeds at 386 r. p. m., 360 r. p. m., 210 r. p. m., and 150 r. p. m., respectively.

The results of these tests clearly indicate that the periodic variation of lift on the airfoil can be fulfilled by cyclic variation of the jet momentum; hence, the lift control problem reduces to simply the problem of pressure control inside the model.

A typical two cycles of pulsating drag and the pulsating pressure inside the model were obtained from the test results for valve speed at 215 r. p. m. The results are plotted in Fig. 48 as a function of time. On account of the inaccuracy of the drag measurement (see Section 4. 3c), the pulsating drag shows a slight phase lag with respect to the pulsating pressure inside the model.

The result of the drag response of the airfoil model to cyclic change in jet mass flow is reduced to the form of nondimensional coefficient C_D versus C_J. The pulsating drag coefficient ratio versus the pulsating jet coefficient ratio is shown in Fig. 49, and the pulsating C_D versus the pulsating C_J is shown in Fig. 50 for valve speed at 215 r. p. m.

4. 6 RESPONSE OF CHORDWISE PRESSURE OF THE MODEL TO CYCLIC CHANGE OF JET

Experiments were made to examine the response of the chordwise static pressure of the elliptical airfoil model of 12-percent-thickness ratio

to a cyclic change in the mass flow. As mentioned in Section 4. 5,the cyclic change in mass flow was accomplished by the use of a rotating butterfly valve which reduced the flow into the model proper. At the fully closed position of the valve, the mass flow was reduced to one-tenth of its maximum value (valve at wide-open position). The instrumentation for these measurements was discussed in Section 3. 4b.

During the tests,two rotational speeds of the valve were used, namely, 300 r. p. m. and 150 r. p. m. These valve speeds correspond to the jet mass flow variation of 10 and 5 cycles per second. Among the data obtained for the cyclic chordwise pressure of the model, the results of eight stations, namely, stations 8, 11, 16, 19, 21, 22, 53, and 55 (see Fig. 20), are presented. A typical seven cycles of pulsating static pressure and the pressure inside the model were obtained for valve speeds at 300 r. p. m. and 150 r. p. m. These results are plotted in Fig. 51 for valve speeds at 300 r. p. m. and in Fig. 52 for 150 r. p. m. as a function of time. It is noted that there is a time lag of about one-fortieth of a second between the pulsating static pressure and the pressure inside the model for both cases. The time lag between the pulsating static pressure and the pressure inside the model is attributed to the effects of the tubing between the static pressure orifices and the pressure transducers.

Figures 53 through 55 are plots of the pulsating pressure coefficient ratio versus the pulsating jet coefficient ratio for valve speed at 300 r. p. m. The pulsating pressure coefficient ratio versus the pulsating jet coefficient ratio for valve speed at 150 r. p. m. is shown in Fig. 56.

The results of the static pressure response of the airfoil model to cyclic changes in jet mass are reduced to the form of nondimensional coefficients, C_p versus C_J. The pulsating C_p versus the pulsating C_J are shown in Figs. 57 through 60 for valve speed at 360 r. p. m. and in Fig. 61 for 150 r. p. m. The results of these tests indicate that not only do the periodic variations of the static pressure follow the cyclic variation of the jet momentum,but they also form a linear relationship.

CONCLUSIONS

Experimental results obtained for elliptical airfoils of both 18-percent- and 12-percent-thickness ratio with trailing edge jets are in good agreement with available theories. Lift forces determined from electric strain-gage data agree very well with those obtained from steady-state pressure measurements. The measured drag data are reasonable but possess more scatter than is desirable; hence, further refinement in the drag force measurement is needed. The pitching moments calculated from the pressure data are reasonable and agree well with the semiempirical expression previously determined.

Most encouraging results were obtained from an experiment performed on the elliptical airfoil of 18-percent-thickness ratio with dual symmetrical jets. These results indicate that the leading edge jet does not disturb the flow and actually furnishes some additional reaction force to the lift. Hence, the important application of the elliptical airfoil (or oval airfoil) with dual jets to the retreating blade of a helicopter rotor is evident.

Furthermore, the results of aerodynamic response measurements of the model to cyclic changes in the blowing jet are surprisingly encouraging. The cyclic valve was tested at frequencies equivalent to twice that of the rotational speed of a conventional helicopter blade, and the response of the lift was found to be excellent with negligible delay. The response of the drag as well as the chordwise pressure distribution to the cyclic changes in the blowing jet were also found to be very good. These results clearly indicate that the periodic variation of lift on the airfoil can be fulfilled by cyclic variation of the jet momentum; hence, the circulation control problem is reduced to simply the problem of pressure control inside the model.

RECOMMENDATIONS

The foregoing test results are very encouraging, since they permit the conclusion that the use of the elliptical airfoil (or oval airfoil) with dual jets on a helicopter would make possible substantial improvements in overall performance. The performance characteristics showing the greatest improvement include a much higher forward flight speed, a higher rate of climb, greater simplicity in rotor construction, a more rigid rotor, and a significant increase in the useful load-lifting capacity. In a VTOL, this system would enable the rotor to experience an advance ratio from zero to infinity.

It is recommended that an accelerated and unified program for further research and development be instituted without delay to obtain complete information on this system. The immediate program should be directed toward obtaining two-dimensional data at high subsonic speeds approaching the transonic range and the static-thrust investigation of this rotor system. Future programs should include a study of the problems expected when this system is applied to the actual design of a prototype helicopter.

BIBLIOGRAPHY

1. Curle, N., and Skan, S. W., "Approximate Method for Predicting Separation Properties of Laminar Boundary Layer," Aeronautical Quarterly (9), August 1957, p. 257.

2. Davidson, I. M., and Stratford, B. S., An Introduction to the Jet Flap, National Gas Turbine Establishment, Report No. R. 155, June 1954.

3. Dimmock, N. A., An Experimental Introduction to the Jet Flap, National Gas Turbine Establishment, Report No. R. 175, July 1955.

4. Golden, J., and House, W., Low Speed Flight Research Program Analysis, Series II, Aerojet Report, No. 509, 1951.

5. Görtler, H., A New Series for the Calculation of Steady Laminar Boundary Layer Flows, Freiburg University, Mathematical Institute Report, September 1955.

6. Küchemann, D., A Method for Calculating the Pressure Distribution Over Jet Flapped Wing, Aeronautical Research Council, Reports and Memoranda No. 3036, 1957.

7. Milne-Thomson, L. M. Theoretical Hydrodynamics, Second Edition, The MacMillan Company, New York, 1950.

8. Schubauer, G. B., Airflow in a Separation Laminar Boundary Layer, NACA Technical Report 527, 1935.

9. Spence, D. A., The Lift Coefficient of a Thin Jet-Flapped Wing, Proceedings of the Royal Society, Series A., Vol. 238, No. 1212, December 1956, pp. 46-68.

10. Theodorson, T., and Garrick, I. E., General Potential Theory of Arbitrary Wing Section, NACA Technical Report No. 451, 1933.

11. Thwaites, B., The Production of Lift Independently of Incidence, Aeronautical Research Council, Reports and Memoranda No. 2611, 1952.

12. Weber, J., The Calculation of the Pressure Distribution Over the Surface of Two-dimensional and Swept Wings with Symmetrical Airfoil Sections, Aeronautical Research Council, Reports and Memoranda No. 2918, 1956.

13. Yuan, S. W., Foundations of Fluid Mechanics, Prentice-Hall, Inc., Englewood Cliffs, New Jersey, to be published.

14. Yuan, S. W., Preliminary Investigation of the von Kármán - Yuan Helicopter Rotor System, Proceedings of the 11th Annual Forum, American Helicopter Society, April 1955, pp. 82-99.

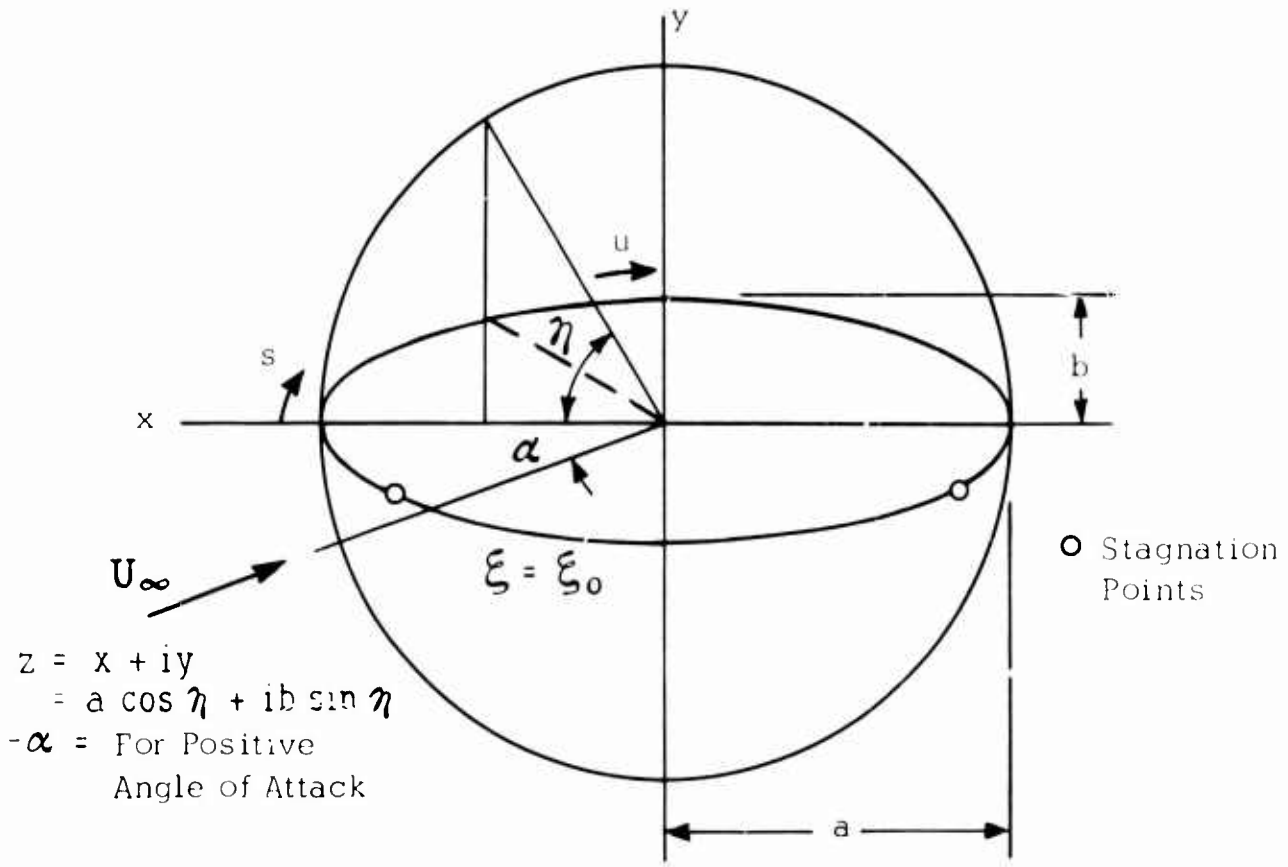

FIG. 1. ELLIPTIC COORDINATES.

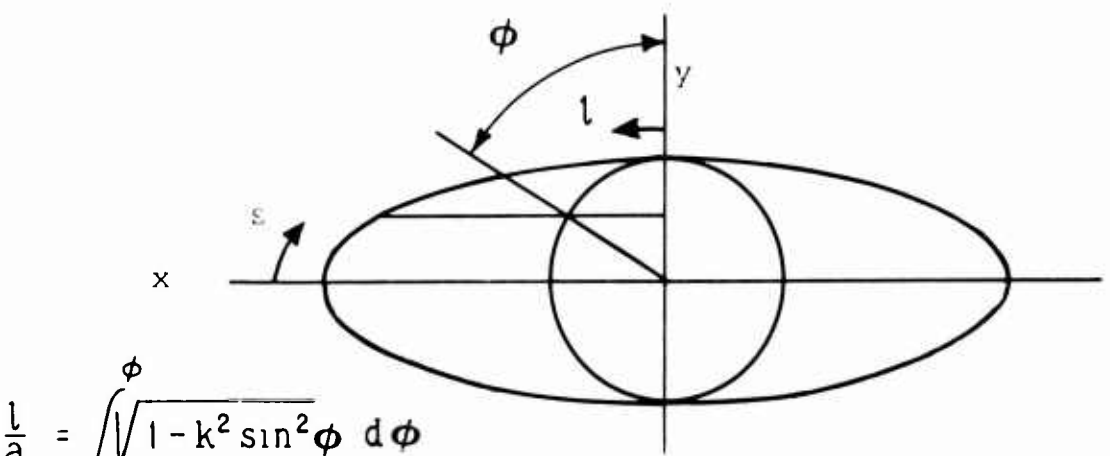

$$\frac{l}{a} = \int_0^{\phi} \sqrt{1 - k^2 \sin^2 \phi}\, d\phi$$

$$k^2 = 1 - \left(\frac{b}{a}\right)^2, \quad a > b$$

$$\eta = 90^\circ - \phi$$

FIG. 2. LENGTH OF THE ARC OF ELLIPSE.

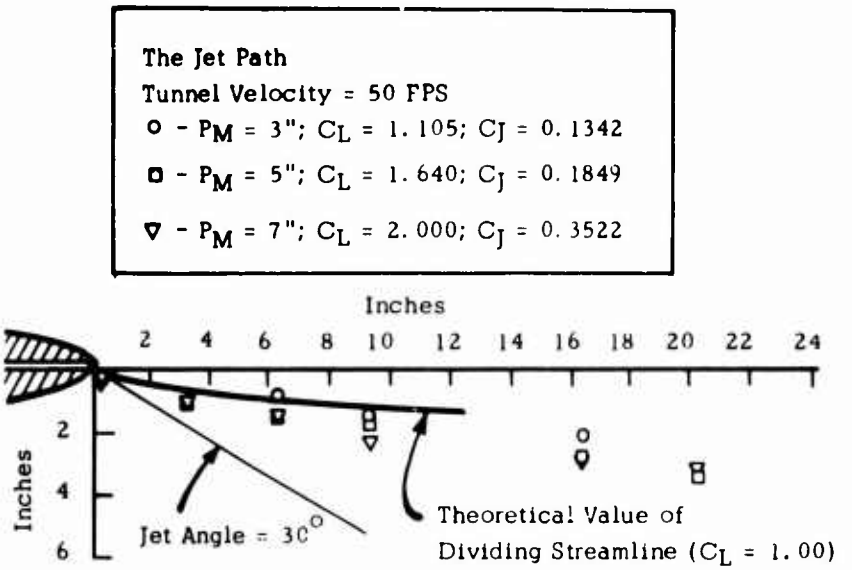

FIG. 3. DIVIDING STREAMLINE AND JET PATH FOR ELLIPTICAL AIRFOIL OF 18-PERCENT-THICKNESS RATIO.

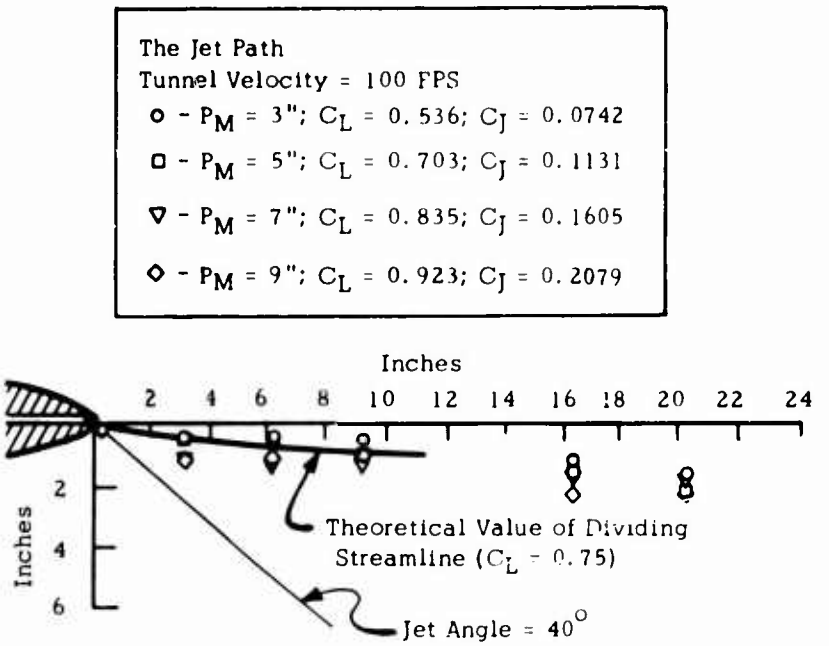

FIG. 4. DIVIDING STREAMLINE AND JET PATH FOR ELLIPTICAL AIRFOIL OF 12-PERCENT-THICKNESS RATIO.

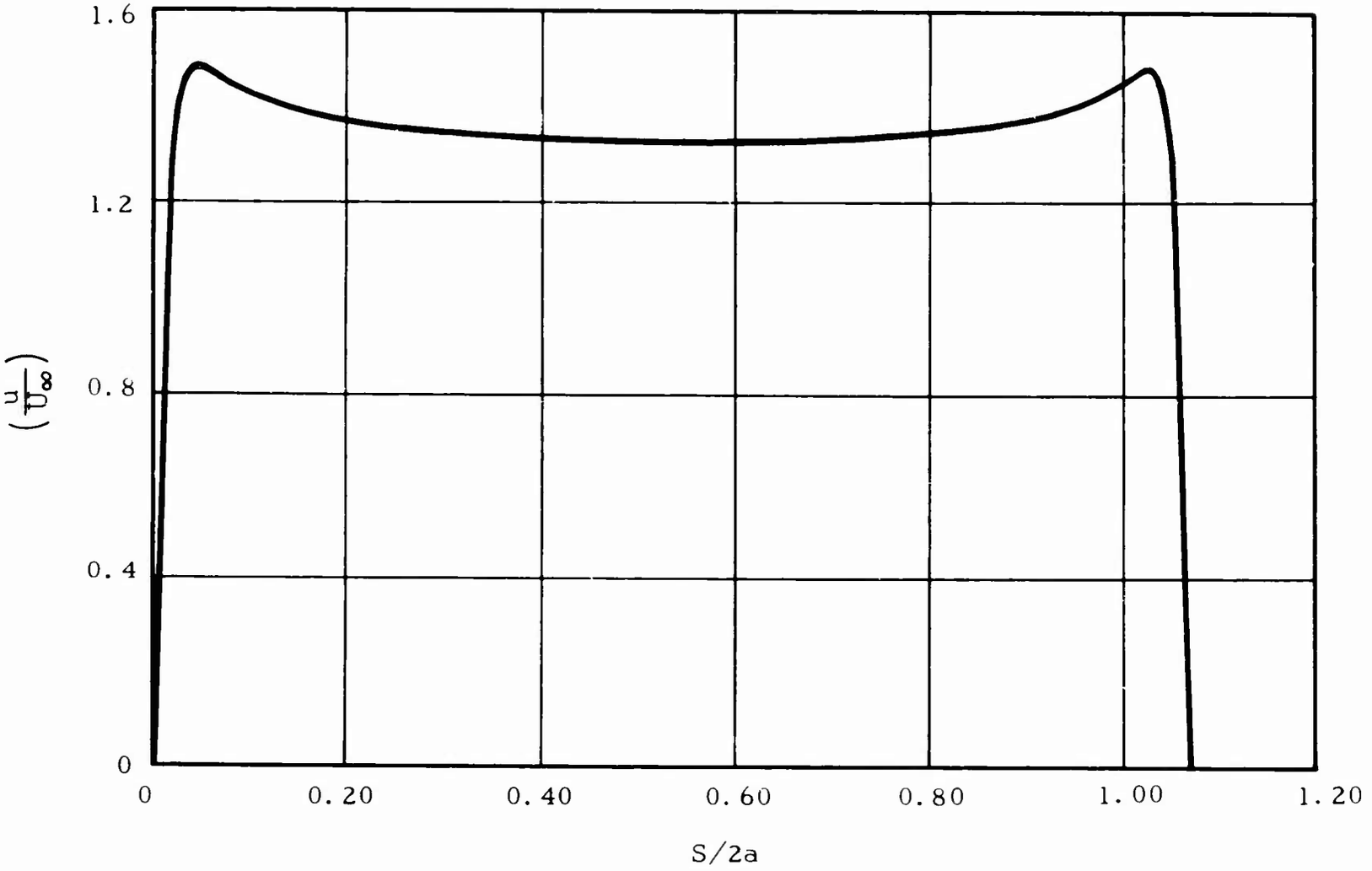

FIG. 5. VELOCITY DISTRIBUTION FOR ELLIPTICAL AIRFOIL OF 18-PERCENT-THICKNESS RATIO WITHOUT TRAILING EDGE JET (C_L = 1.0, $\theta = 30^\circ$).

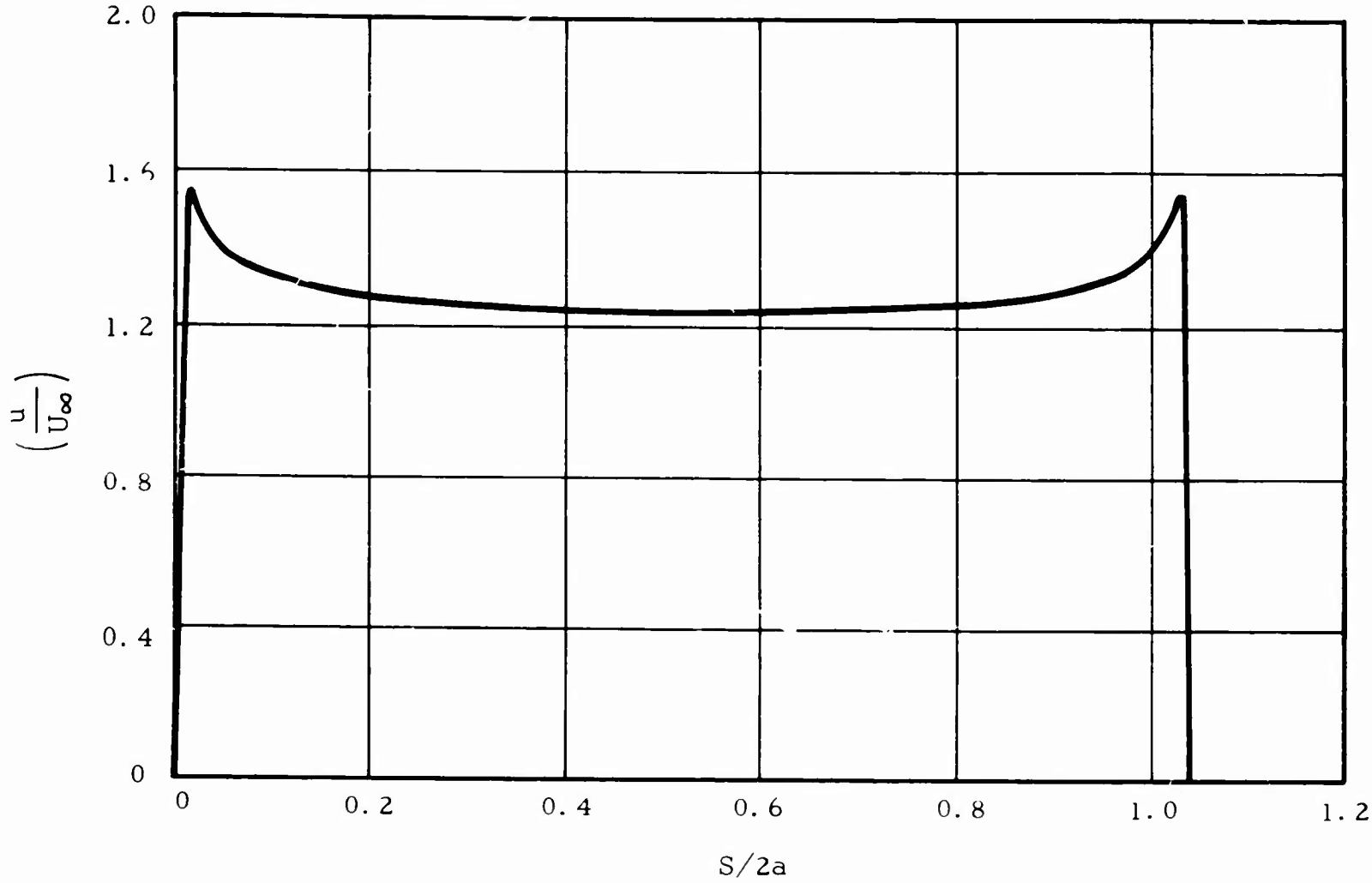

FIG. 6. VELOCITY DISTRIBUTION FOR ELLIPTICAL AIRFOIL OF 12-PERCENT-THICKNESS RATIO WITHOUT TRAILING EDGE JET (C_L = 0.75, θ = 40°).

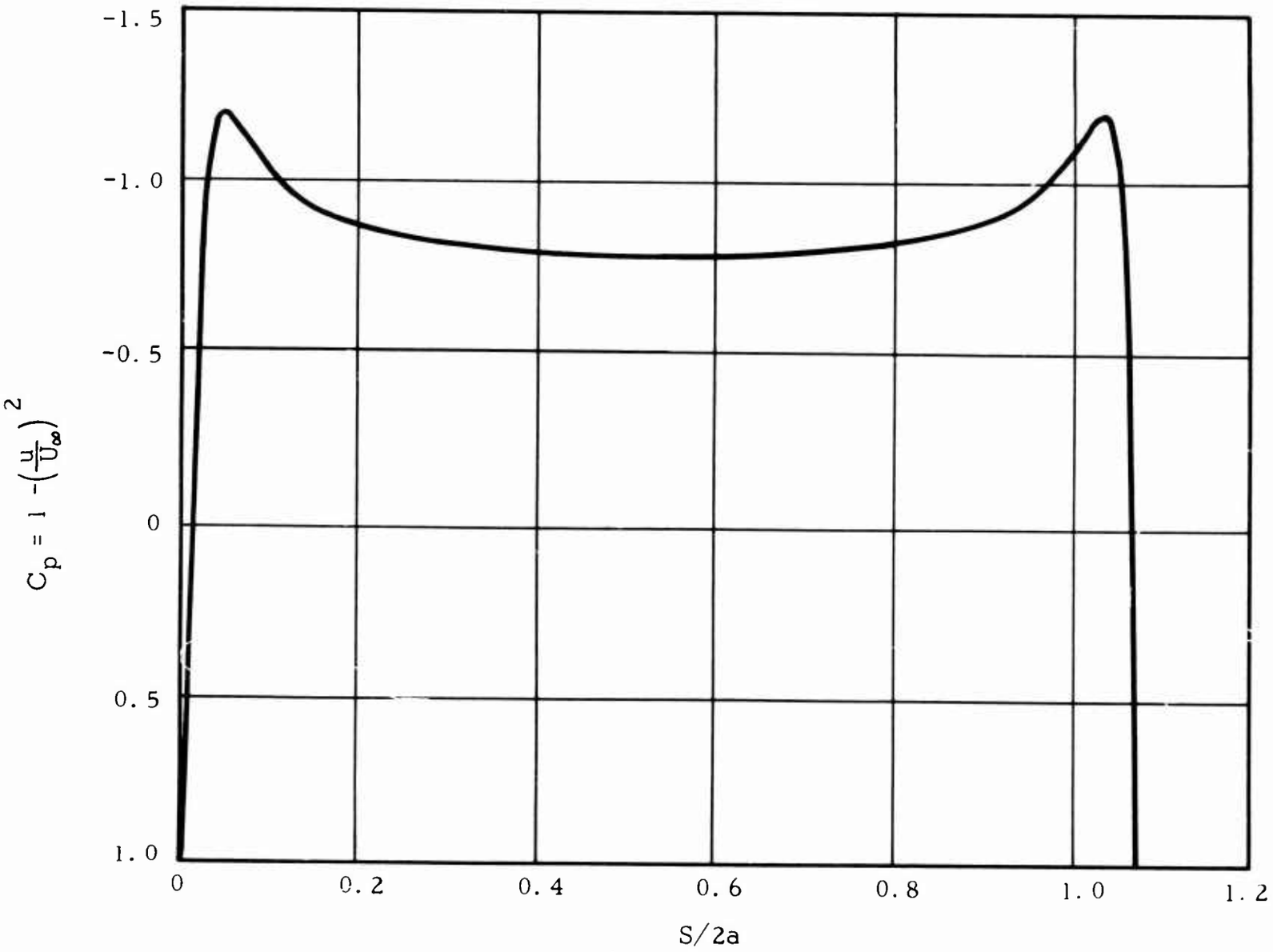

FIG. 7. PRESSURE DISTRIBUTION FOR ELLIPTICAL AIRFOIL OF 18-PERCENT-THICKNESS RATIO WITHOUT TRAILING EDGE JET (C_L = 1.0, $\theta = 30^\circ$).

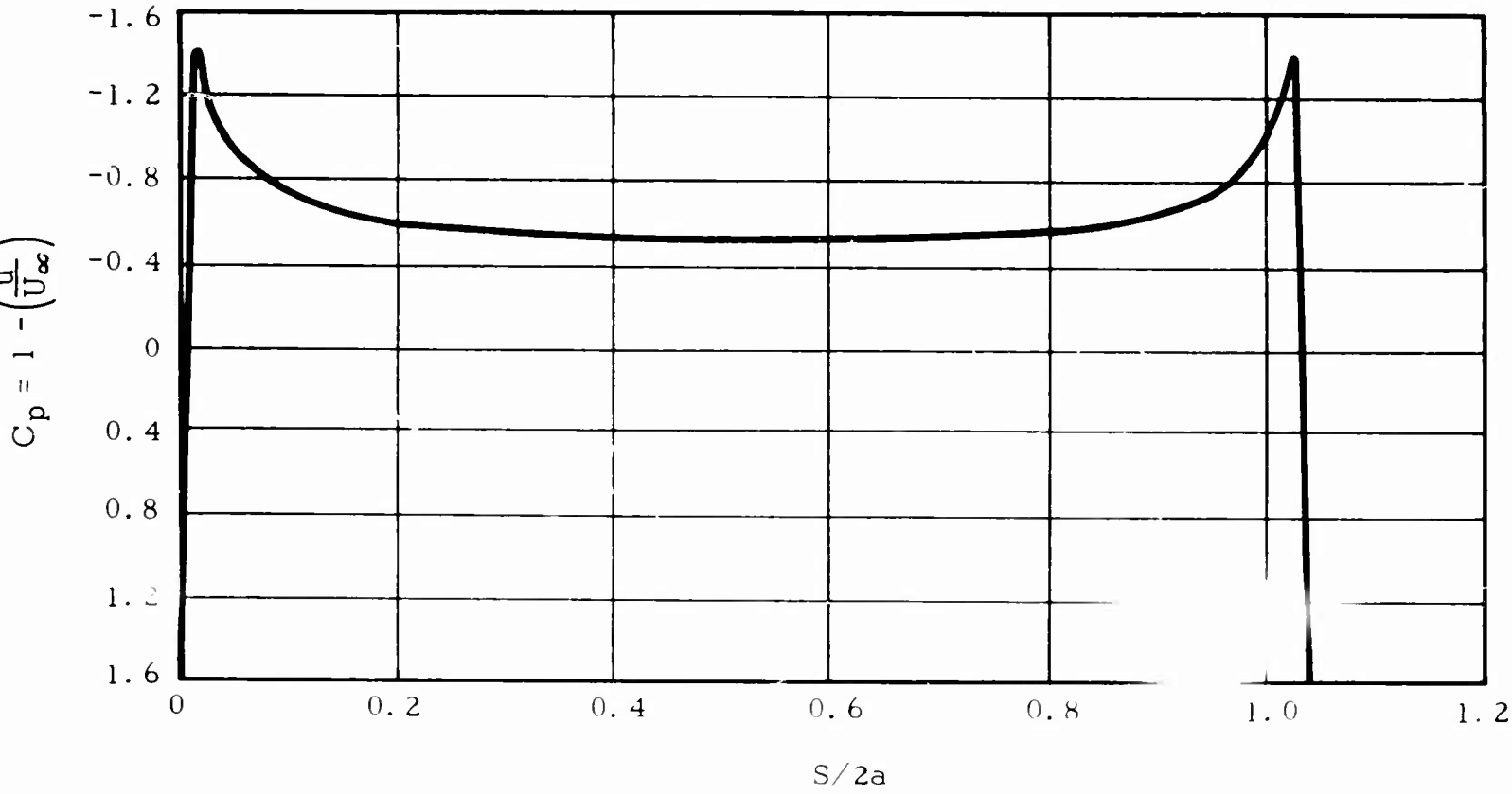

FIG. 8. PRESSURE DISTRIBUTION FOR ELLIPTICAL AIRFOIL OF 12-PERCENT-THICKNESS RATIO WITHOUT TRAILING EDGE JET ($C_L = 0.75$, $\theta = 40^\circ$).

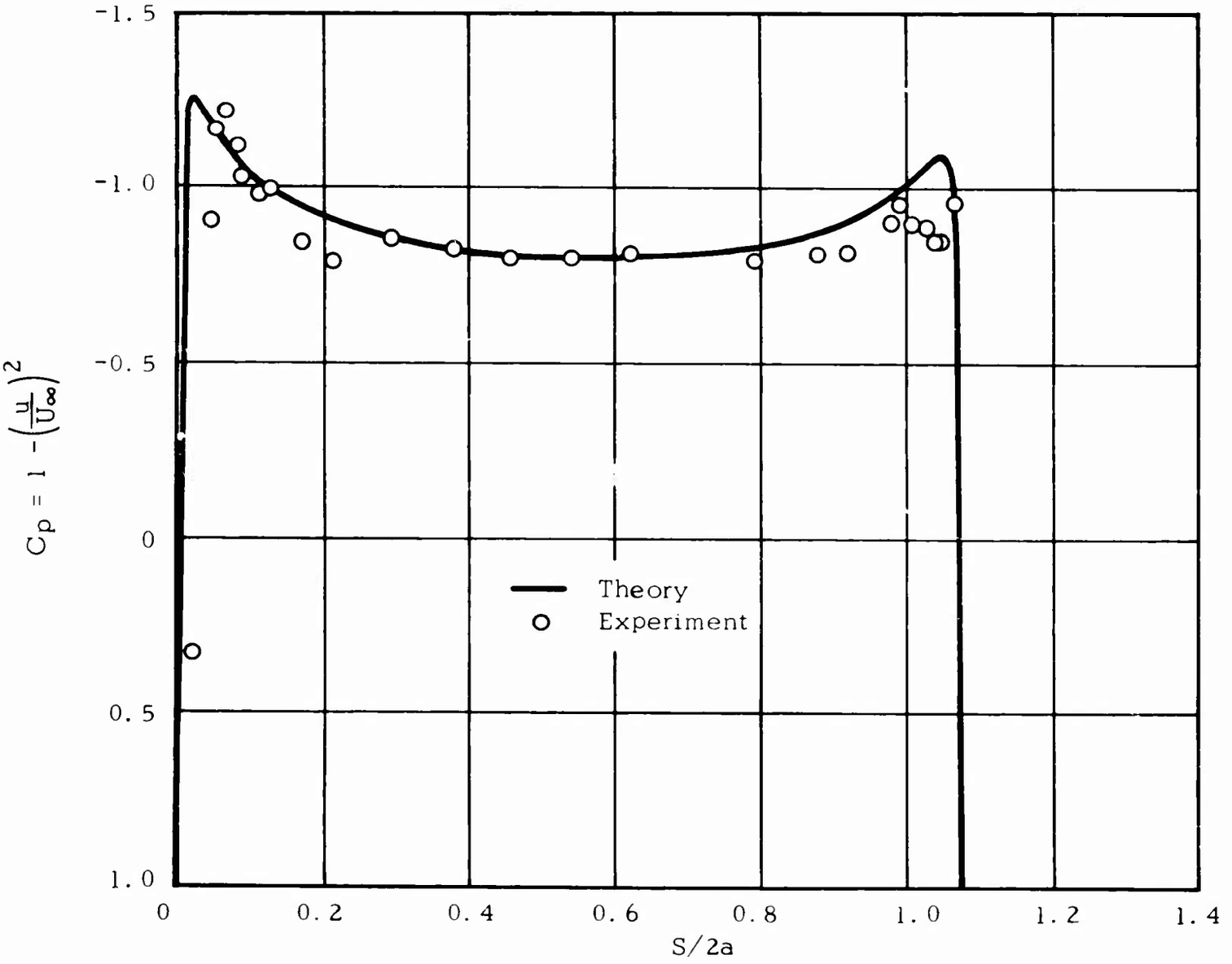

FIG. 9. PRESSURE DISTRIBUTION OF ELLIPTICAL AIRFOIL OF 18-PERCENT-THICKNESS RATIO WITH TRAILING EDGE JET (C_L = 1.1, C_J = 0.154, $\theta = 30^\circ$).

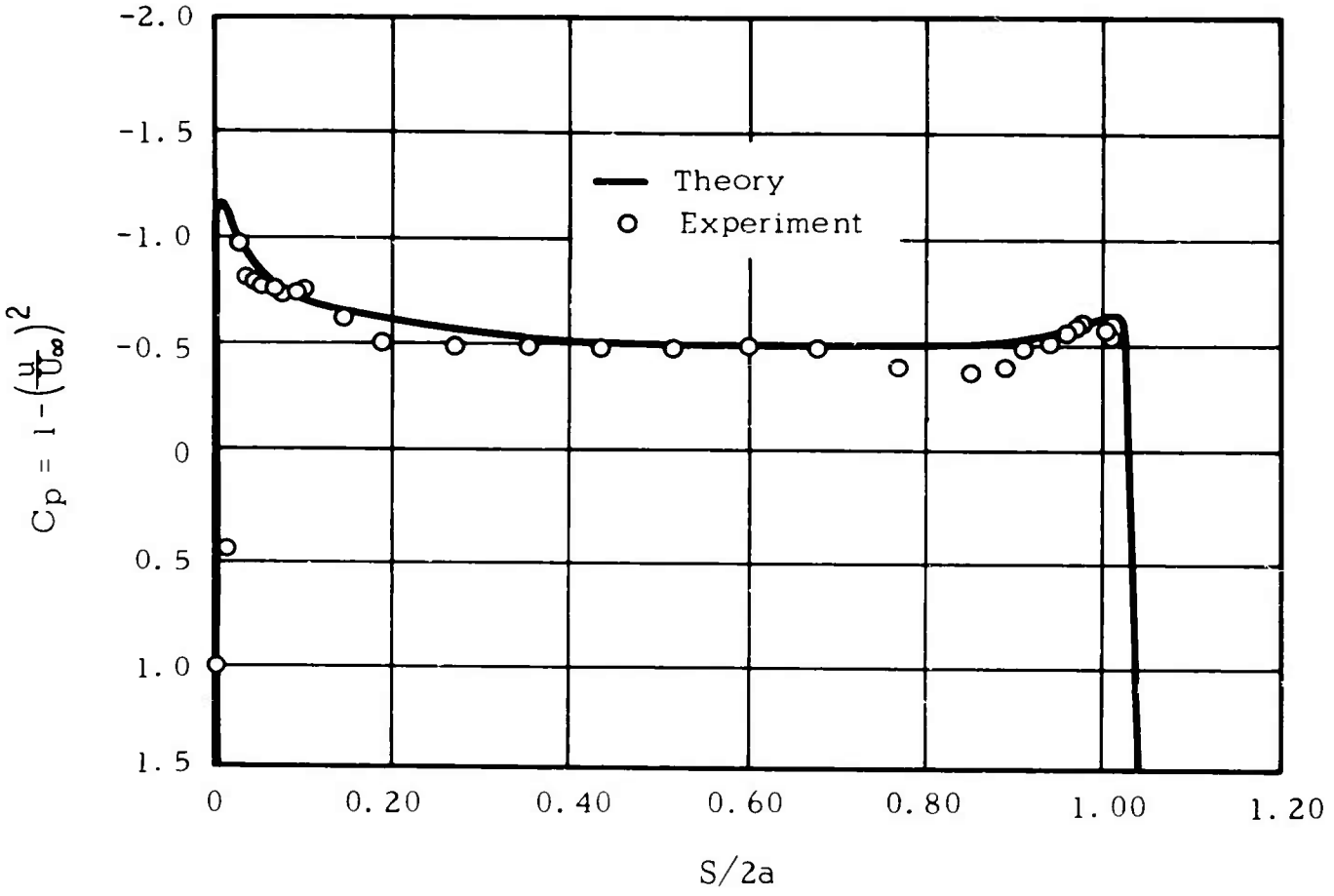

FIG. 10. PRESSURE DISTRIBUTION OF ELLIPTICAL AIRFOIL OF 12-PERCENT-THICKNESS RATIO WITH TRAILING EDGE JET ($C_L = 0.70$, $C_J = 0.084$, $\theta = 40^\circ$).

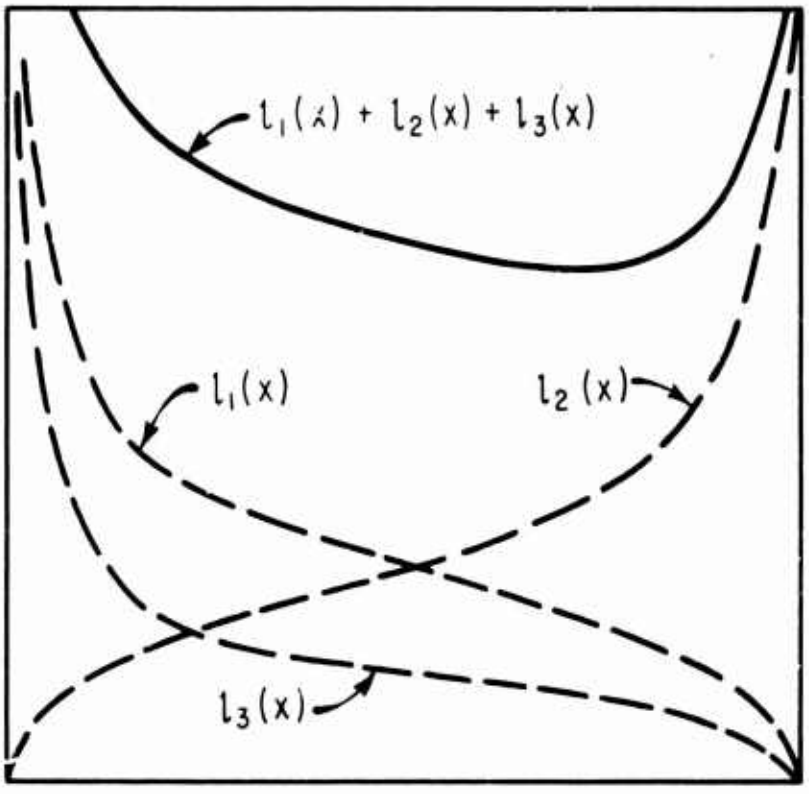

FIG. 11. FLAT-PLATE ASYMMETRICAL LOADING ($\alpha = 0$).

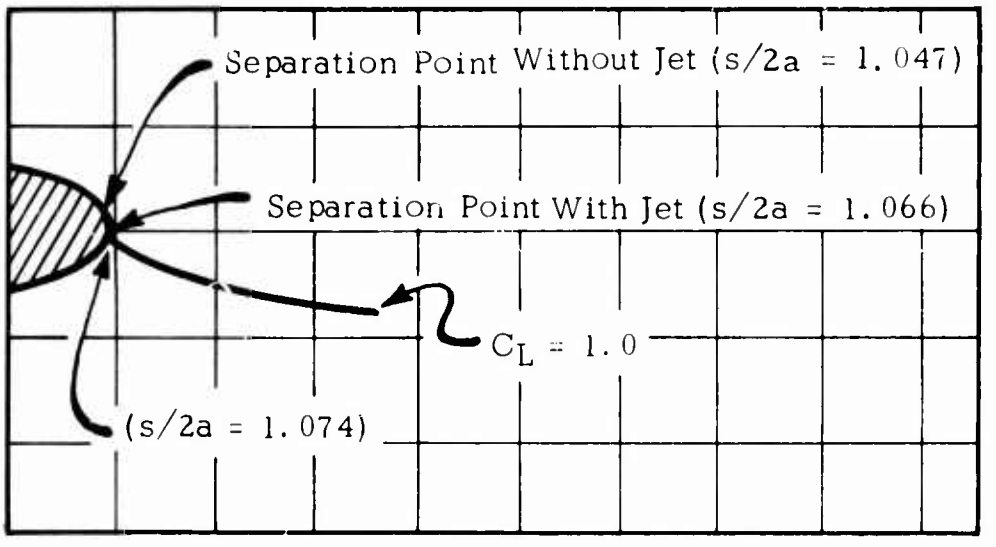

FIG. 12. LOCATION OF POINTS OF SEPARATION FOR ELLIPTICAL AIRFOIL OF 18-PERCENT-THICKNESS RATIO WITH AND WITHOUT TRAILING EDGE JET.

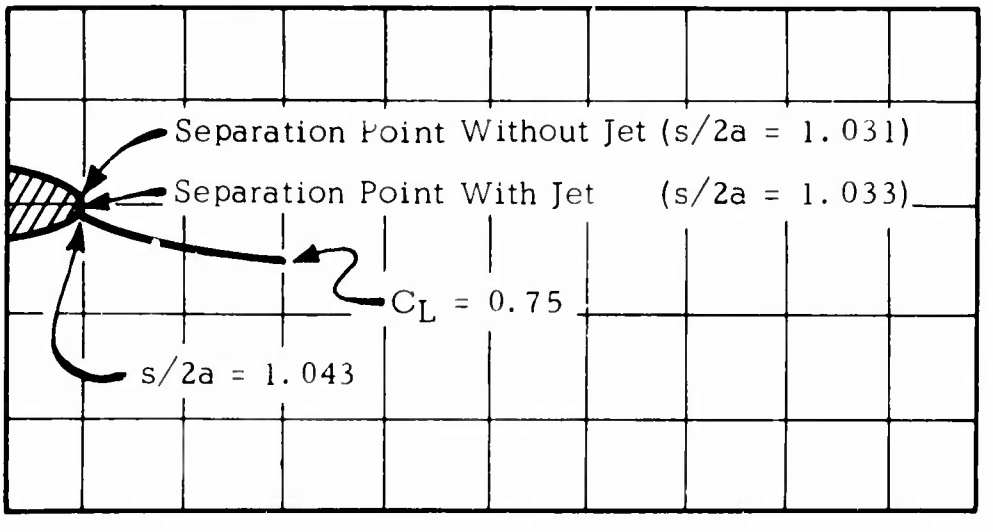

FIG. 13. LOCATION OF POINTS OF SEPARATION FOR ELLIPTICAL AIRFOIL OF 12-PERCENT-THICKNESS RATIO WITH AND WITHOUT TRAILING EDGE JET.

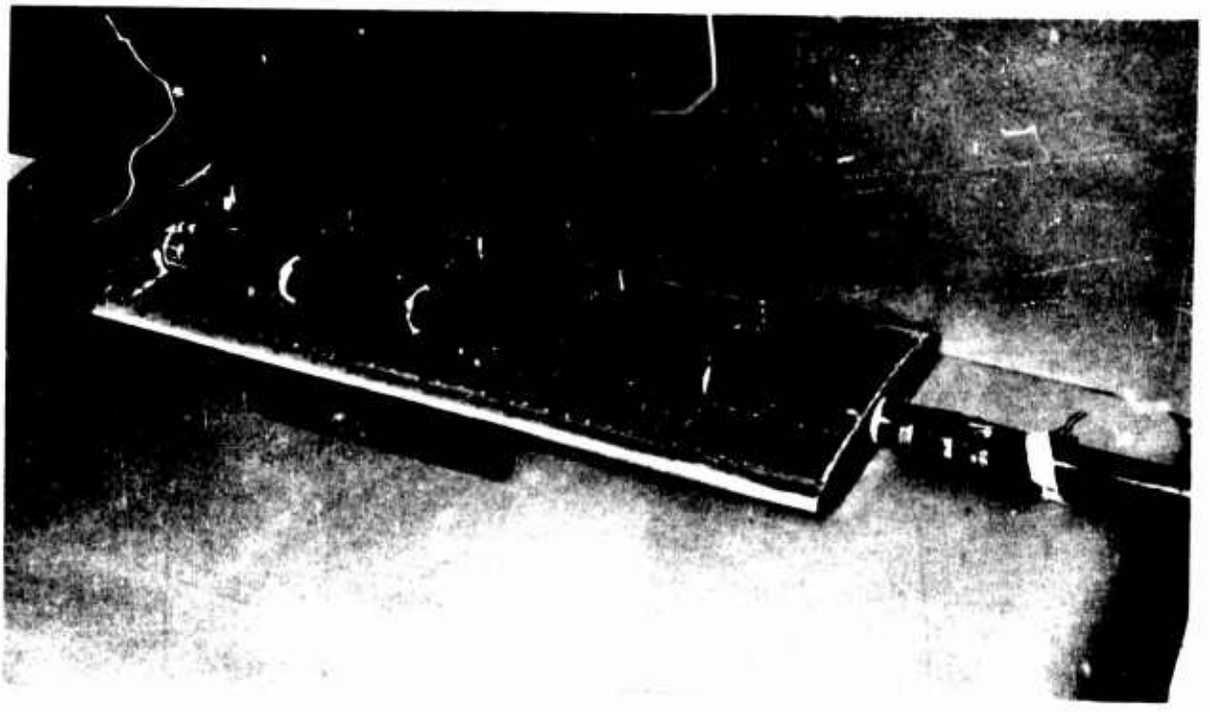

FIG. 14. GENERAL VIEW OF THE 18-PERCENT MODEL ARRANGEMENT.

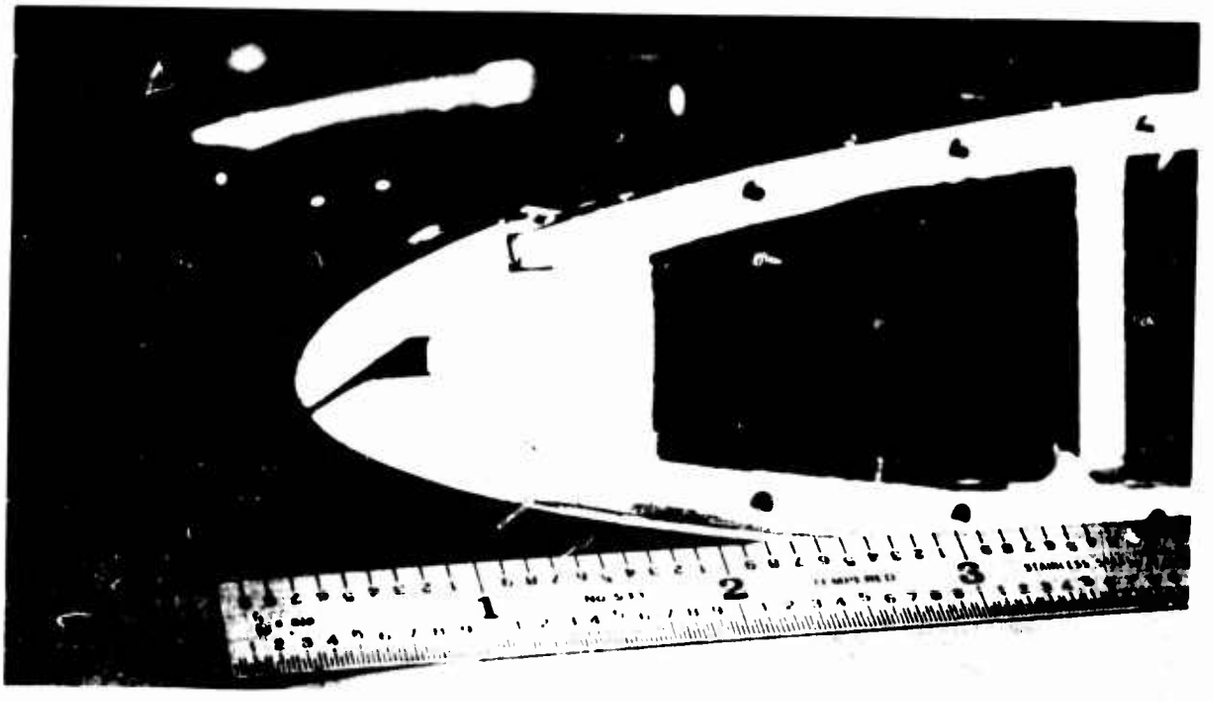

FIG. 15. JET SLOT CONFIGURATION FOR THE 18-PERCENT MODEL.

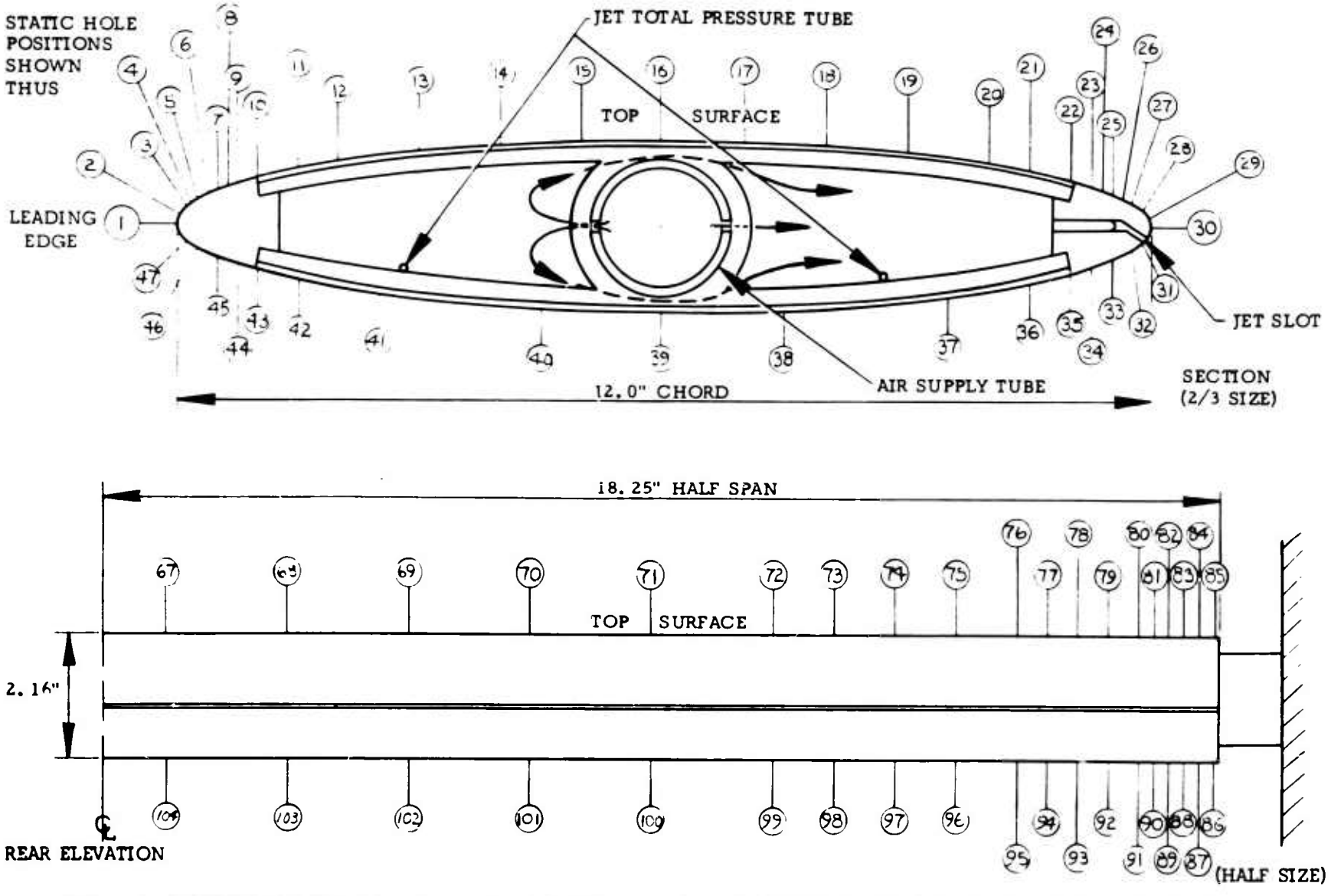

FIG. 16. SECTION OF MODEL SHOWING LOCATIONS OF THE STATIC PRESSURE TAPS (18-PERCENT-THICKNESS RATIO).

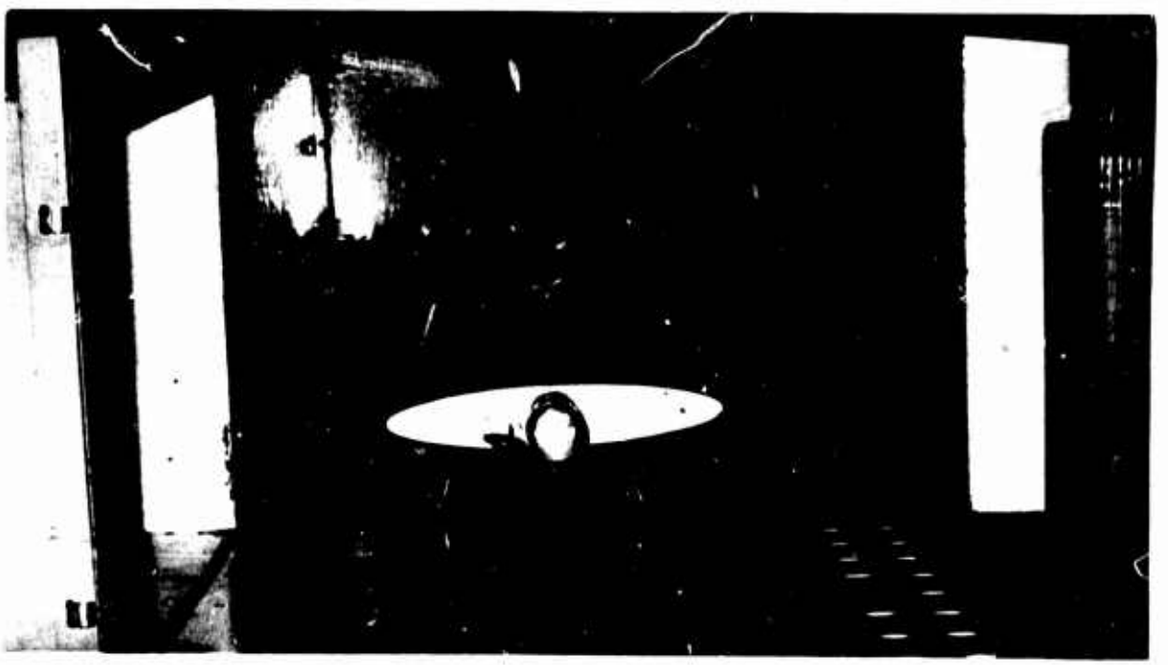

FIG. 17. MODEL MOUNTING IN THE TEST SECTION.

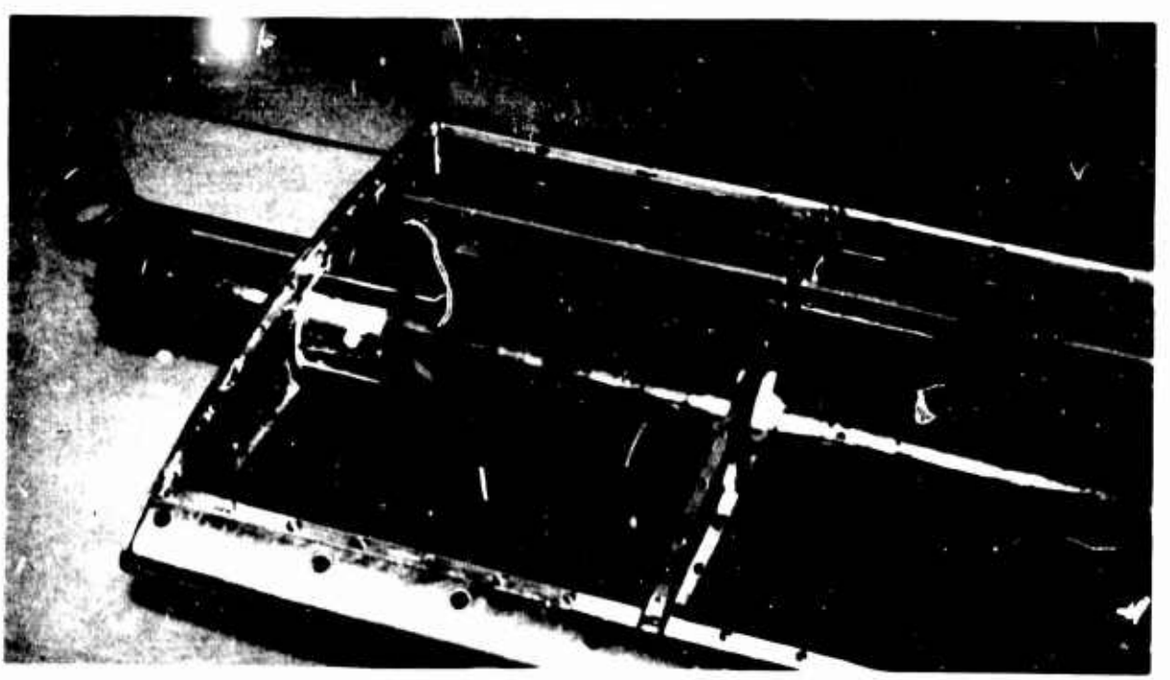

FIG. 18. MULTIPLE-GATE TYPE VALVE FOR CONTROLLING THE FRONT JET OF 18-PERCENT MODEL.

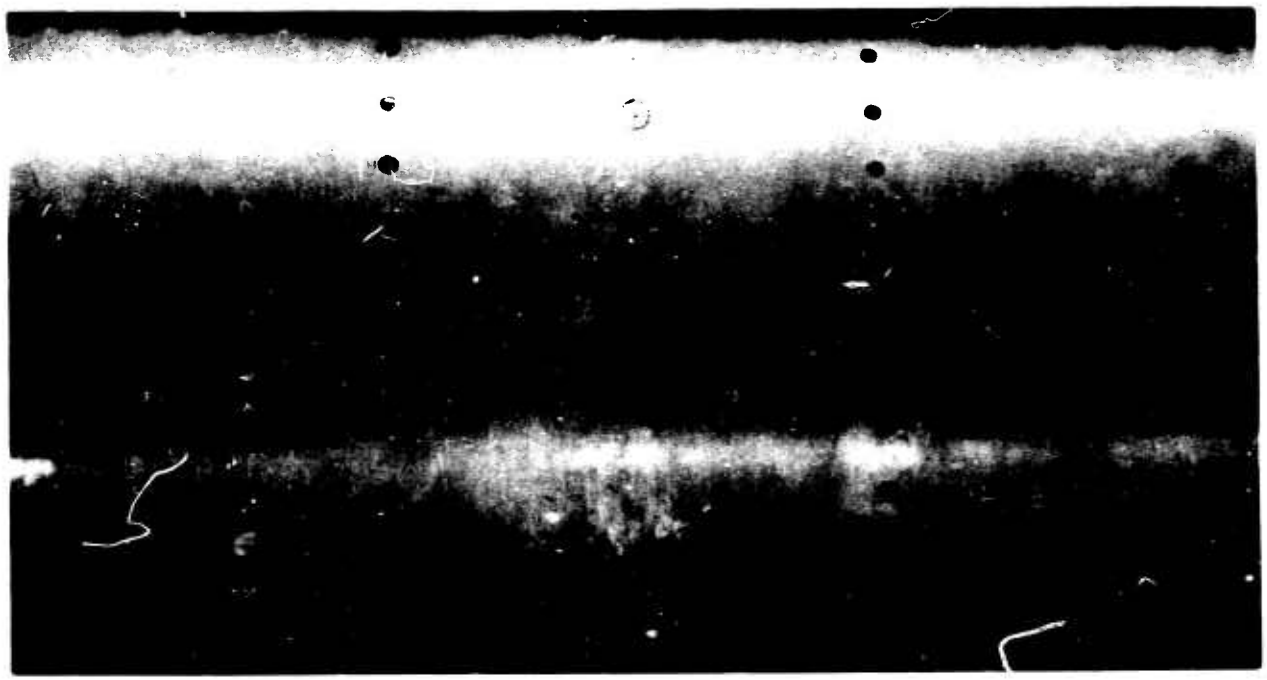

FIG. 19. THE MODEL EXTERIOR SHOWING THE PRESSURE TAPS.

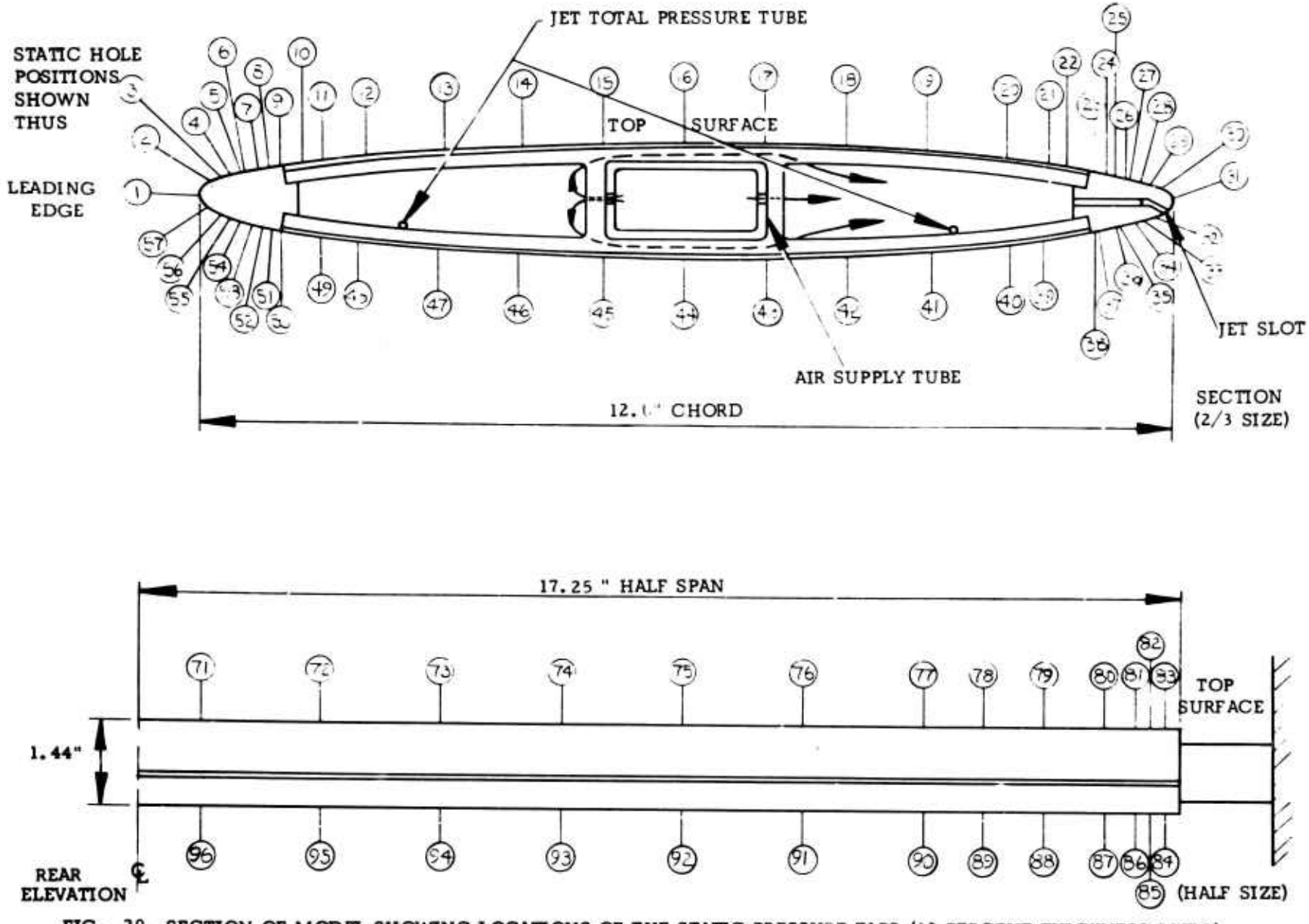

FIG. 20. SECTION OF MODEL SHOWING LOCATIONS OF THE STATIC PRESSURE TAPS (12-PERCENT-THICKNESS RATIO).

FIG. 21. AIR SUPPLY SYSTEM.

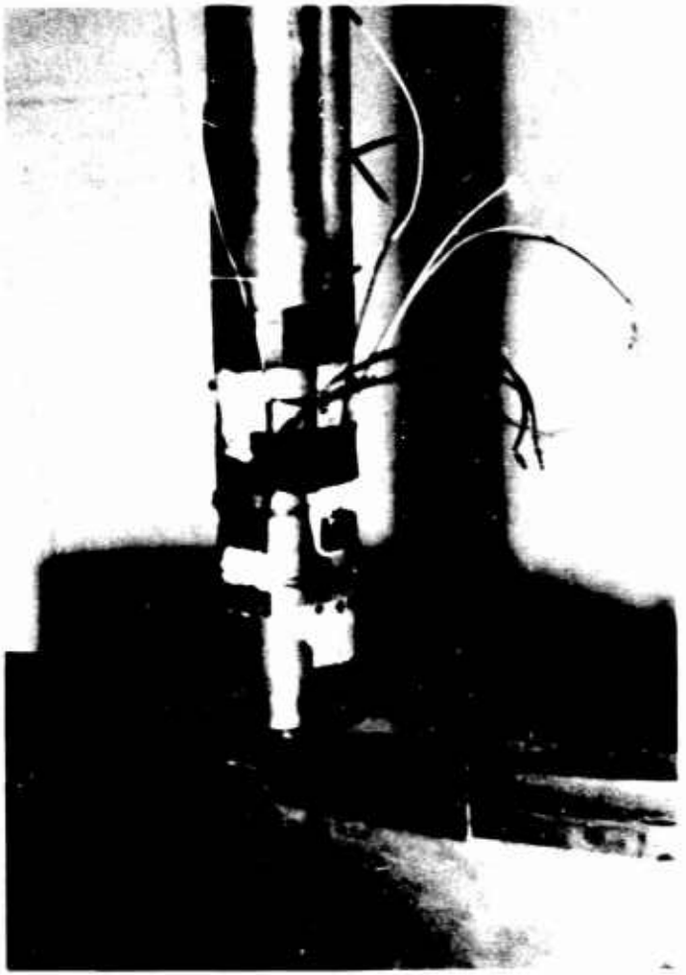

FIG. 22. FORCE AND MOMENT STRAIN GAGES.

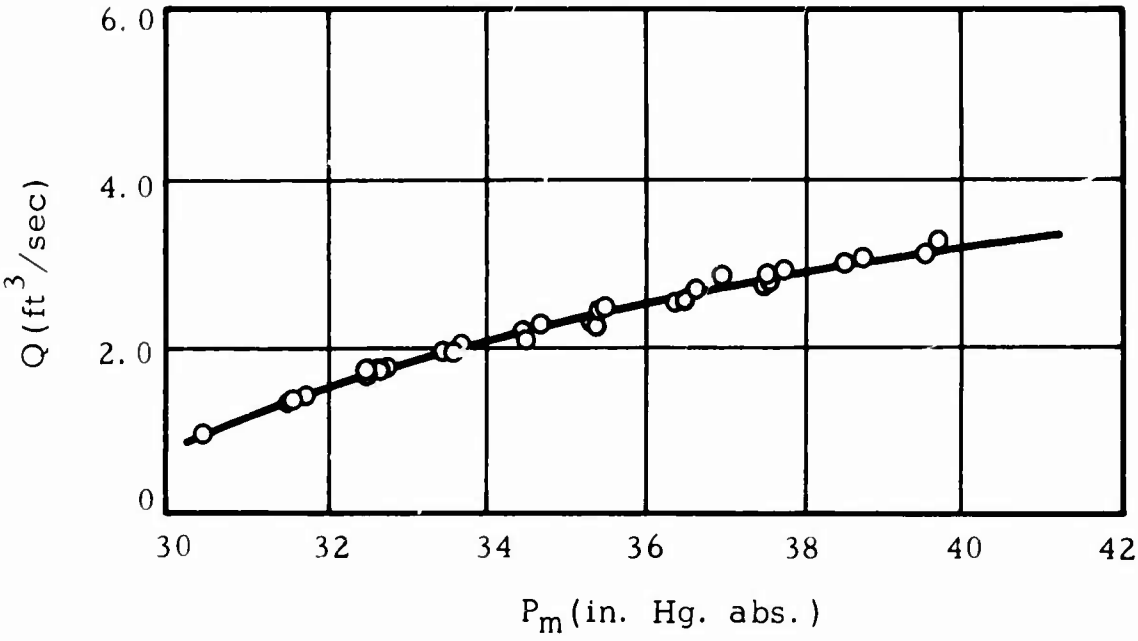

FIG. 23. VOLUME FLOW RATE VERSUS THE PLENUM PRESSURE OF THE MODEL (18-PERCENT MODEL).

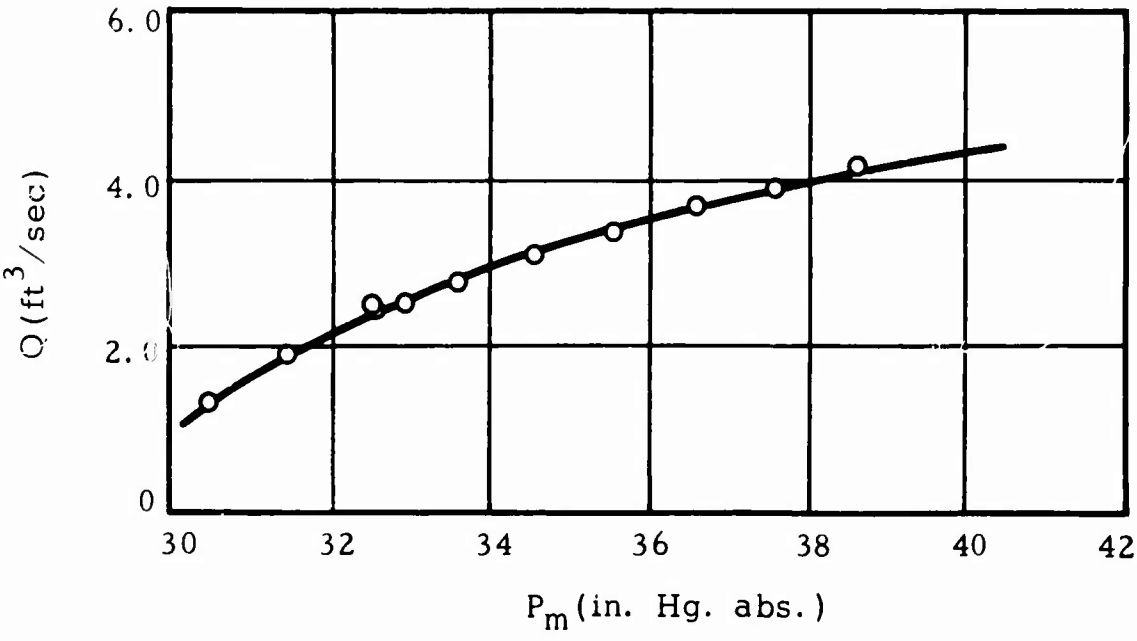

FIG. 24. VOLUME FLOW RATE VERSUS THE PLENUM PRESSURE OF THE MODEL (12-PERCENT MODEL).

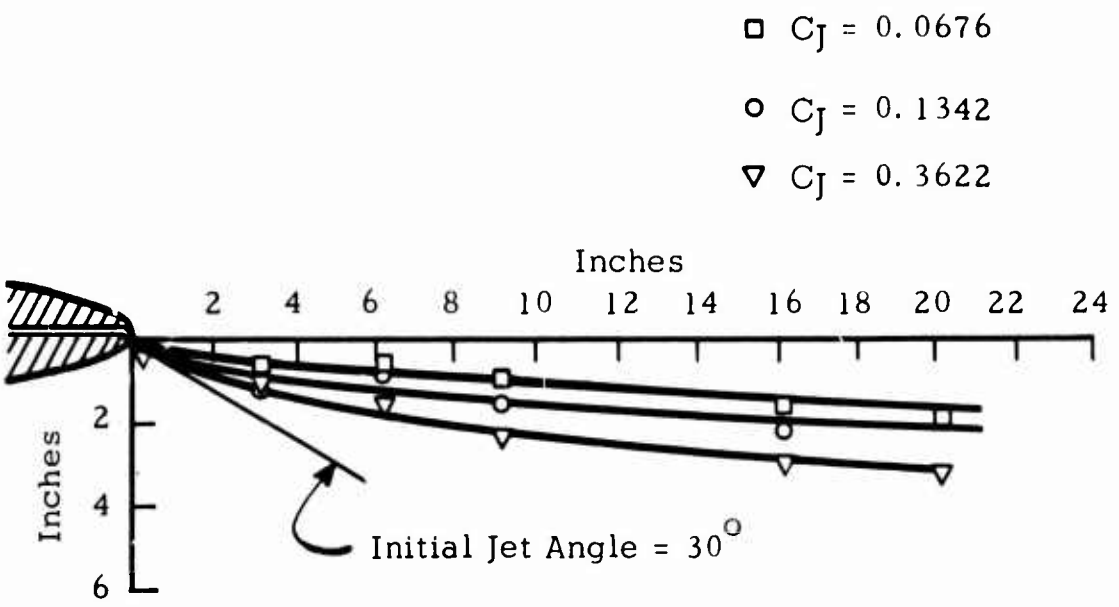

FIG. 25. JET PATH FOR THE ELLIPTICAL AIRFOIL OF 18-PERCENT-THICKNESS RATIO ($\theta = 30^{\circ}$, $\alpha = 0$).

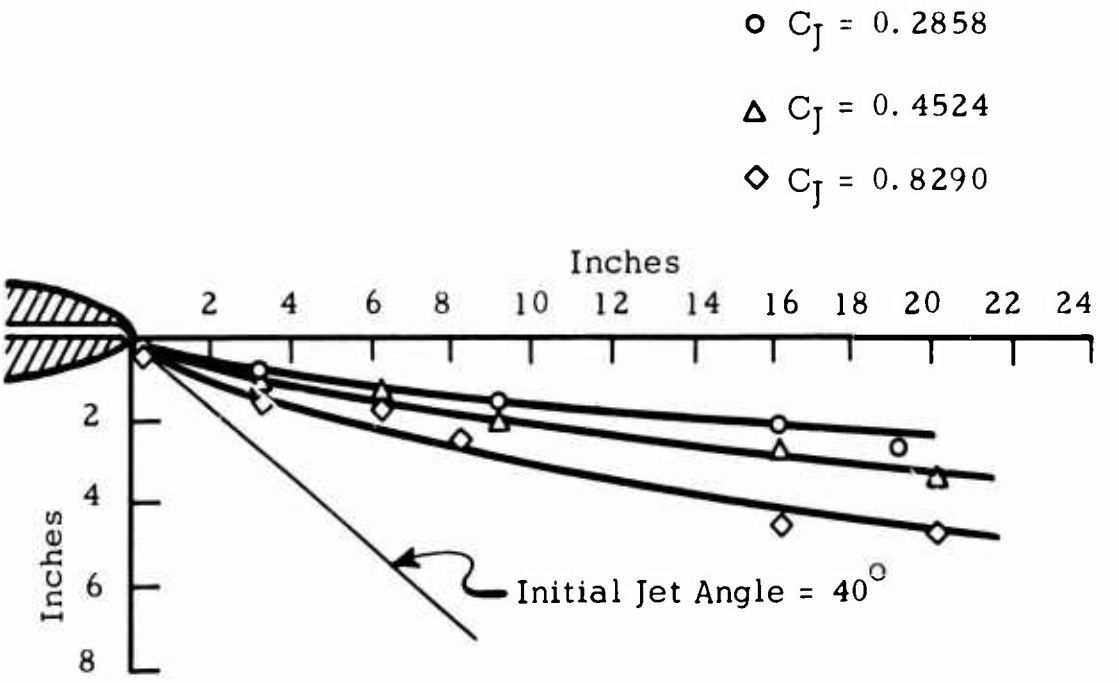

FIG. 26. JET PATH FOR THE ELLIPTICAL AIRFOIL OF 12-PERCENT-THICKNESS RATIO ($\theta = 40^{\circ}$, $\alpha = 0$).

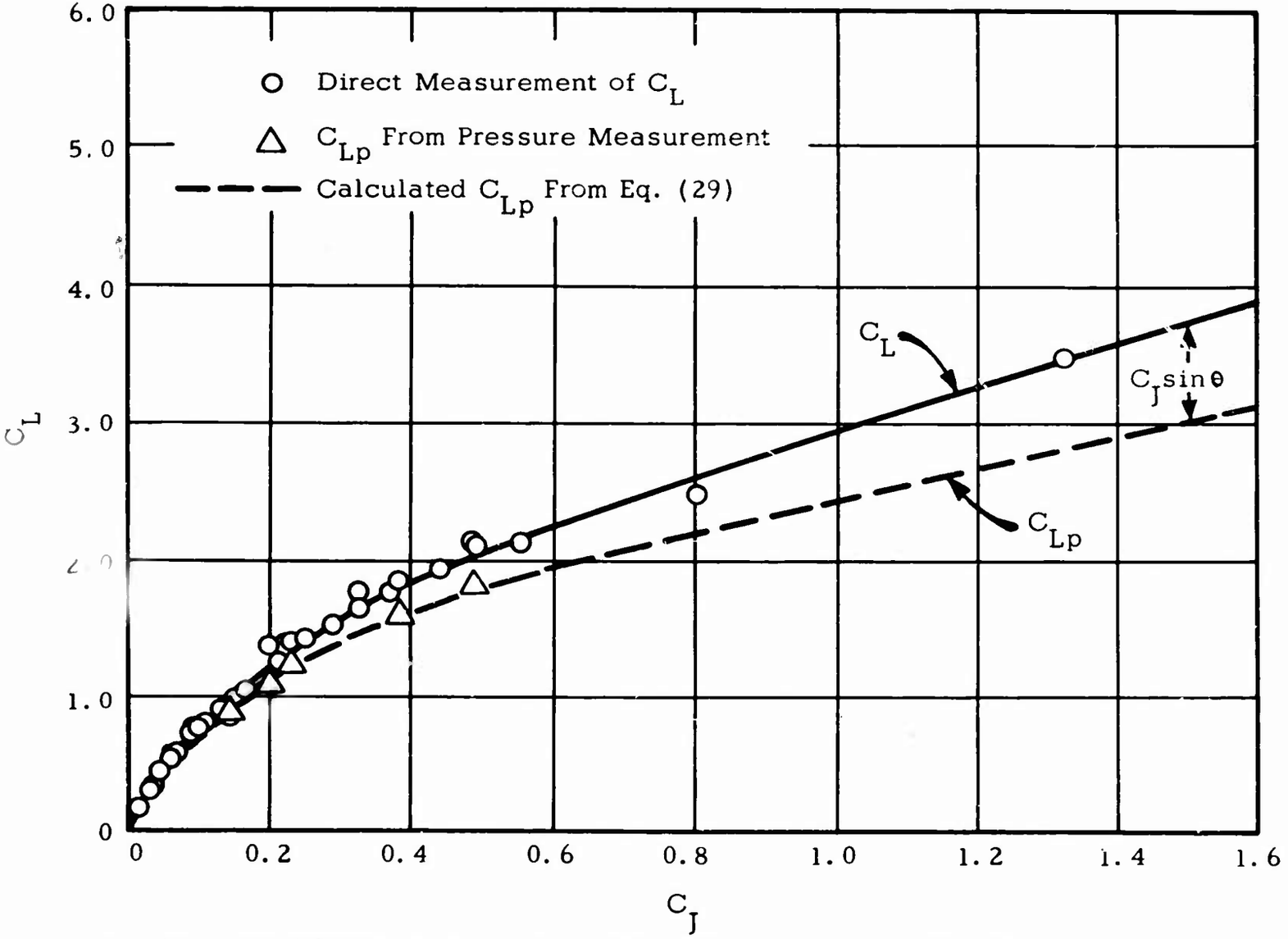

FIG. 27. LIFT COEFFICIENT VERSUS JET COEFFICIENT FOR ELLIPTICAL AIRFOIL OF 18-PERCENT-THICKNESS RATIO ($\theta = 30^{\circ}$, $\alpha = 0$).

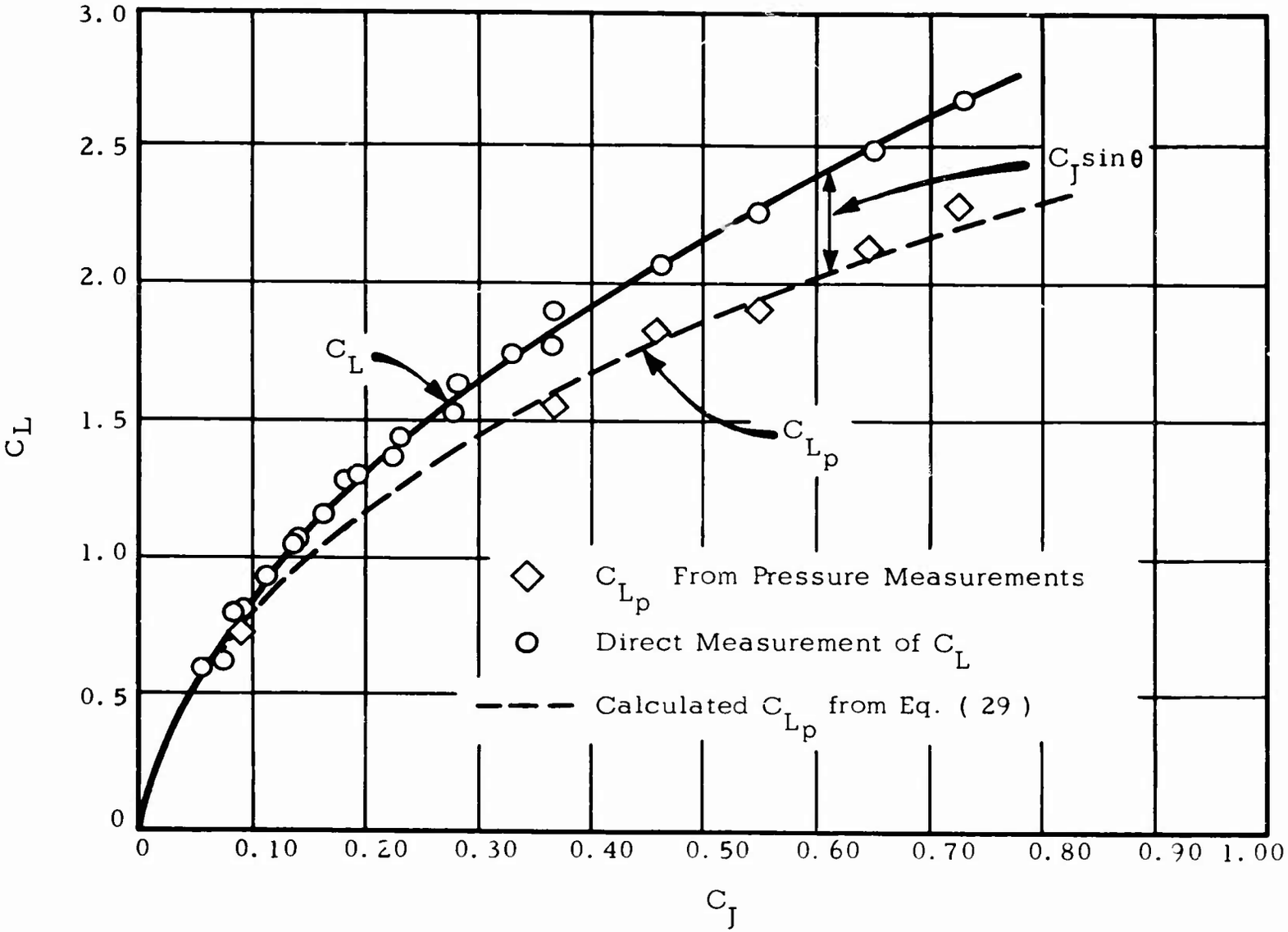

FIG. 28. LIFT COEFFICIENT VERSUS JET COEFFICIENT FOR ELLIPTICAL AIRFOIL OF 12-PERCENT-THICKNESS RATIO ($\theta = 40^{\circ}$, $\alpha = 0$).

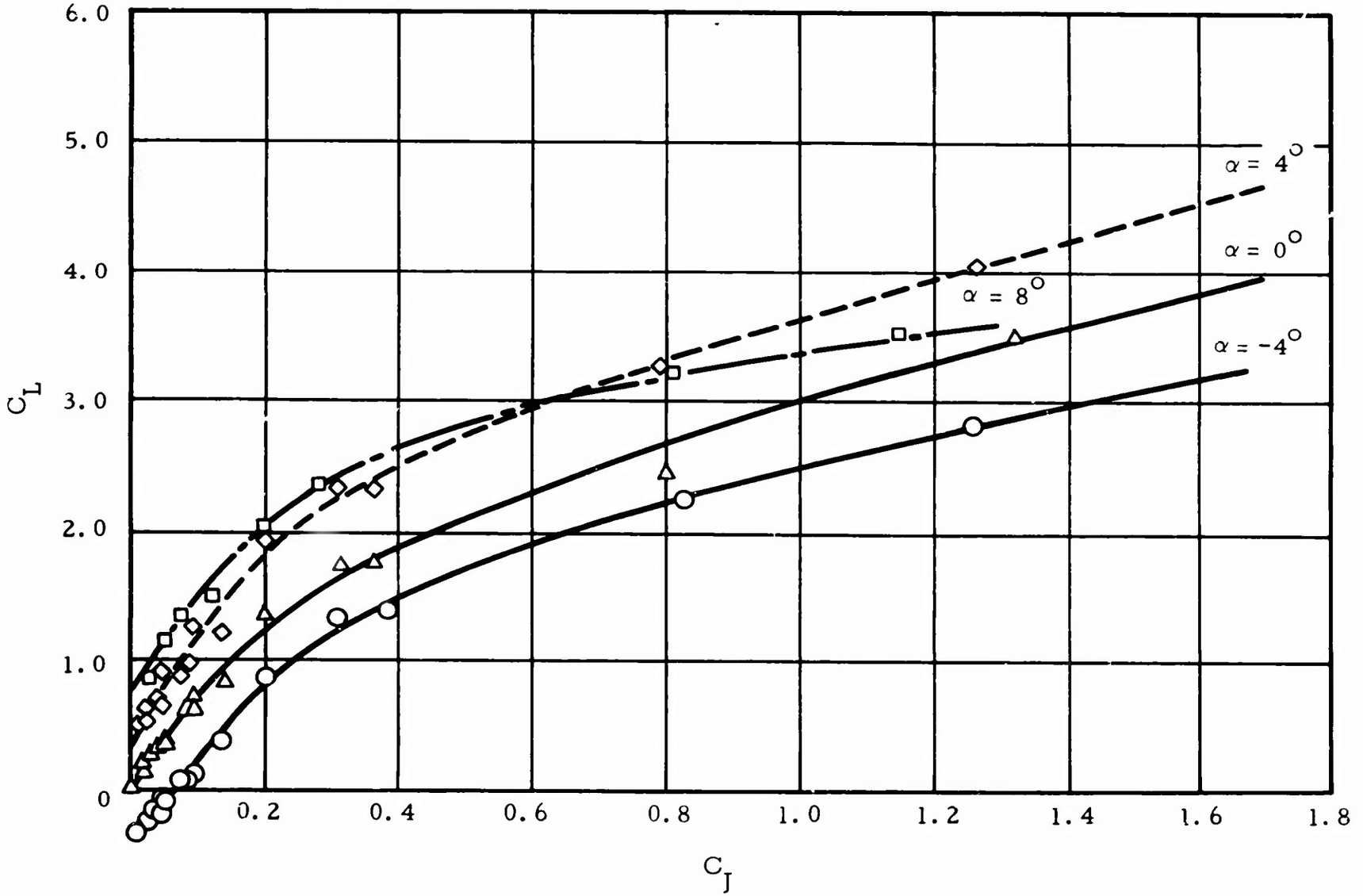

FIG. 29. TOTAL LIFT COEFFICIENT VERSUS THE JET COEFFICIENT AT VARIOUS ANGLES OF ATTACK ($\frac{b}{a}$ = 18%).

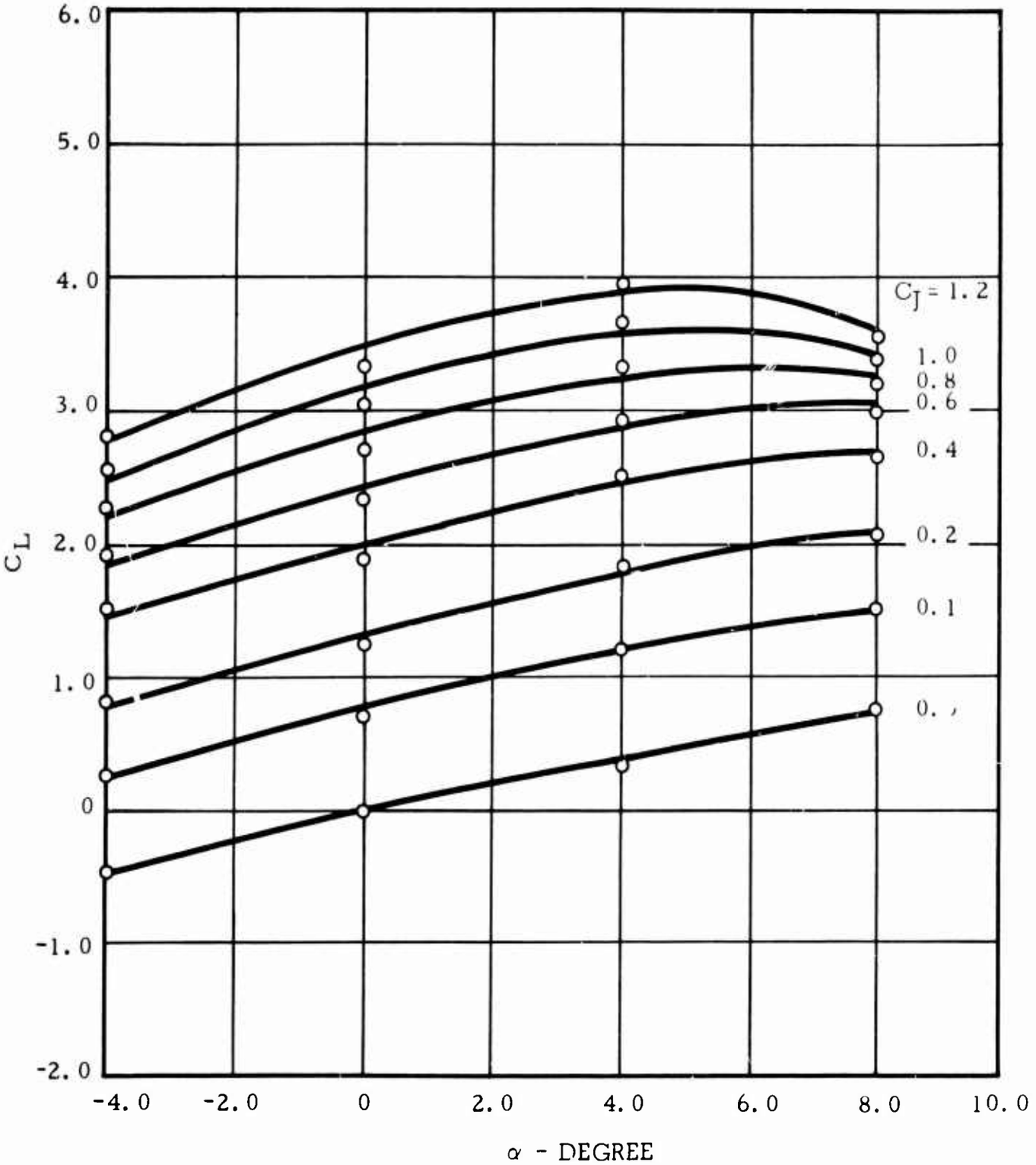

FIG. 30. TOTAL LIFT COEFFICIENT VERSUS ANGLE OF ATTACK AT VARIOUS VALUES OF C_J ($\frac{b}{a}$ = 18%).

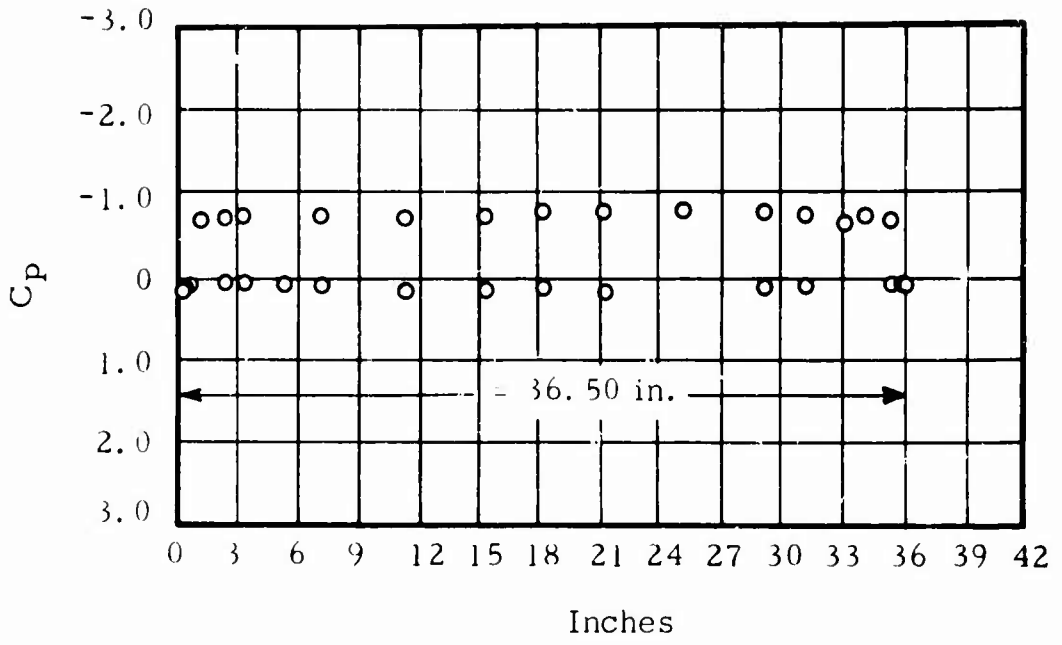

FIG. 31. PRESSURE DISTRIBUTION IN THE SPANWISE DIRECTION FOR THE ELLIPTICAL AIRFOIL OF 18-PERCENT-THICKNESS RATIO (C_J = 0.154).

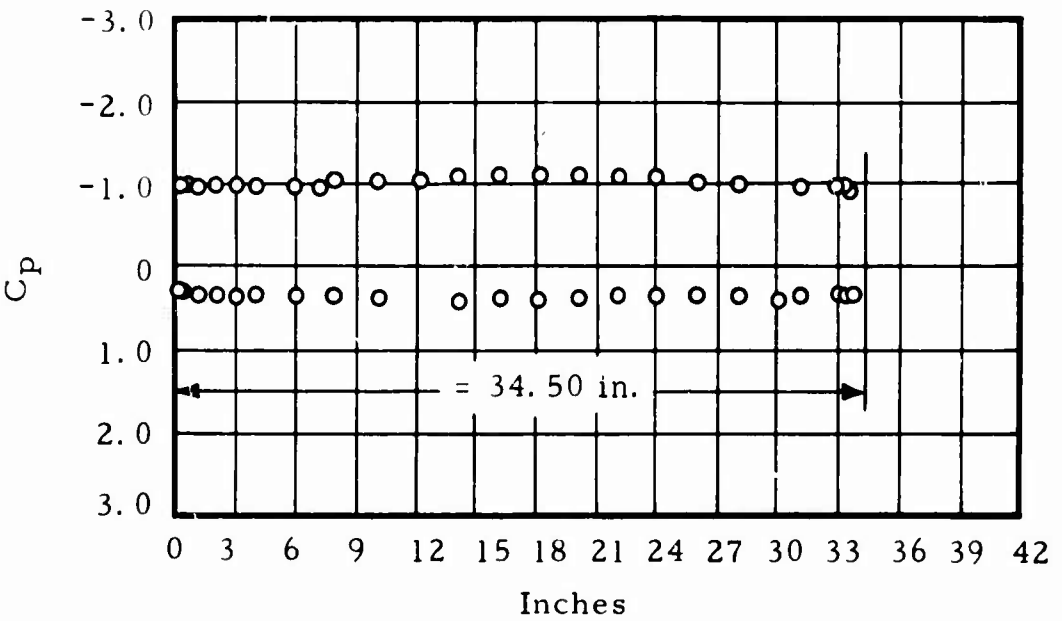

FIG. 32. PRESSURE DISTRIBUTION IN THE SPANWISE DIRECTION FOR THE ELLIPTICAL AIRFOIL OF 12-PERCENT-THICKNESS RATIO (C_J = 0.461).

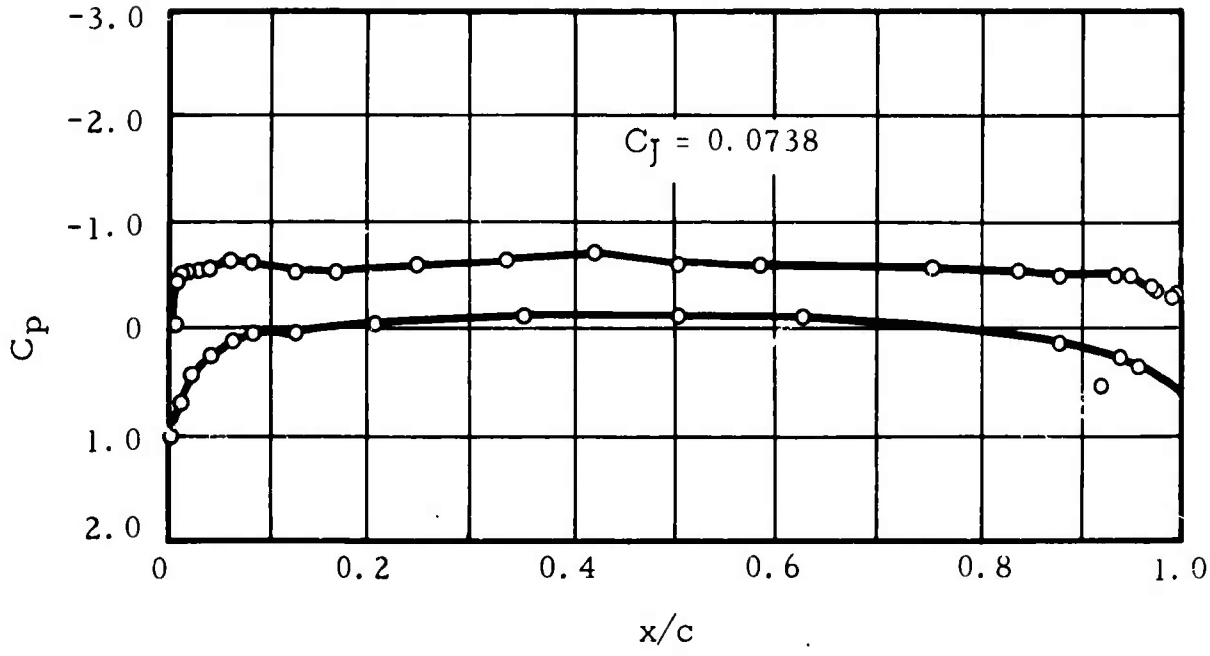

FIG. 33a. PRESSURE DISTRIBUTION IN THE CHORDWISE DIRECTION FOR THE ELLIPTICAL AIRFOIL OF 18-PERCENT-THICKNESS RATIO.

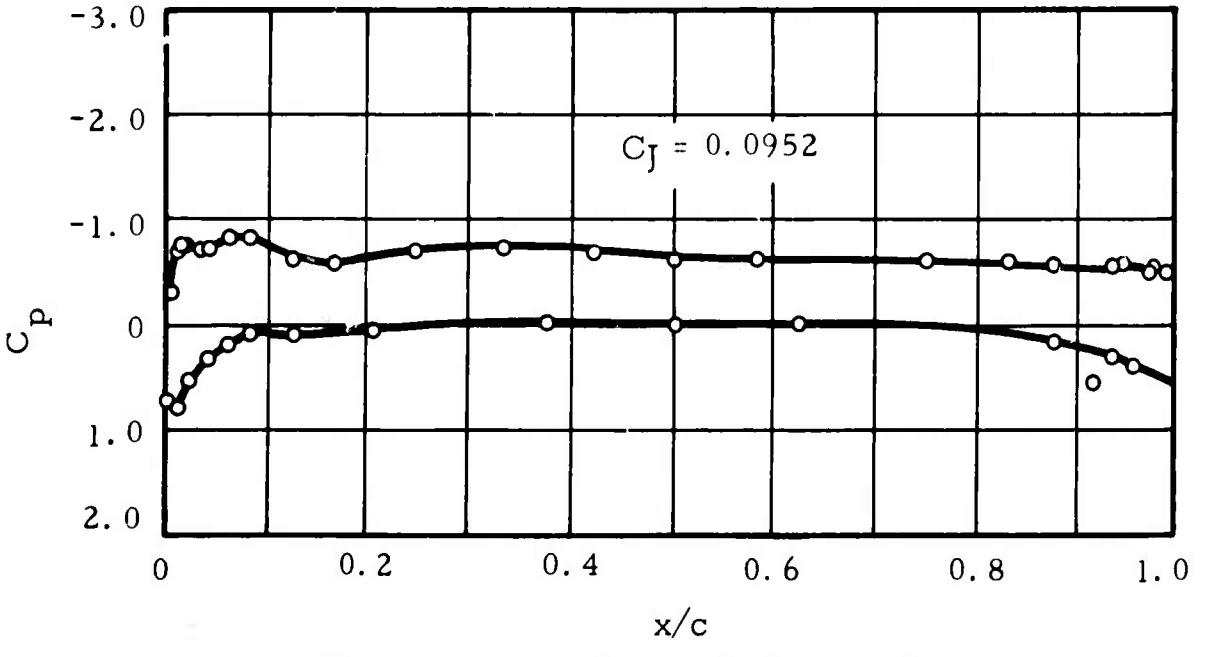

FIG. 33b. PRESSURE DISTRIBUTION IN THE CHORDWISE DIRECTION FOR THE ELLIPTICAL AIRFOIL OF 18-PERCENT-THICKNESS RATIO.

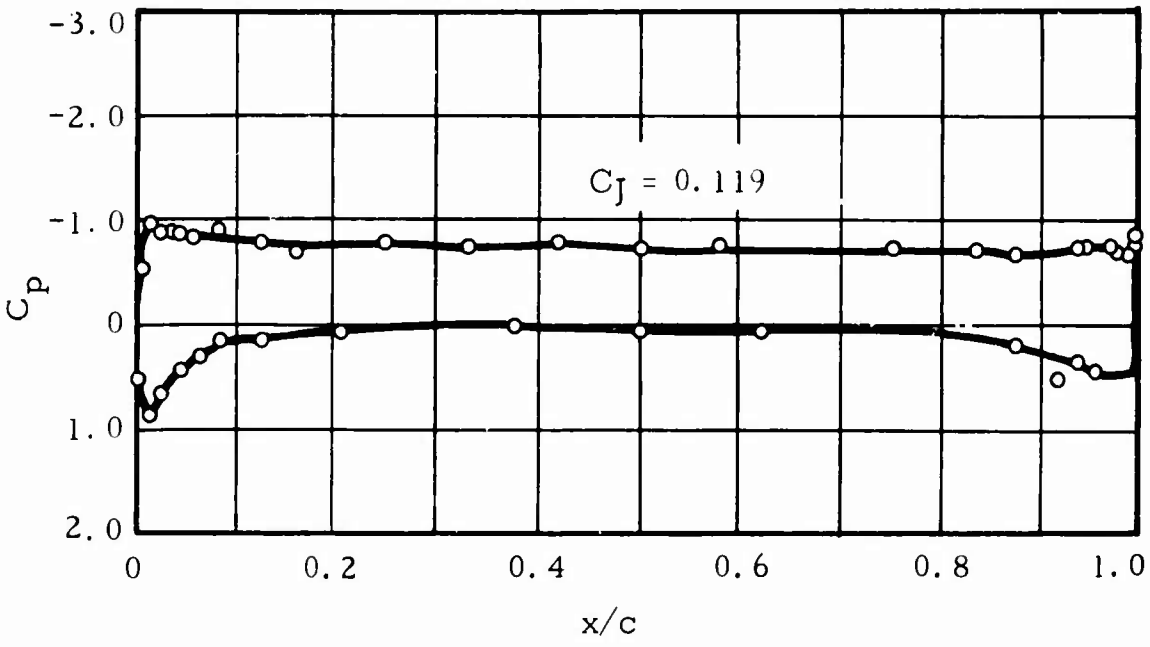

FIG. 33c. PRESSURE DISTRIBUTION IN THE CHORDWISE DIRECTION FOR THE ELLIPTICAL AIRFOIL OF 18-PERCENT-THICKNESS RATIO.

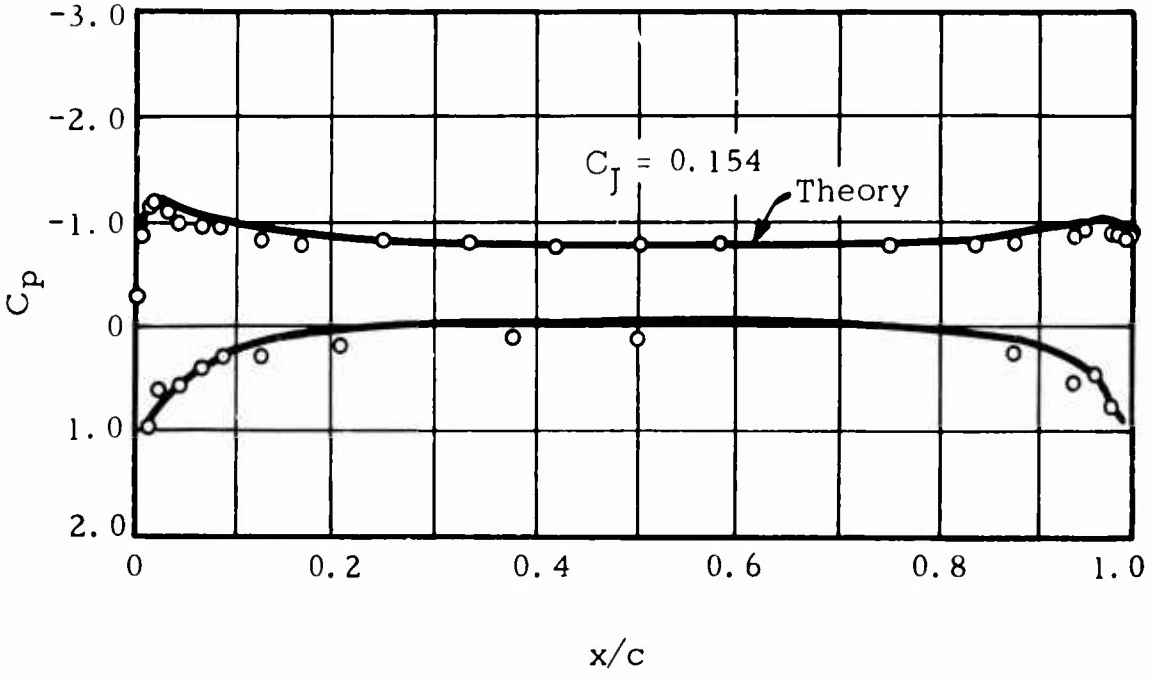

FIG. 33d. PRESSURE DISTRIBUTION IN THE CHORDWISE DIRECTION FOR THE ELLIPTICAL AIRFOIL OF 18-PERCENT-THICKNESS RATIO.

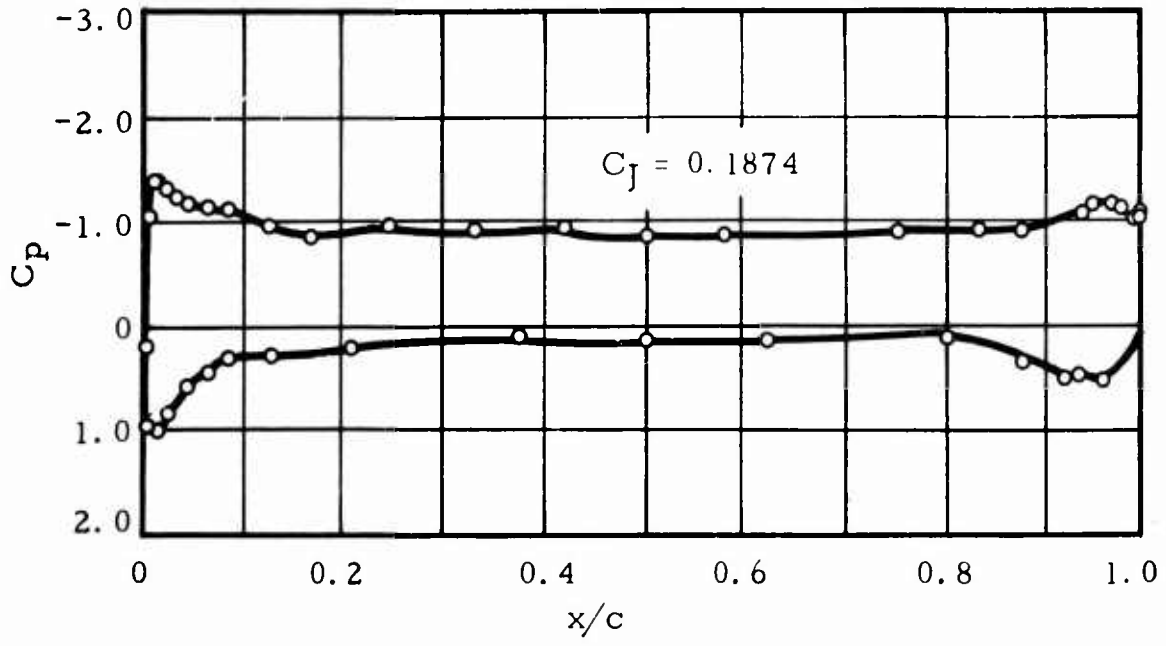

FIG. 33e. PRESSURE DISTRIBUTION IN THE CHORDWISE DIRECTION FOR THE ELLIPTICAL AIRFOIL OF 18-PERCENT-THICKNESS RATIO.

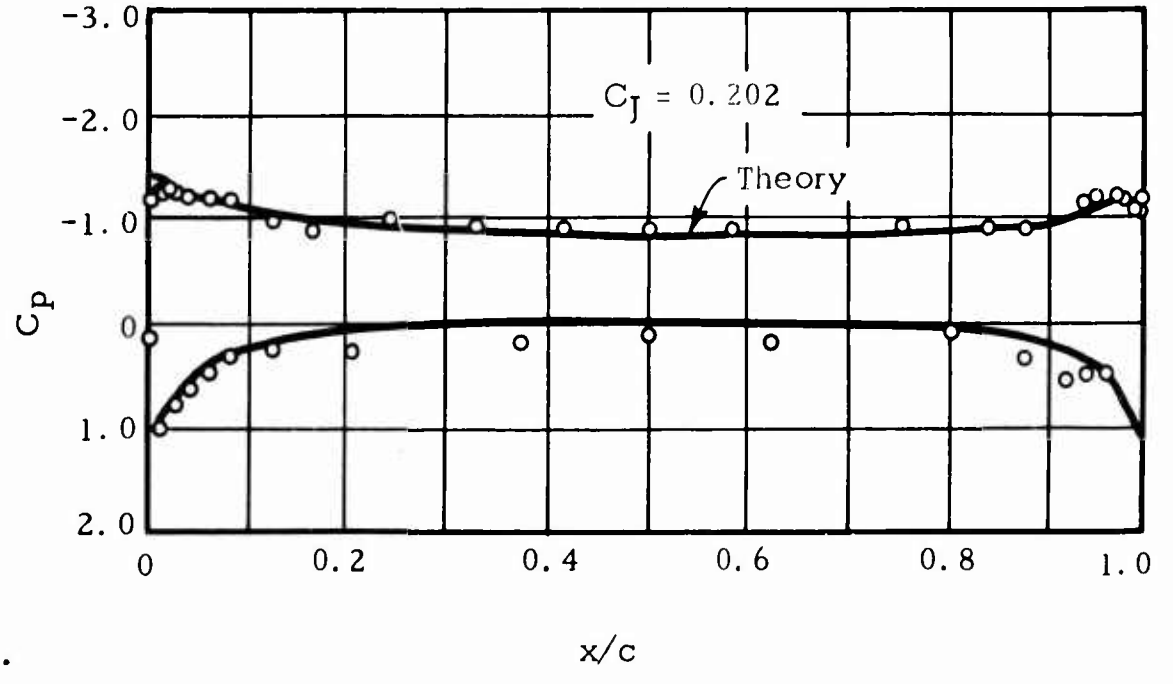

FIG. 33f. PRESSURE DISTRIBUTION IN THE CHORDWISE DIRECTION FOR THE ELLIPTICAL AIRFOIL OF 18-PERCENT-THICKNESS RATIO.

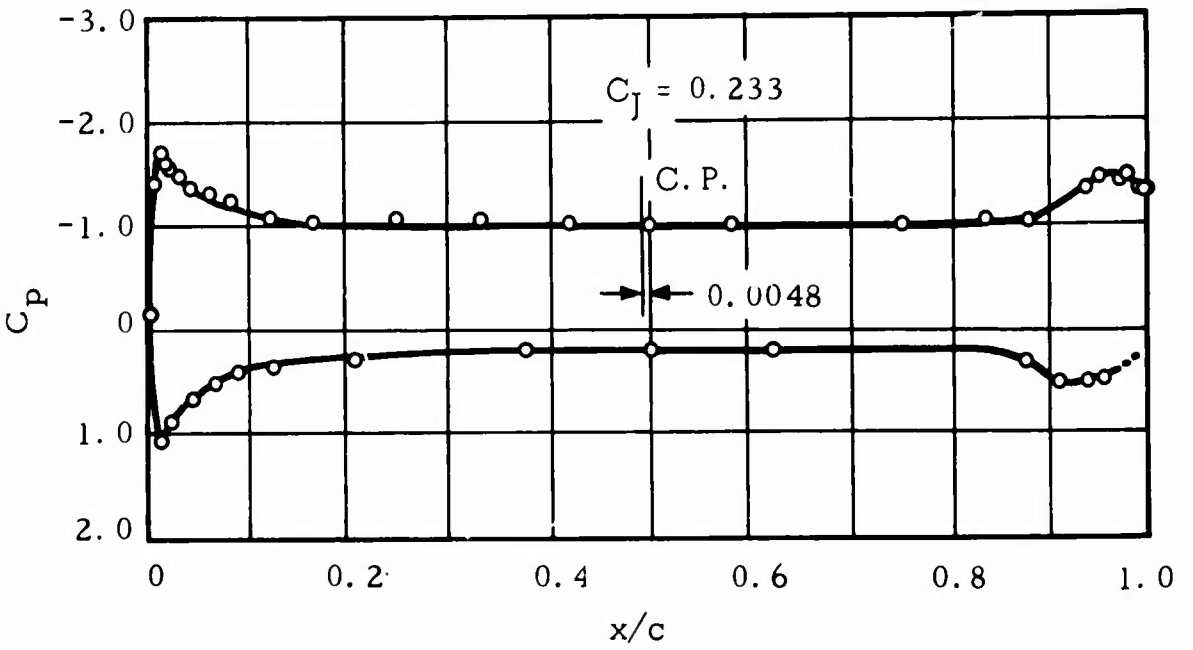

FIG. 33g. PRESSURE DISTRIBUTION IN THE CHORDWISE DIRECTION FOR THE ELLIPTICAL AIRFOIL OF 18-PERCENT-THICKNESS RATIO.

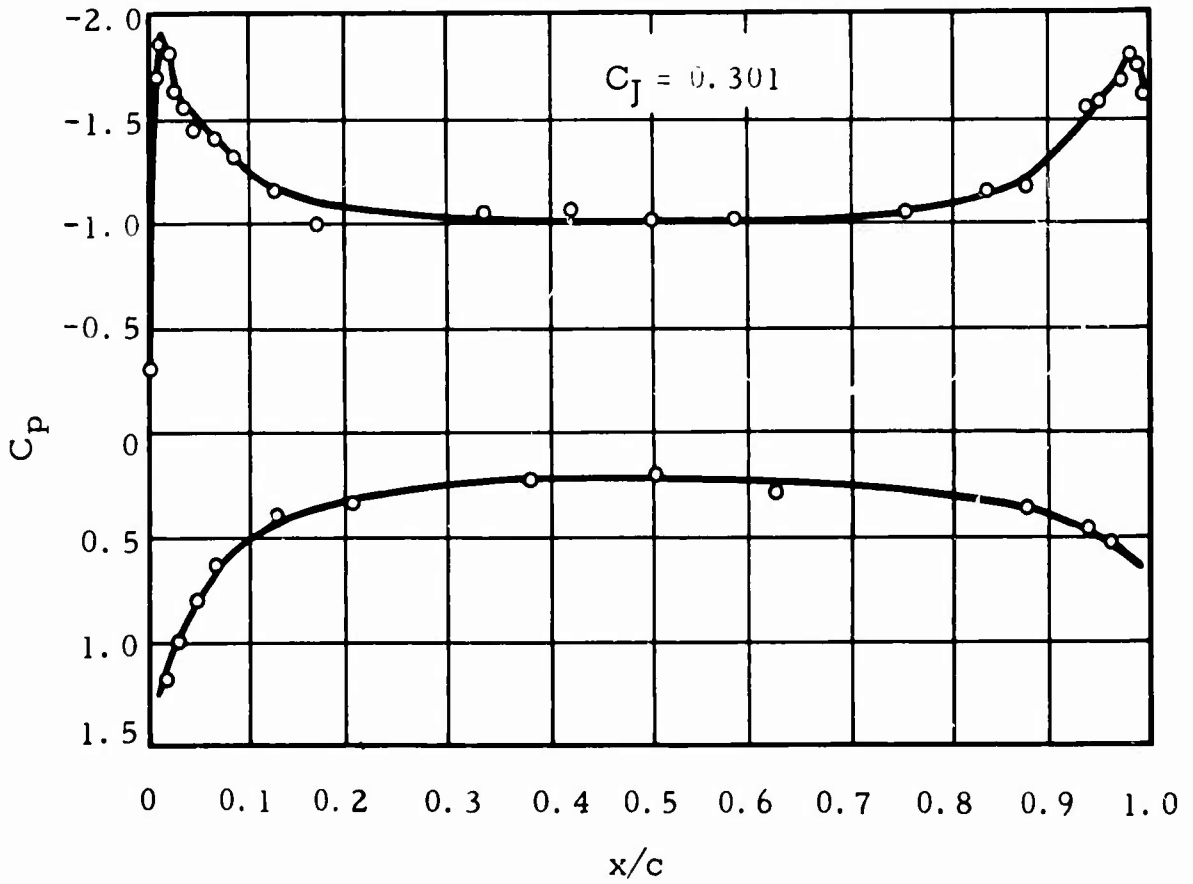

FIG. 33h. PRESSURE DISTRIBUTION IN THE CHORDWISE DIRECTION FOR THE ELLIPTICAL AIRFOIL OF 18-PERCENT-THICKNESS RATIO.

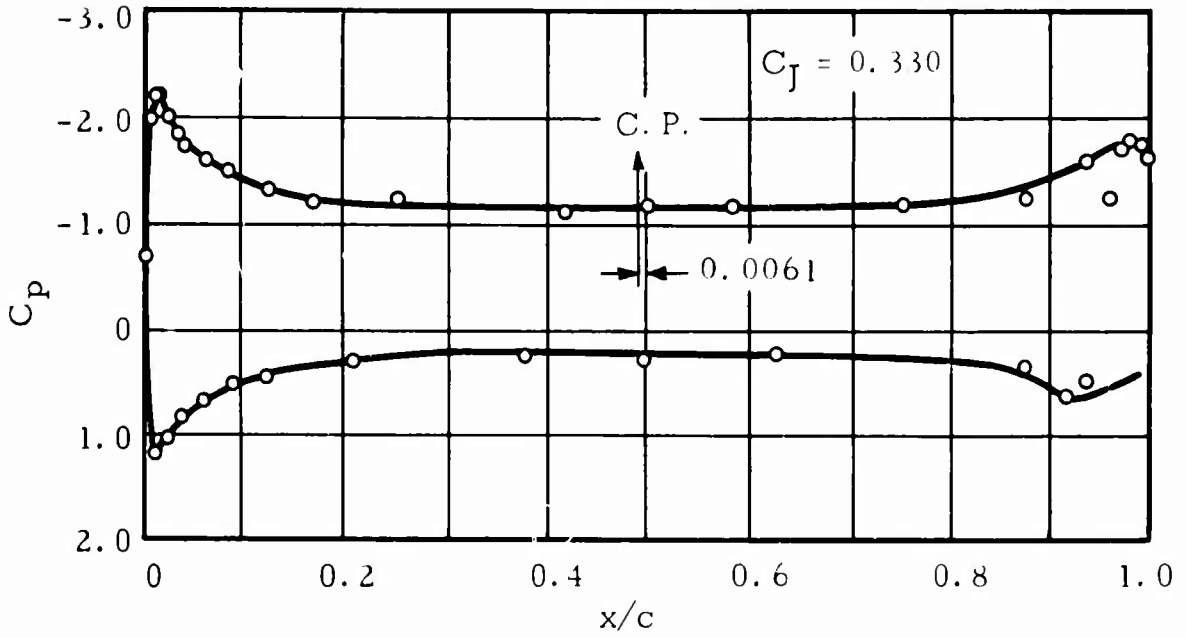

FIG. 33i. PRESSURE DISTRIBUTION IN THE CHORDWISE DIRECTION FOR THE ELLIPTICAL AIRFOIL OF 18-PERCENT-THICKNESS RATIO.

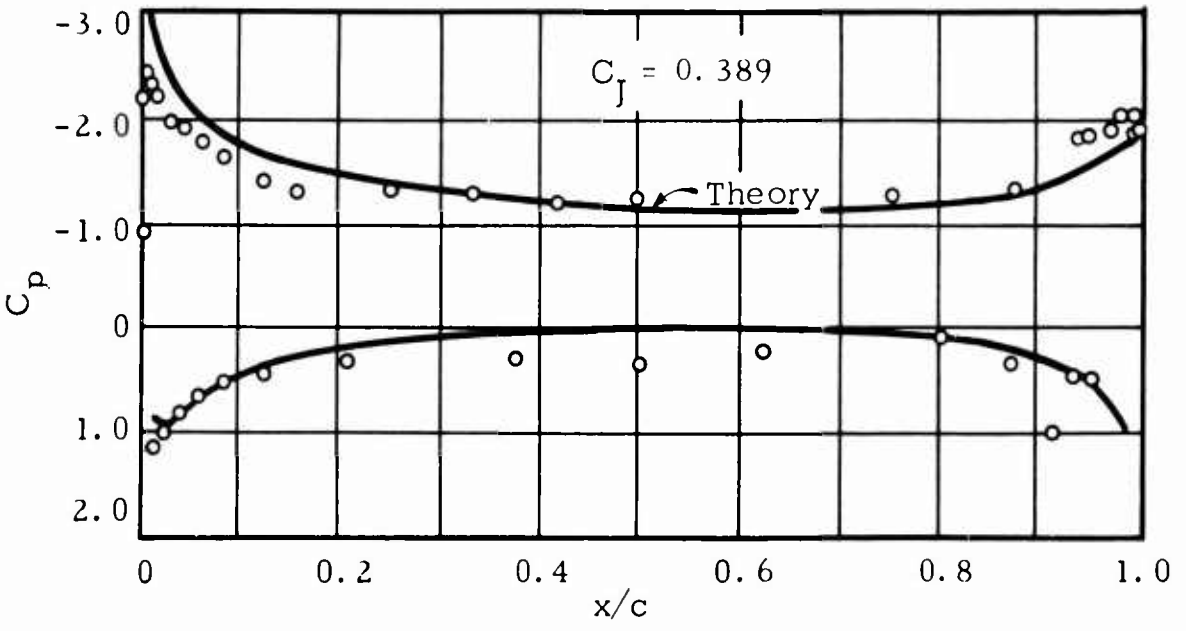

FIG. 33j. PRESSURE DISTRIBUTION IN THE CHORDWISE DIRECTION FOR THE ELLIPTICAL AIRFOIL OF 18-PERCENT-THICKNESS RATIO.

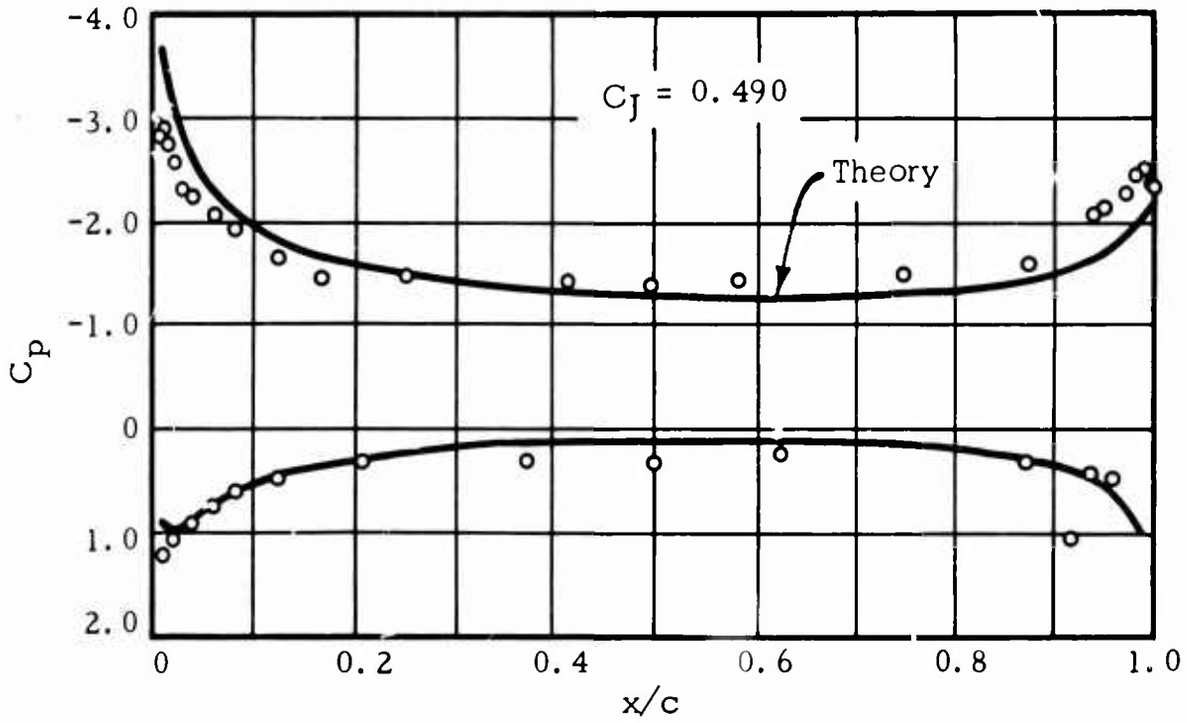

FIG. 33k. PRESSURE DISTRIBUTION IN THE CHORDWISE DIRECTION FOR THE ELLIPTICAL AIRFOIL OF 18-PERCENT-THICKNESS RATIO.

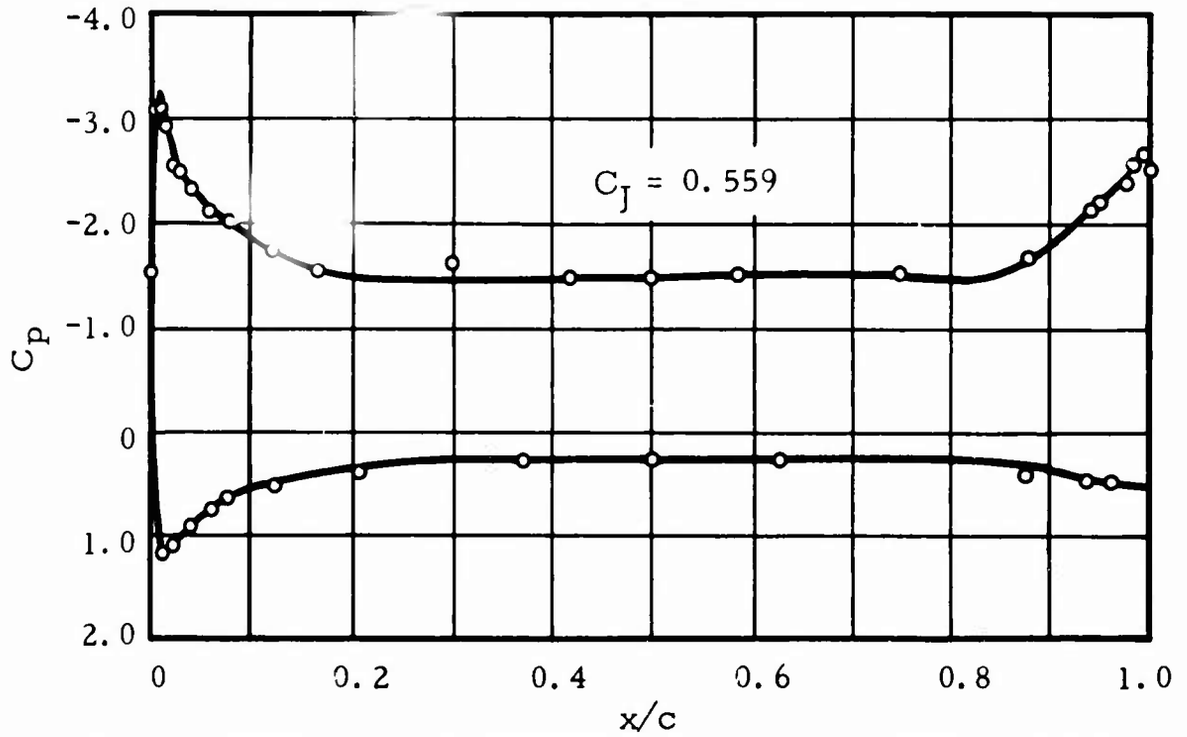

FIG. 33l. PRESSURE DISTRIBUTION IN THE CHORDWISE DIRECTION FOR THE ELLIPTICAL AIRFOIL OF 18-PERCENT-THICKNESS RATIO.

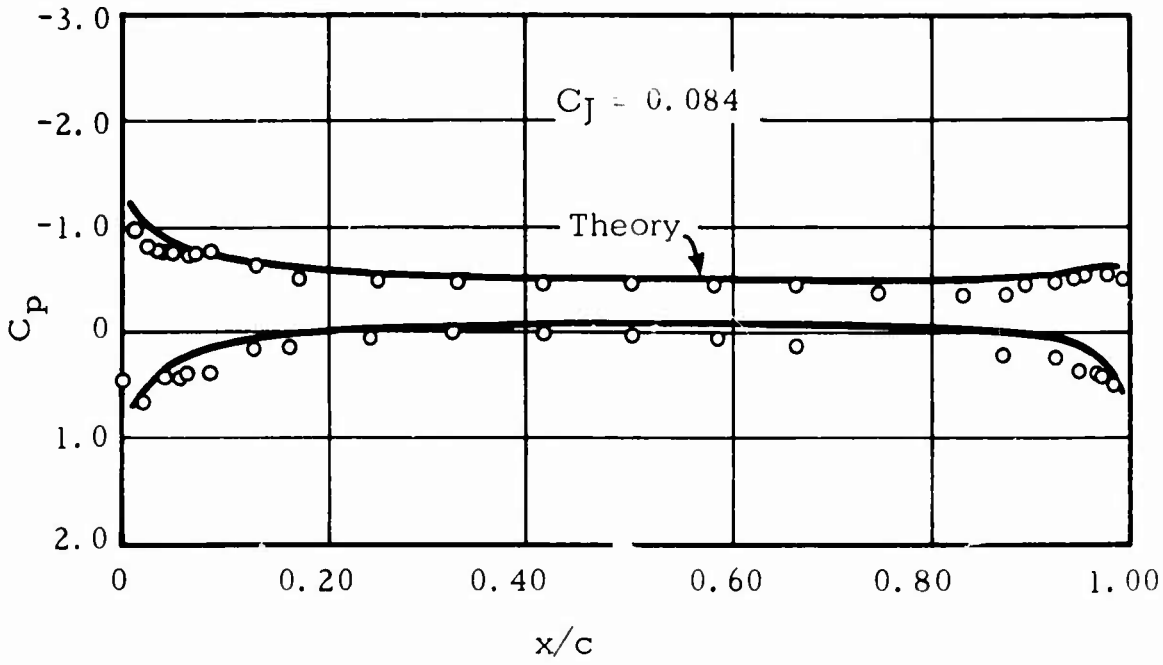

FIG. 34a. PRESSURE DISTRIBUTION IN THE CHORDWISE DIRECTION FOR THE ELLIPTICAL AIRFOIL OF 12-PERCENT-THICKNESS RATIO.

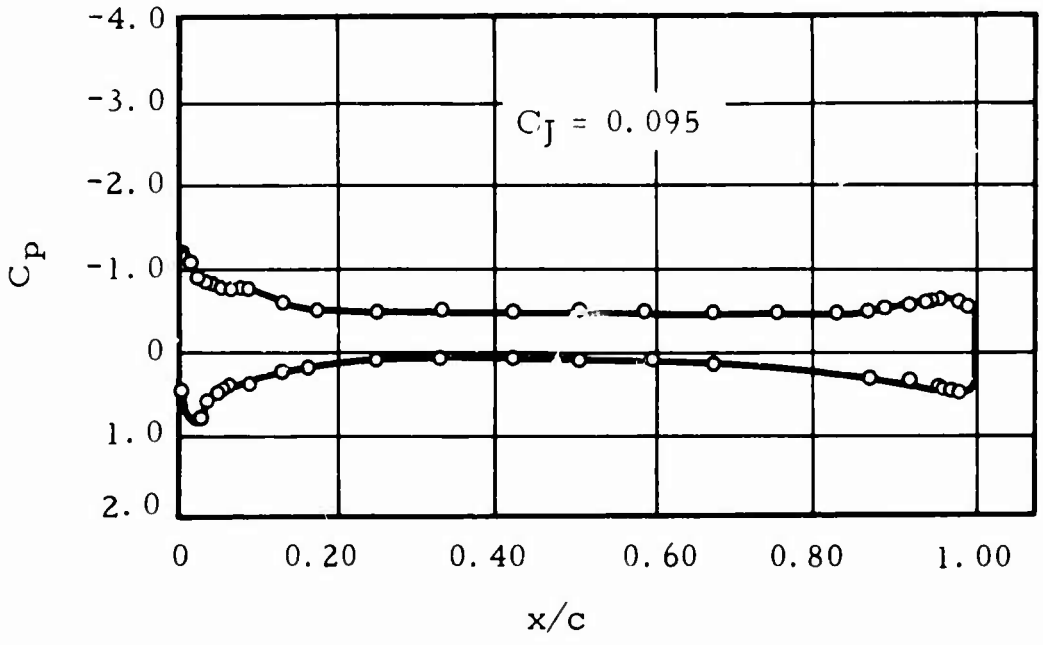

FIG. 34b. PRESSURE DISTRIBUTION IN THE CHORDWISE DIRECTION FOR THE ELLIPTICAL AIRFOIL OF 12-PERCENT-THICKNESS RATIO.

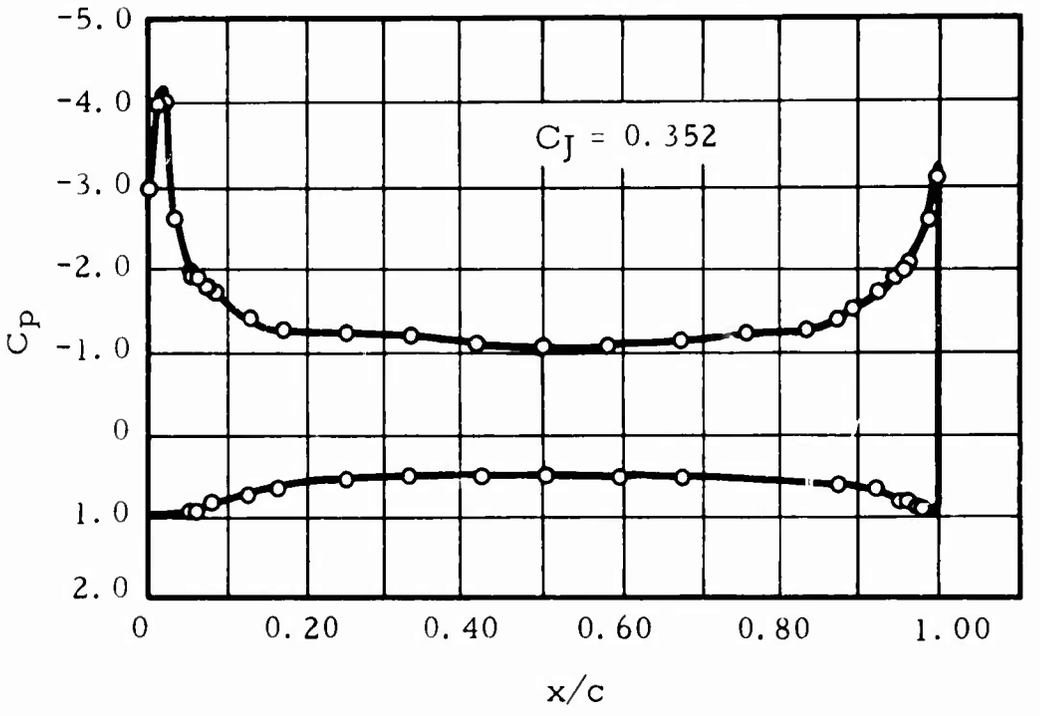

FIG. 34c. PRESSURE DISTRIBUTION IN THE CHORDWISE DIRECTION FOR THE ELLIPTICAL AIRFOIL OF 12-PERCENT-THICKNESS RATIO.

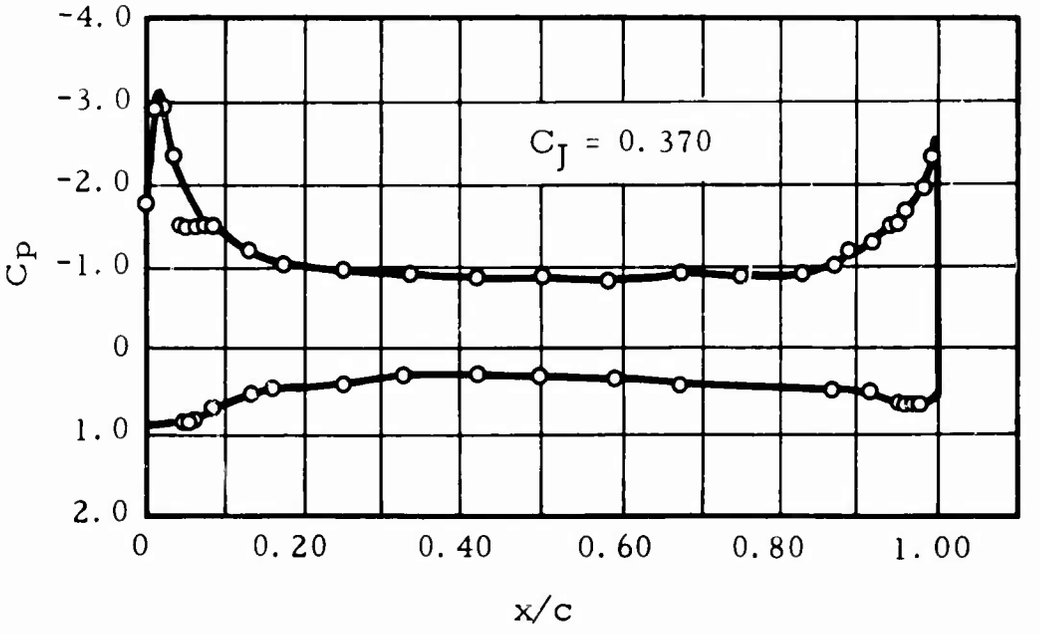

FIG. 34d. PRESSURE DISTRIBUTION IN THE CHORDWISE DIRECTION FOR THE ELLIPTICAL AIRFOIL OF 12-PERCENT-THICKNESS RATIO.

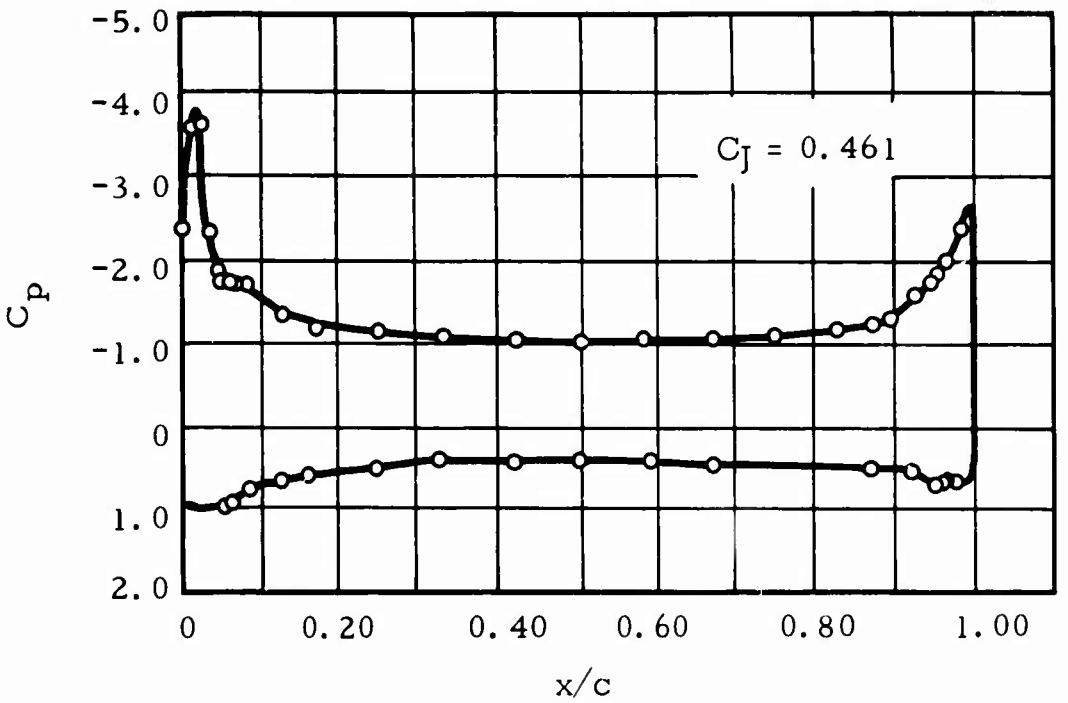

FIG. 34e. PRESSURE DISTRIBUTION IN THE CHORDWISE DIRECTION FOR THE ELLIPTICAL AIRFOIL OF 12-PERCENT-THICKNESS RATIO.

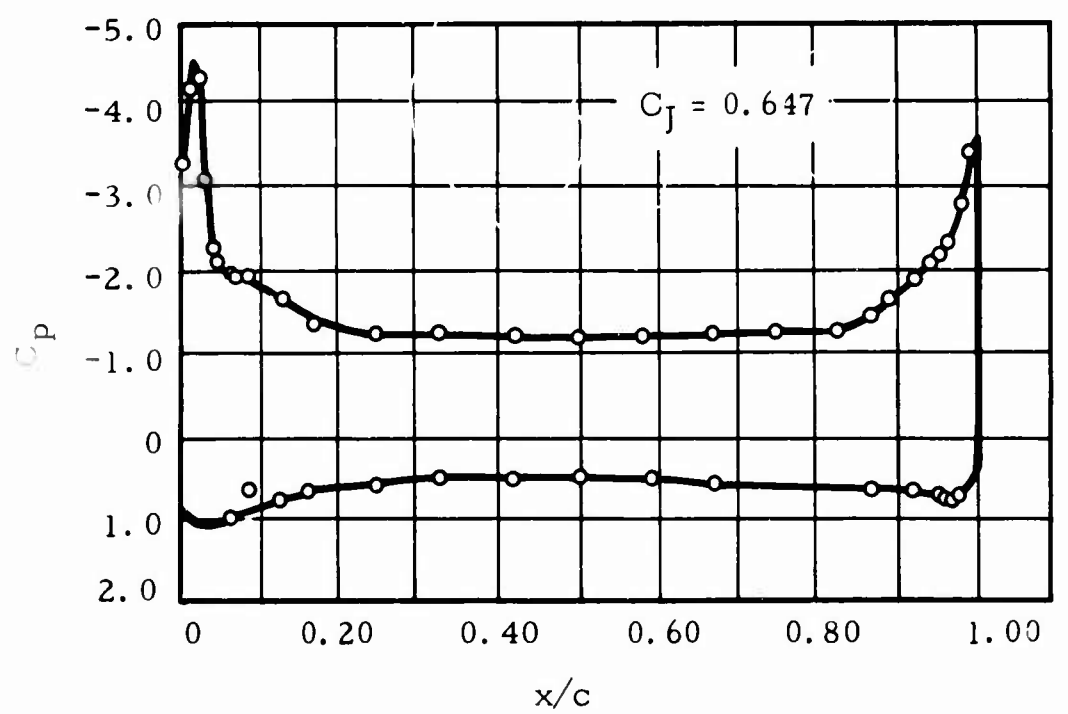

FIG. 34f. PRESSURE DISTRIBUTION IN THE CHORDWISE DIRECTION FOR THE ELLIPTICAL AIRFOIL OF 12-PERCENT-THICKNESS RATIO.

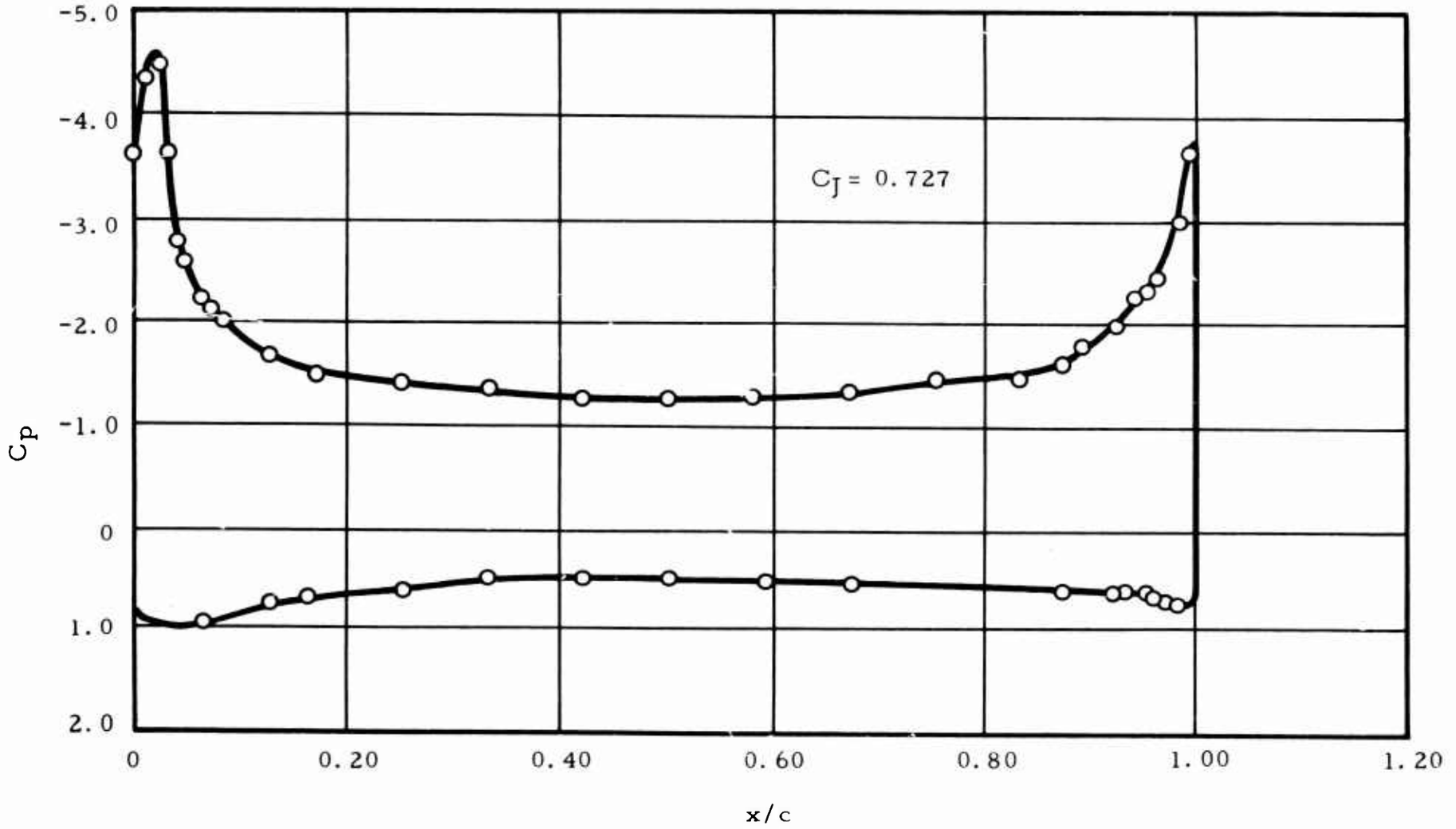

FIG. 34(g). PRESSURE DISTRIBUTION IN THE CHORDWISE DIRECTION FOR THE ELLIPTICAL AIRFOIL OF 12-PERCENT-THICKNESS RATIO.

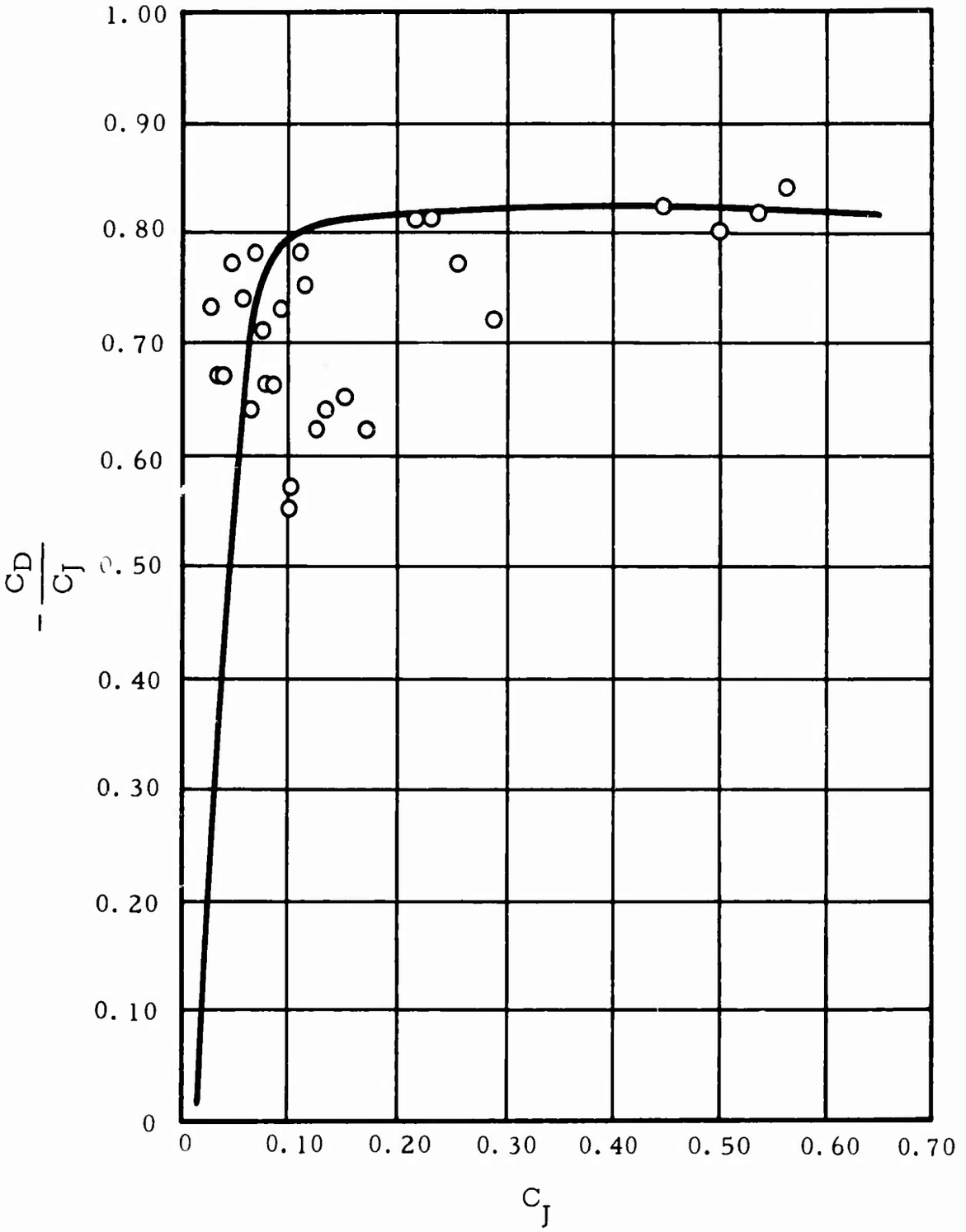

FIG. 35. MEASURED THRUST FOR THE ELLIPTICAL AIRFOIL OF 18-PERCENT-THICKNESS RATIO ($\theta = 30^{\circ}$, $\alpha = 0$).

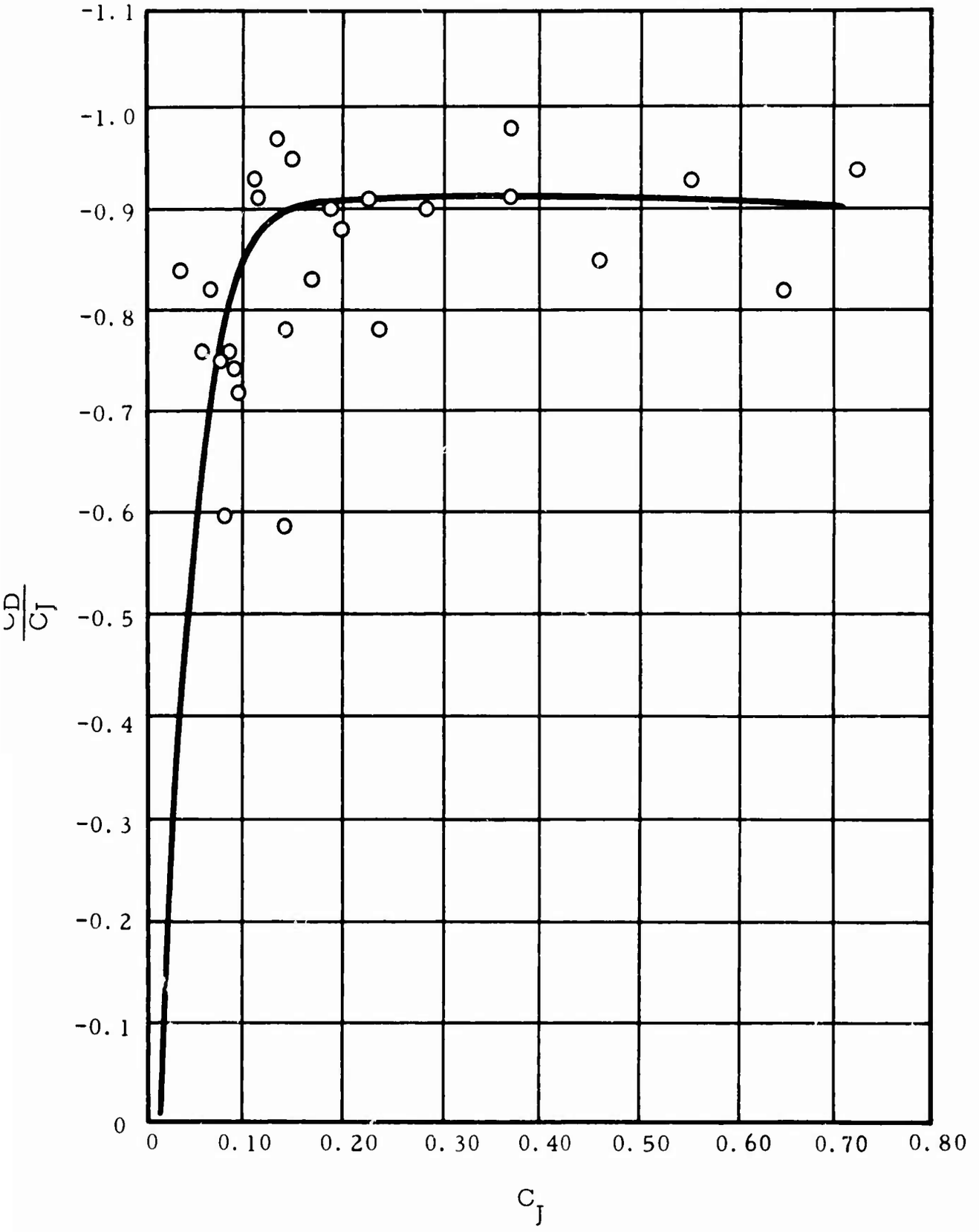

FIG. 36. MEASURED THRUST FOR THE ELLIPTICAL AIRFOIL OF 12-PERCENT—THICKNESS RATIO ($\theta = 40^{\circ}$, $\alpha = 0$).

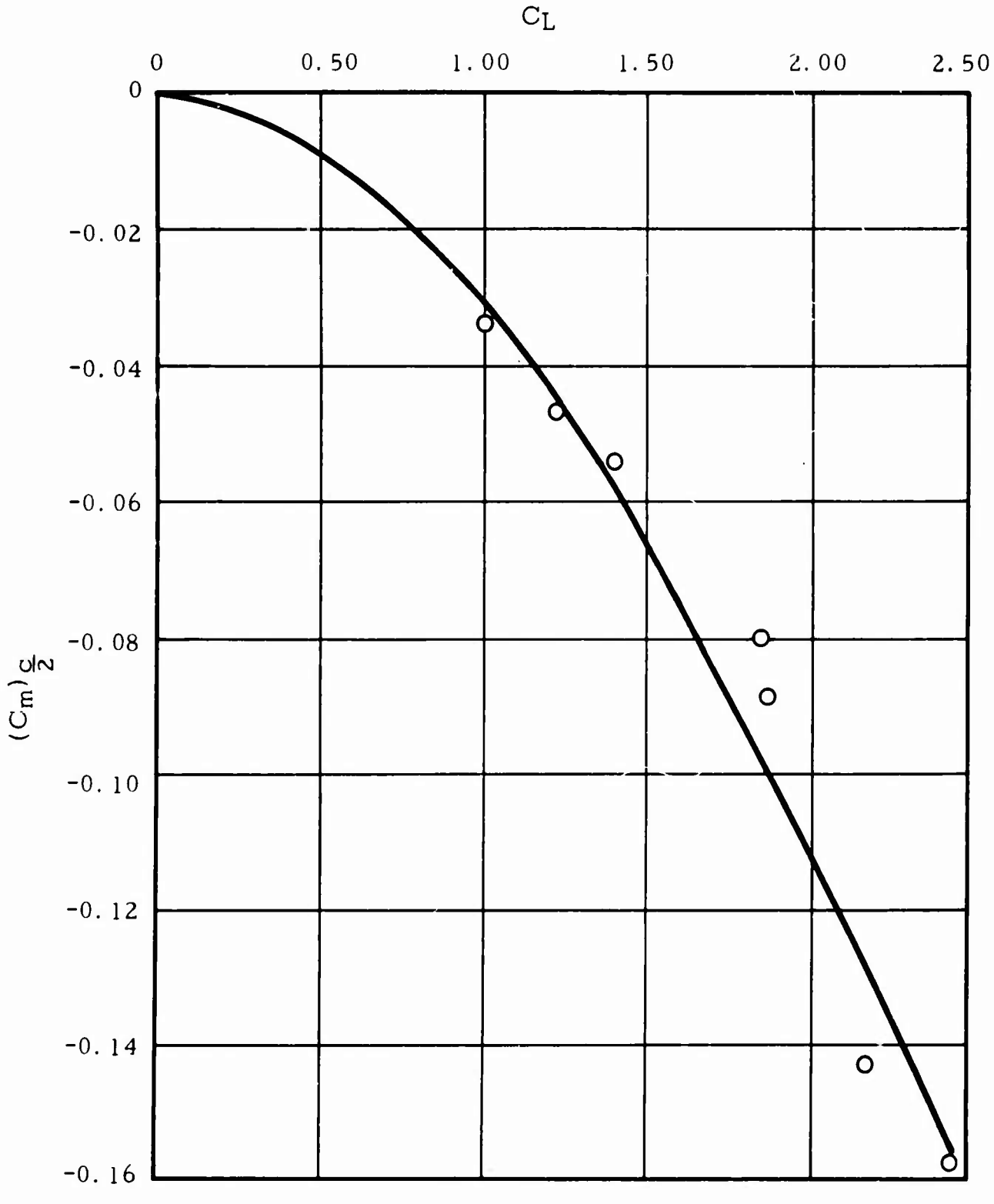

FIG. 37. PITCHING MOMENT COEFFICIENT VERSUS LIFT COEFFICIENT (RELATIVE TO MID-CHORD POINT) FOR MODEL OF 18-PERCENT-THICKNESS RATIO.

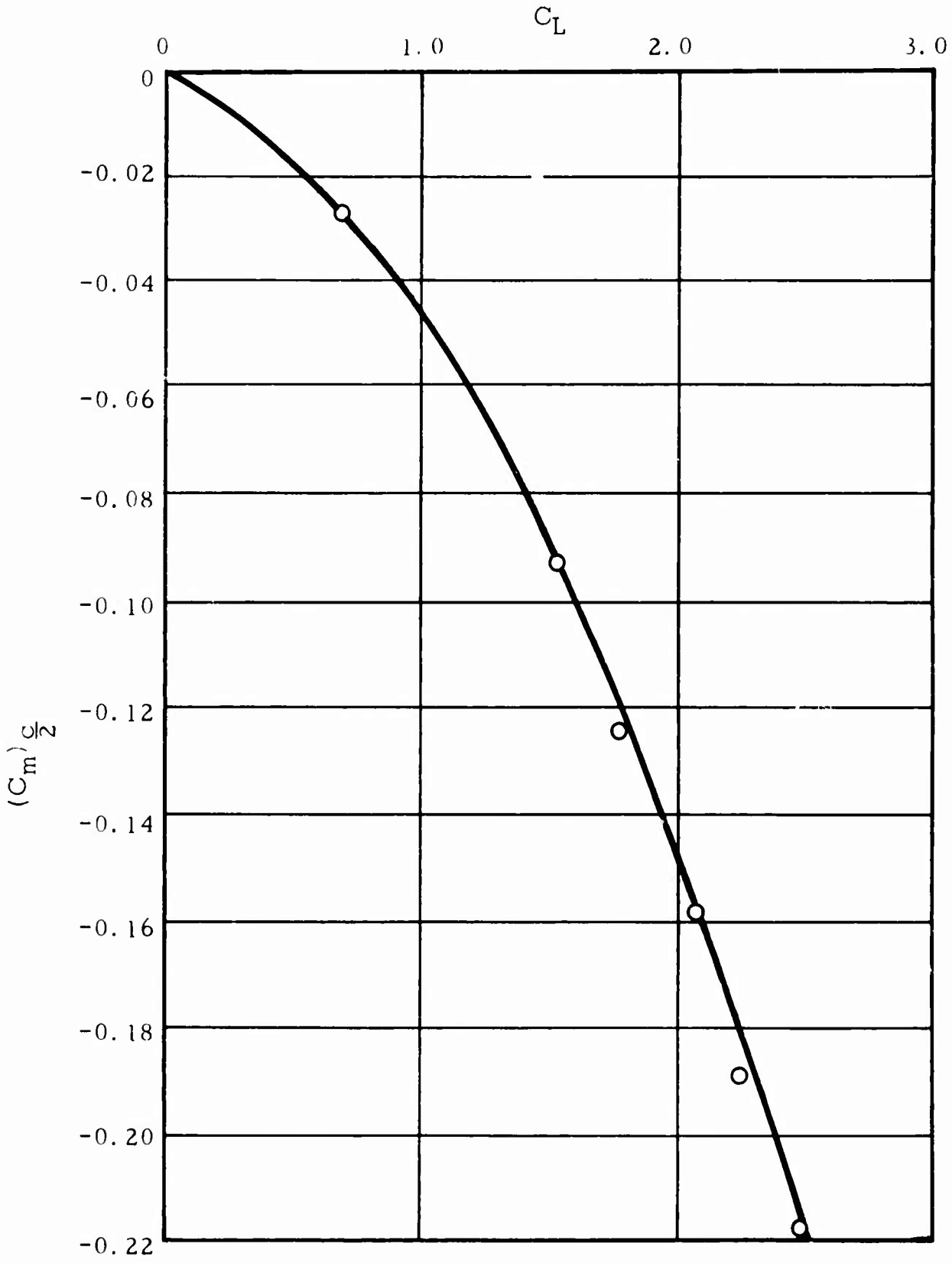

FIG. 38. PITCHING MOMENT COEFFICIENT VERSUS LIFT COEFFICIENT (RELATIVE TO MID-CHORD POINT) FOR MODEL OF 12-PERCENT-THICKNESS RATIO.

FIG. 39. ELLIPTICAL AIRFOIL MODEL OF 18 PERCENT WITH DUAL JETS.

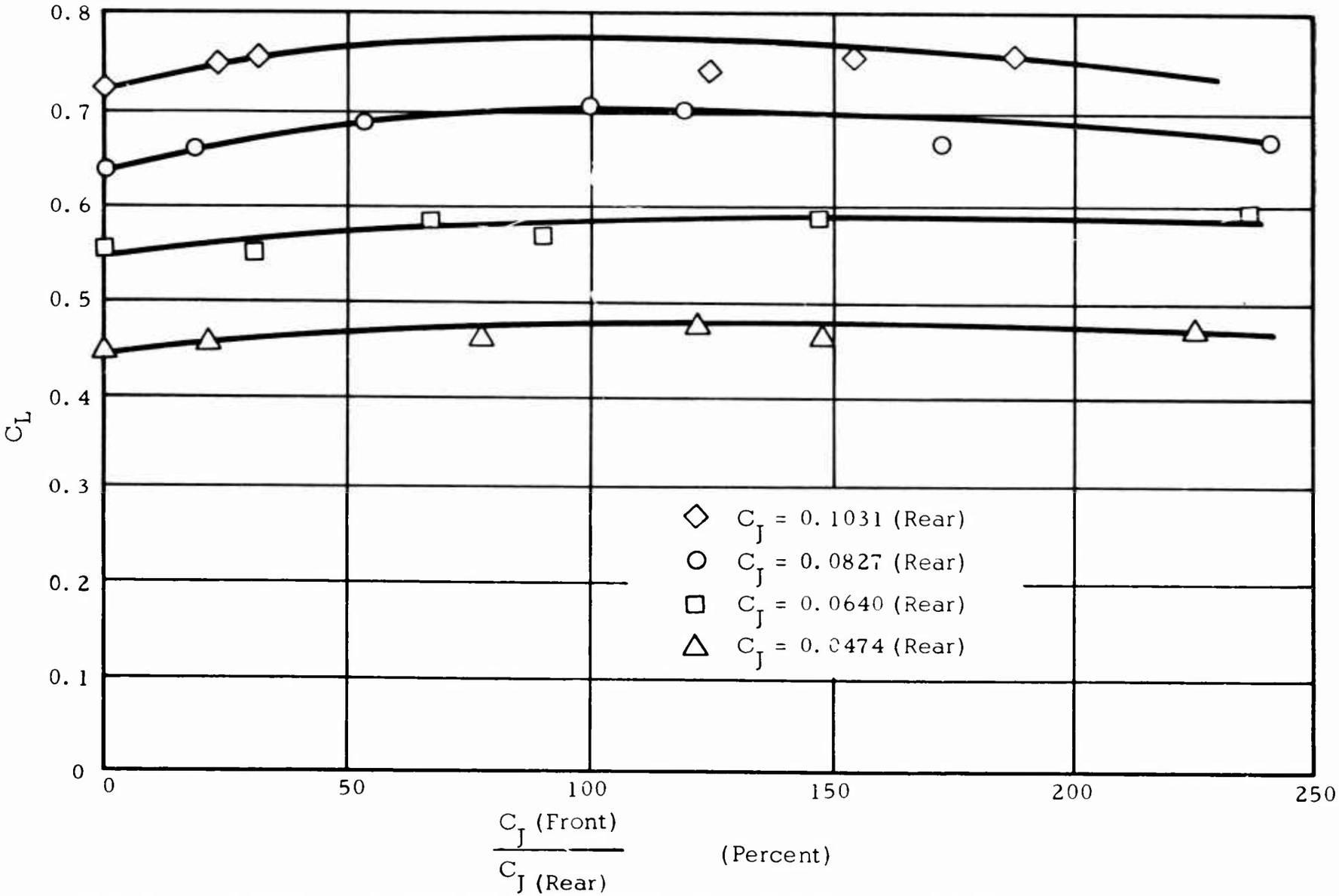

FIG. 40. THE TOTAL LIFT COEFFICIENT VERSUS THE RATIO OF LEADING EDGE JET COEFFICIENT TO TRAILING EDGE JET COEFFICIENT (18-PERCENT-THICKNESS RATIO).

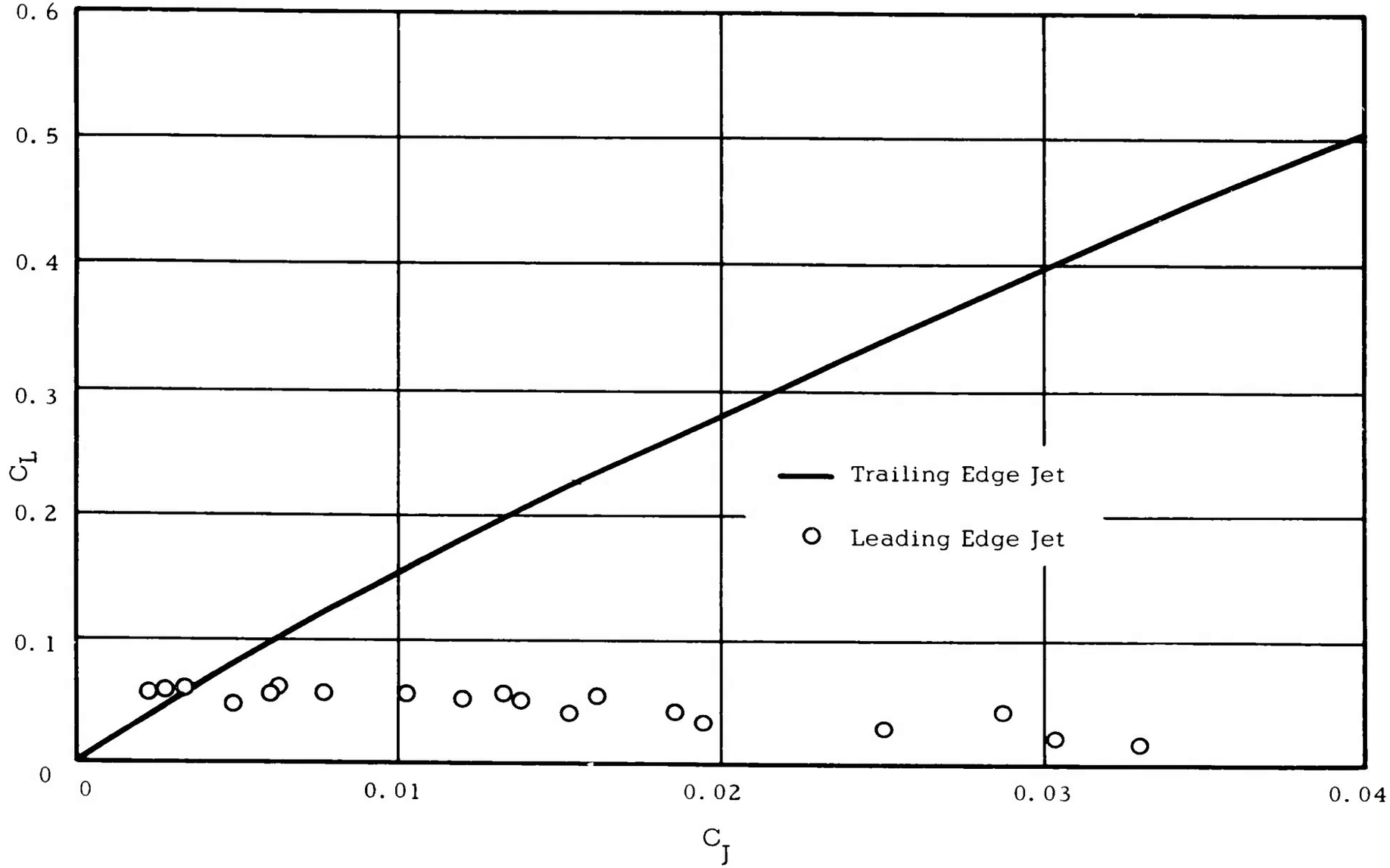

FIG. 41. C_L VERSUS C_J FOR SINGLE LEADING EDGE JET (18-PERCENT MODEL).

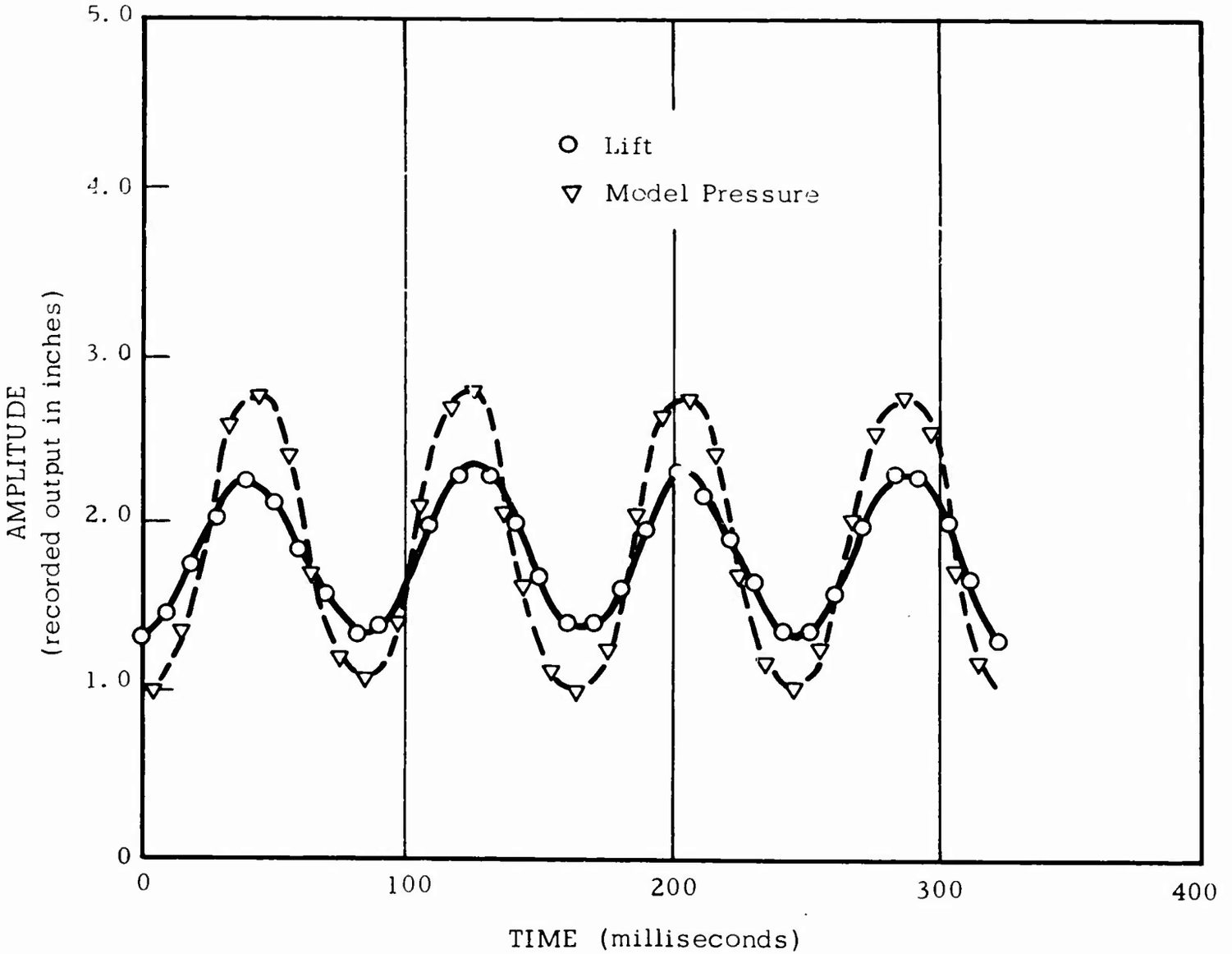

FIG. 42. PULSATING LIFT AND MODEL PRESSURE FOR ELLIPTICAL AIRFOIL OF 18-PERCENT-THICKNESS RATIO (VALVE SPEED = 360 r. p. m.).

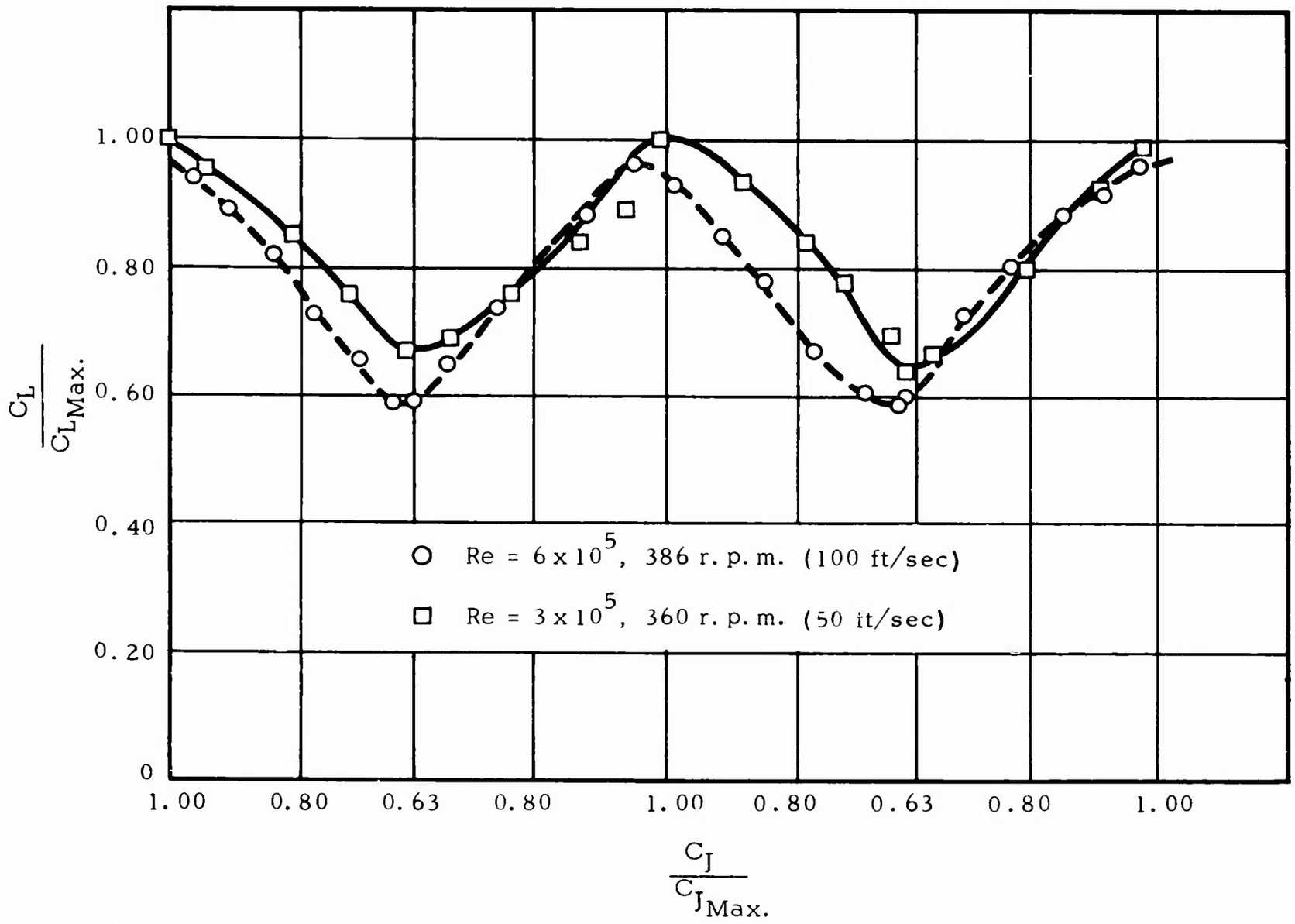

FIG. 43. PULSATING LIFT COEFFICIENT RATIO VERSUS PULSATING JET COEFFICIENT RATIO FOR 18-PERCENT MODEL.

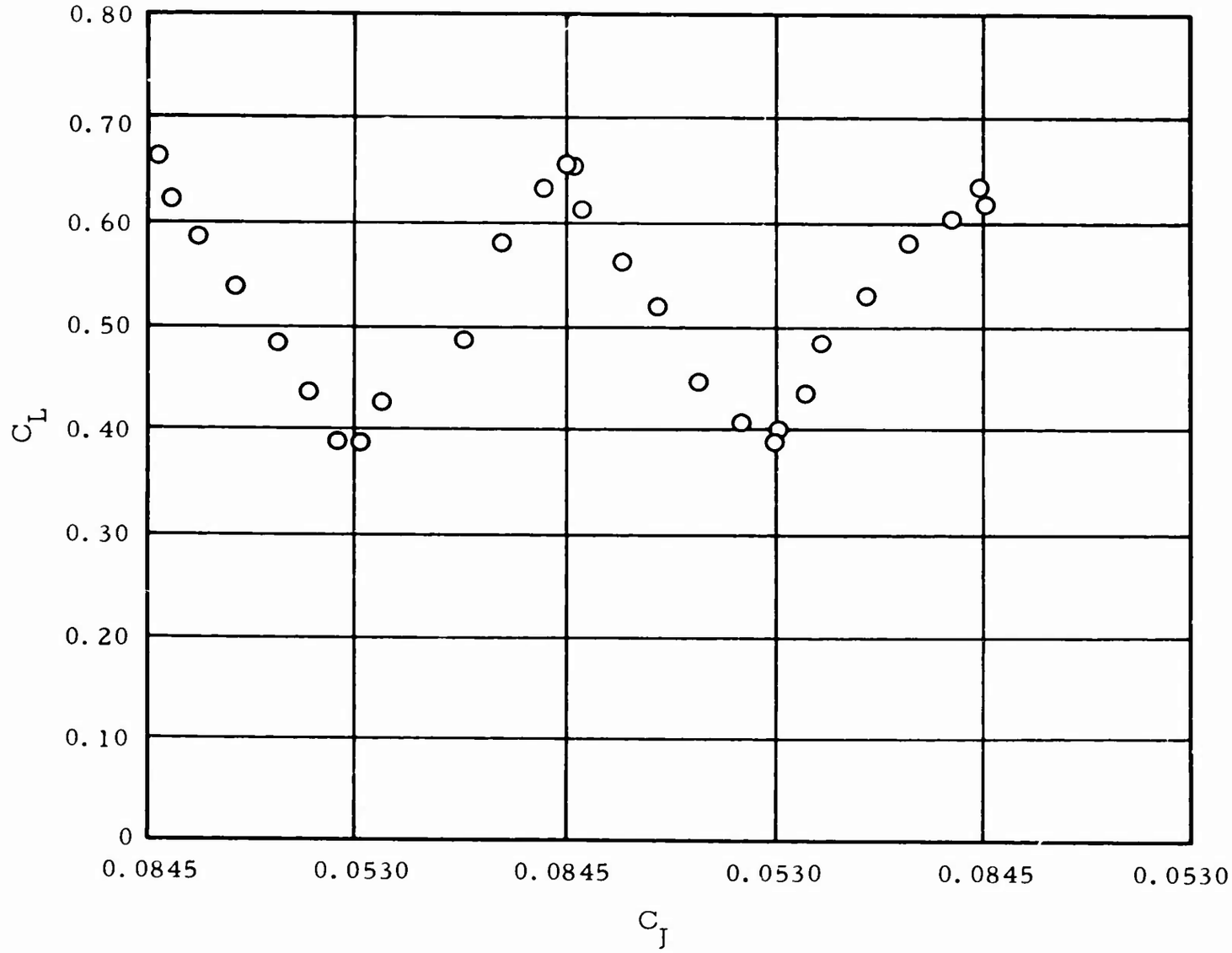

FIG. 44. PULSATING LIFT COEFFICIENT VERSUS PULSATING JET COEFFICIENT FOR 18-PERCENT MODEL AT VALVE SPEED 386 r. p. m.

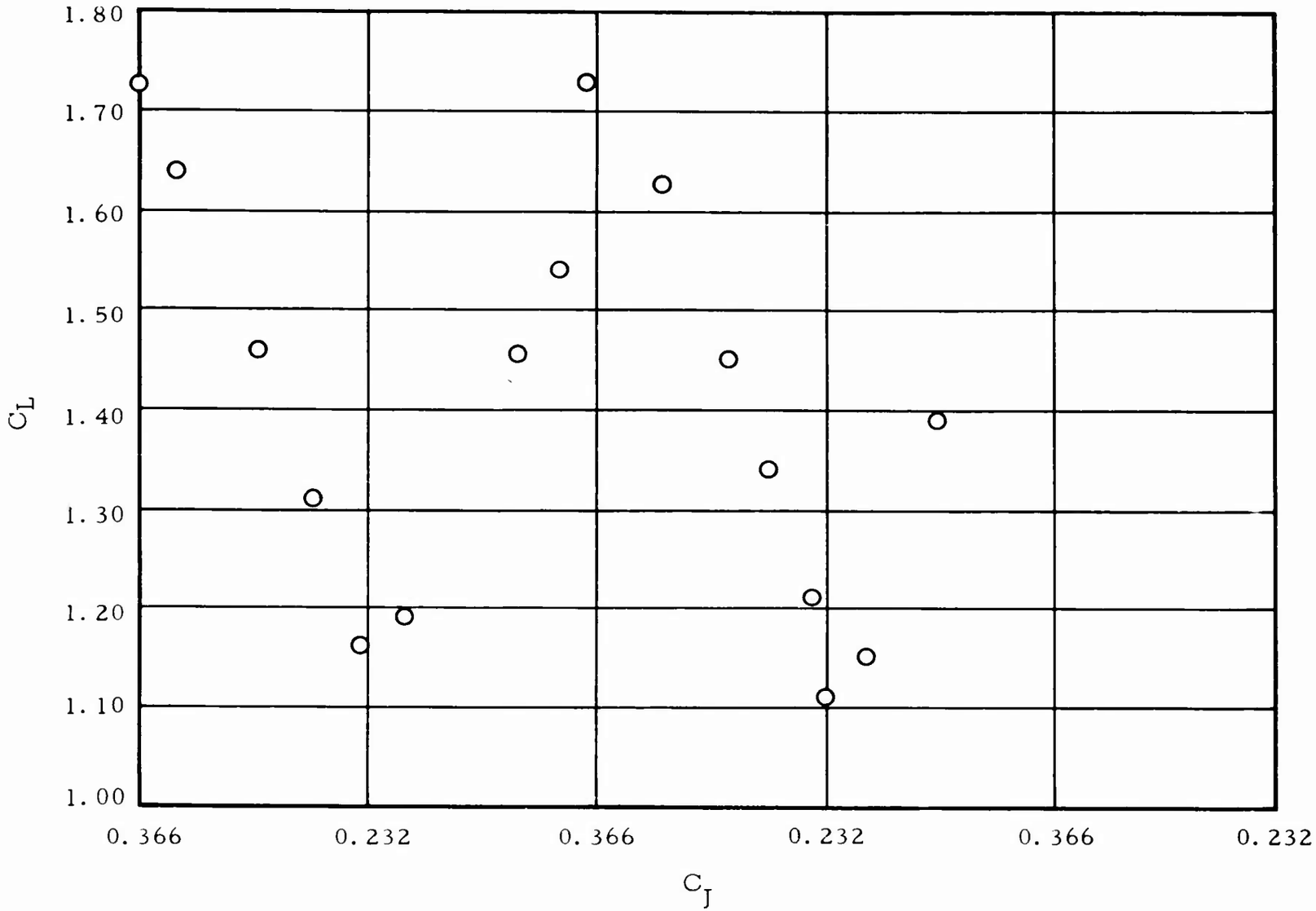

FIG. 45. PULSATING LIFT COEFFICIENT VERSUS PULSATING JET COEFFICIENT FOR 18-PERCENT MODEL AT VALVE SPEED 360 r. p. m.

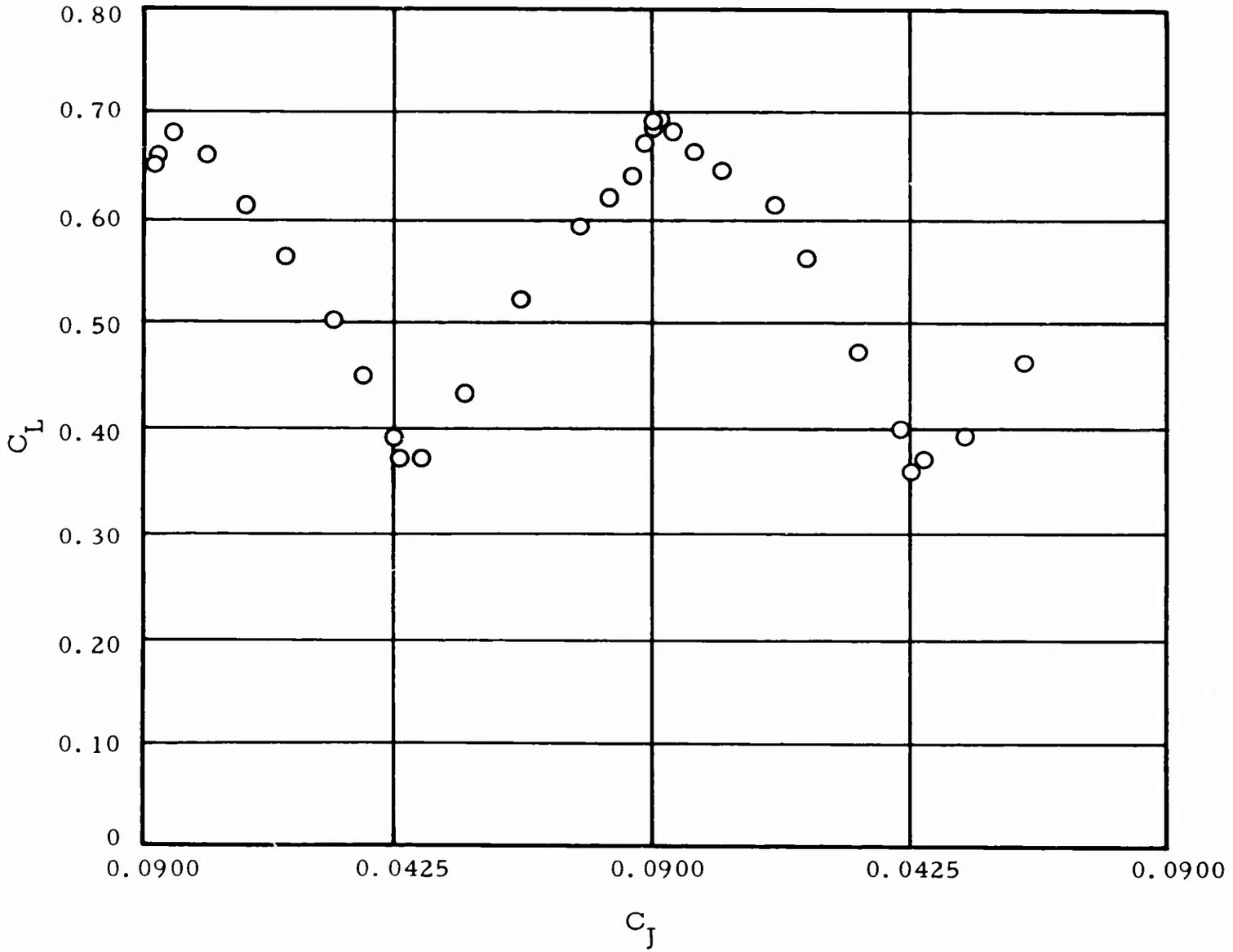

FIG. 46. PULSATING LIFT COEFFICIENT VERSUS PULSATING JET COEFFICIENT FOR 18-PERCENT MODEL AT VALVE SPEED 210 r. p. m.

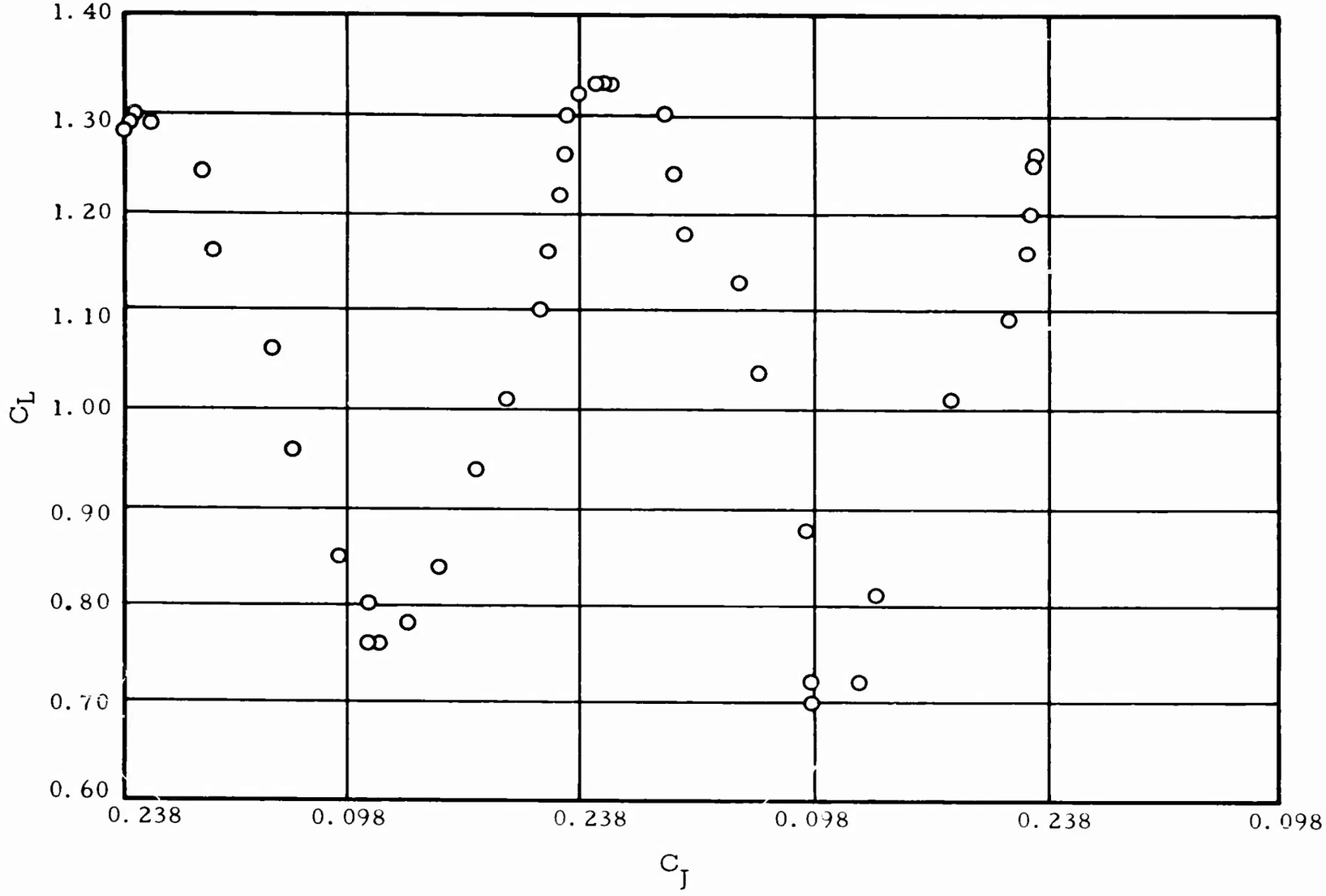

FIG. 47. PULSATING LIFT COEFFICIENT VERSUS PULSATING JET COEFFICIENT FOR 18-PERCENT MODEL AT VALVE SPEED 150 r. p. m.

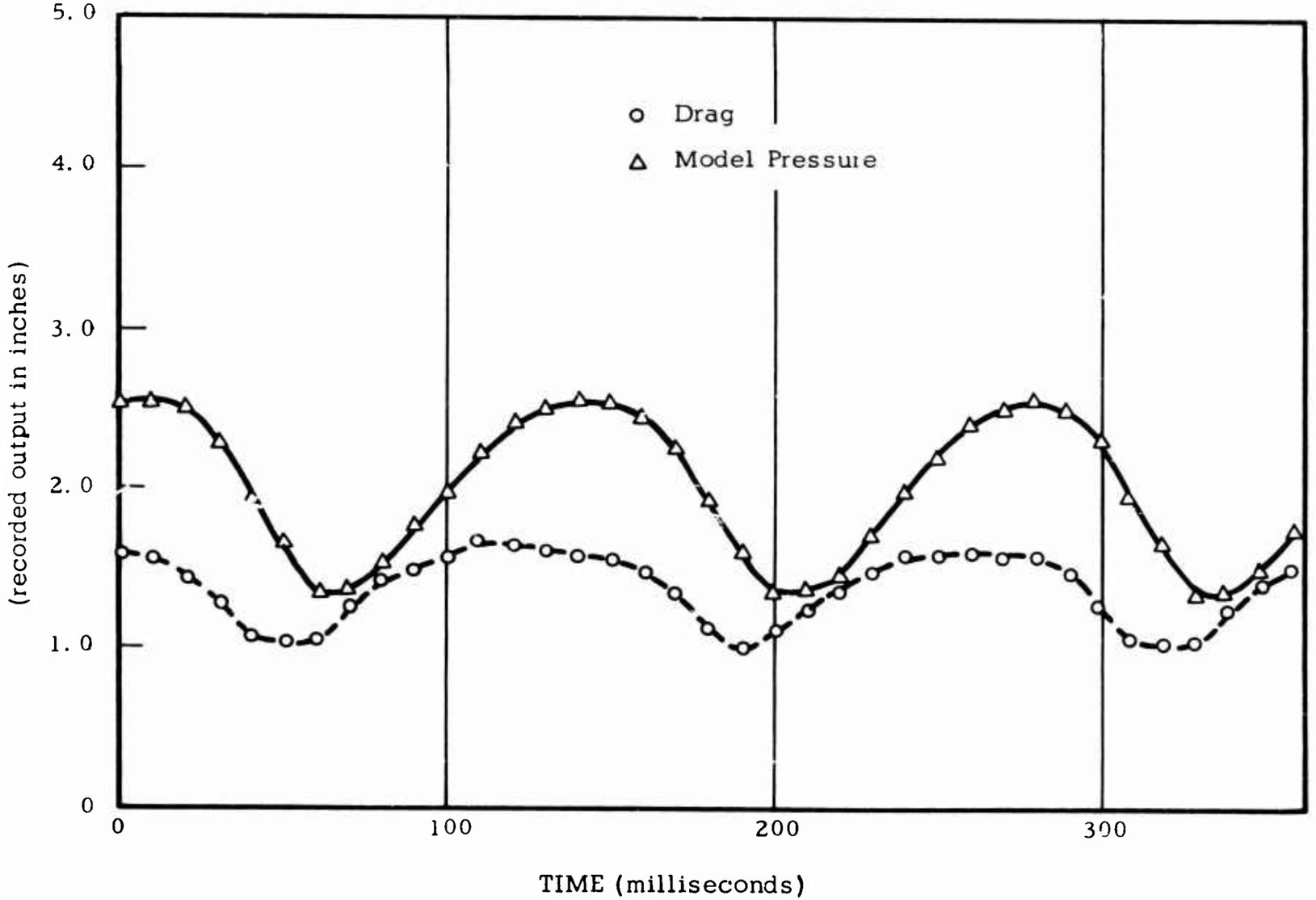

FIG. 48. PULSATING DRAG AND MODEL PRESSURE FOR ELLIPTICAL AIRFOIL OF 18-PERCENT-THICKNESS RATIO (VALVE SPEED = 215 r. p. m.).

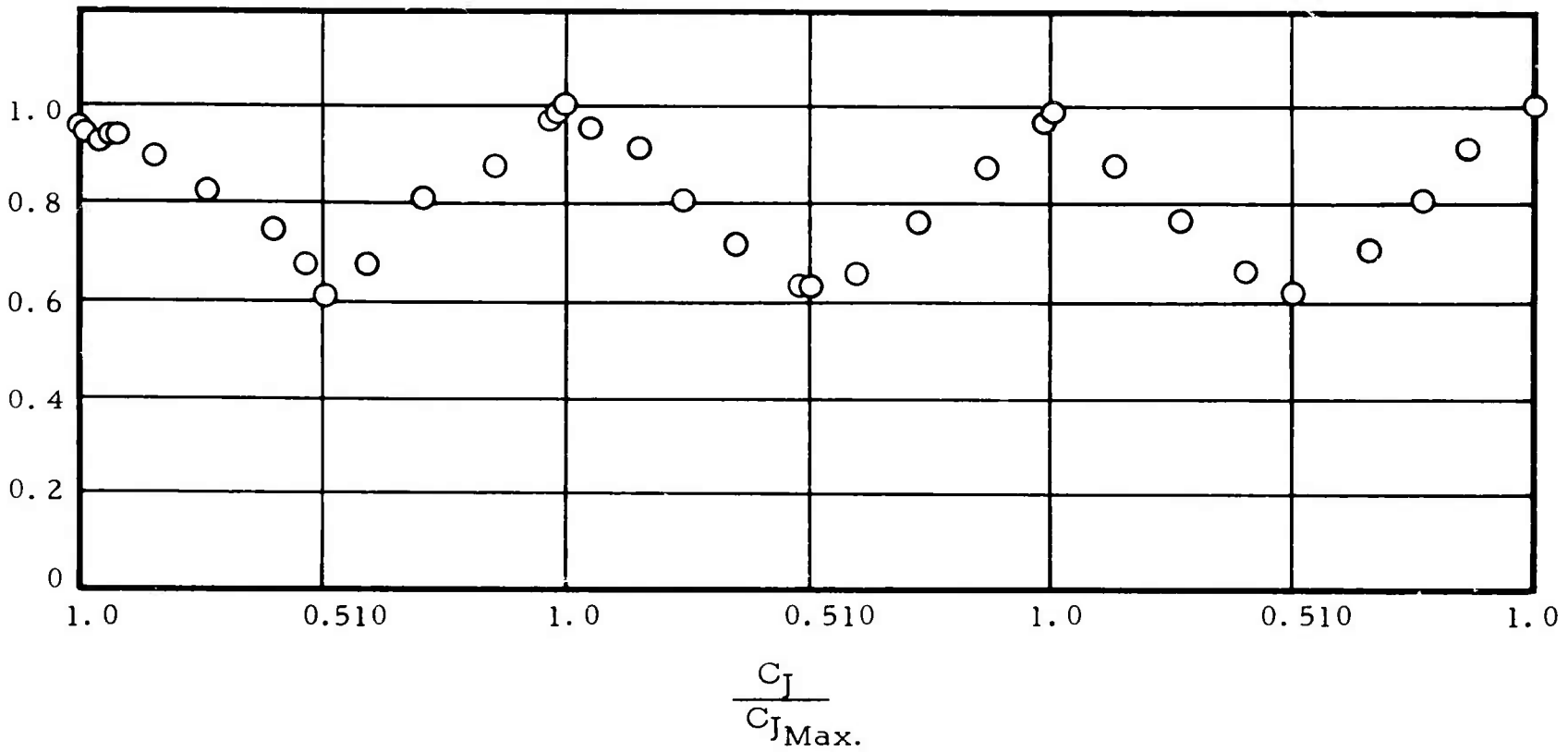

FIG. 49. PULSATING DRAG COEFFICIENT RATIO VERSUS PULSATING JET COEFFICIENT RATIO FOR 18-PERCENT MODEL.

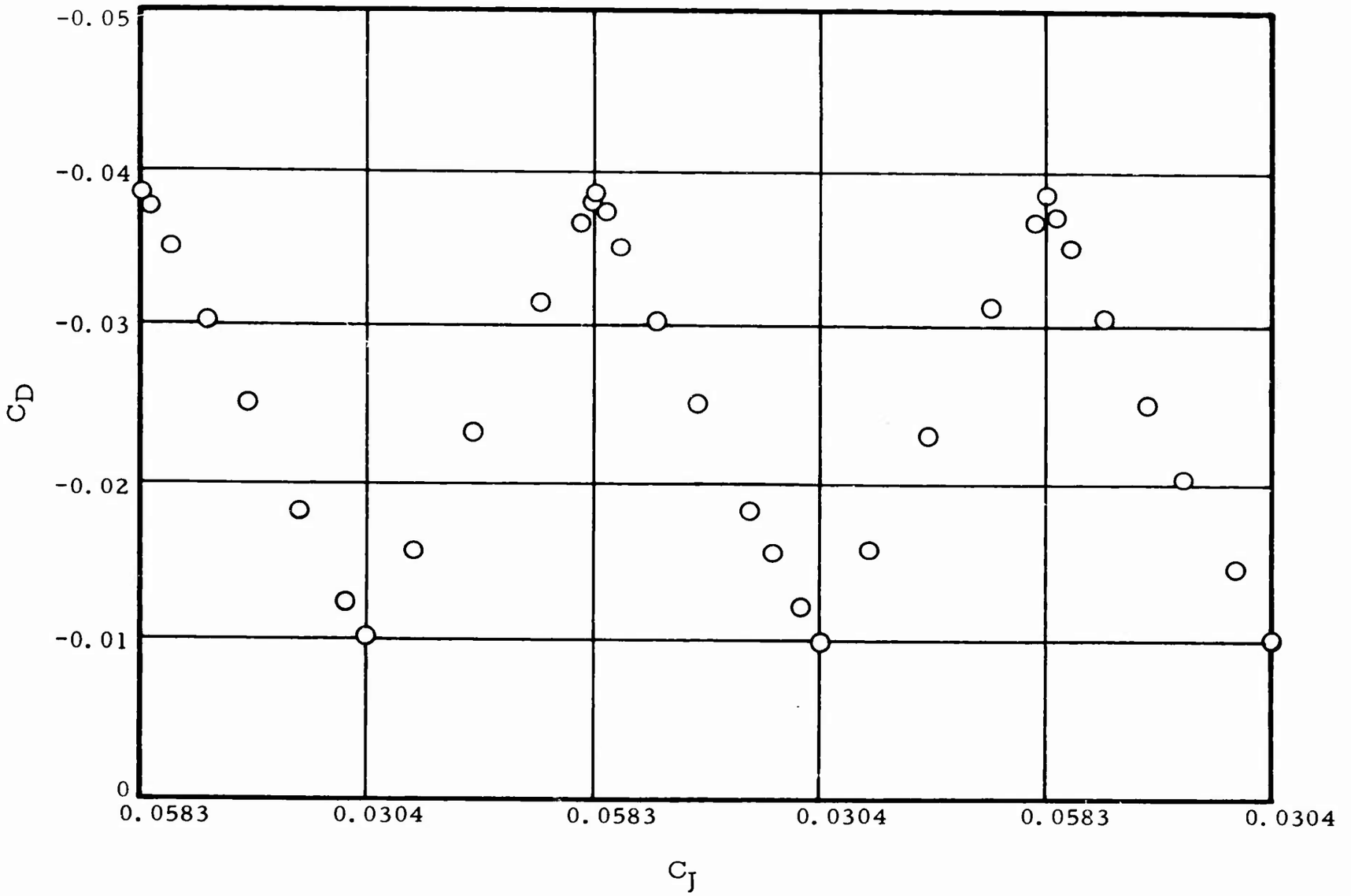

FIG. 50. PULSATING DRAG COEFFICIENT VERSUS PULSATING JET COEFFICIENT FOR 18-PERCENT MODEL AT VALVE SPEED 215 r. p. m.

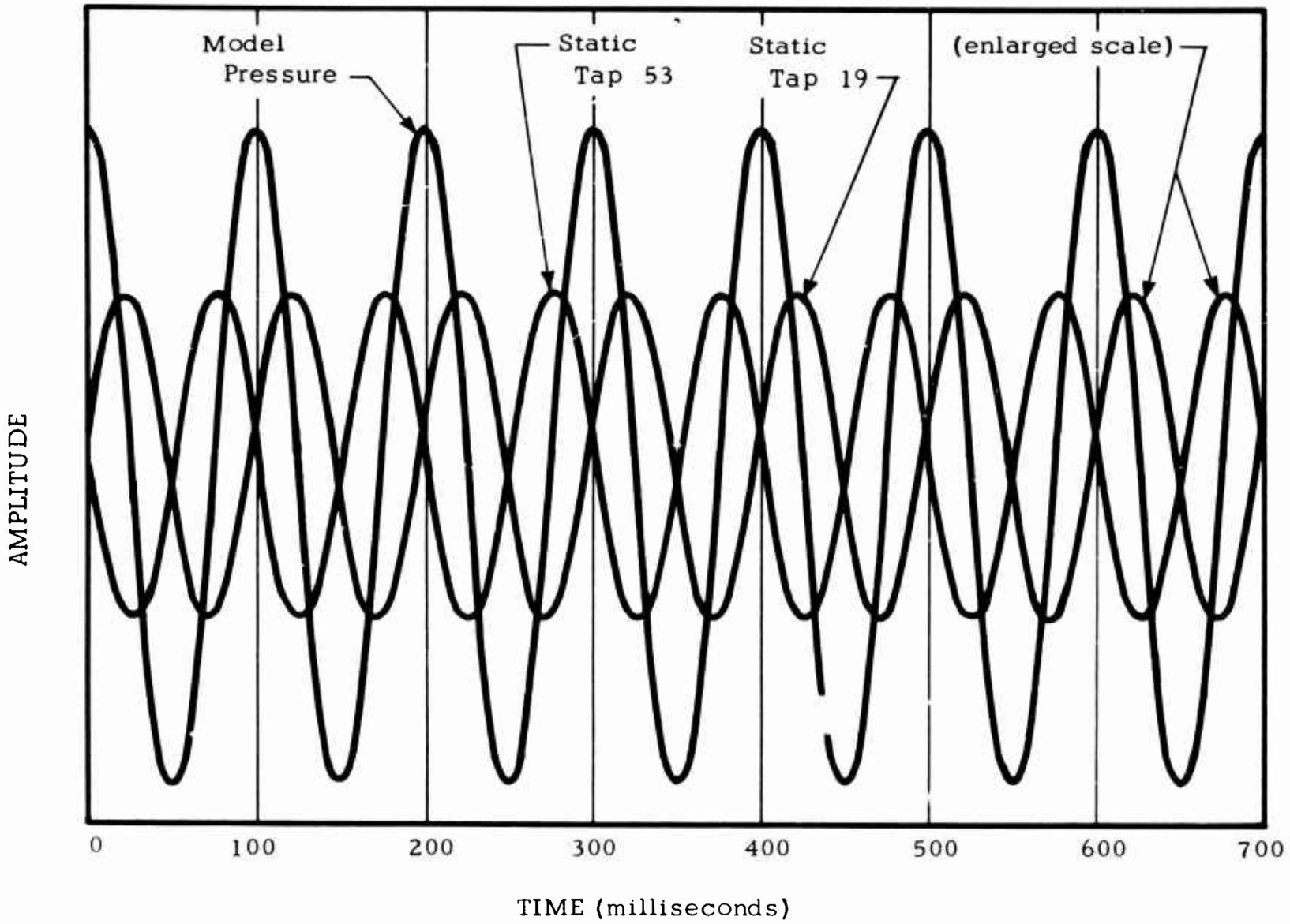

FIG. 51. PULSATING STATIC PRESSURE AND MODEL PRESSURE FOR ELLIPTICAL AIRFOIL OF 12-PERCENT-THICKNESS RATIO (VALVE SPEED = 300 r. p. m.).

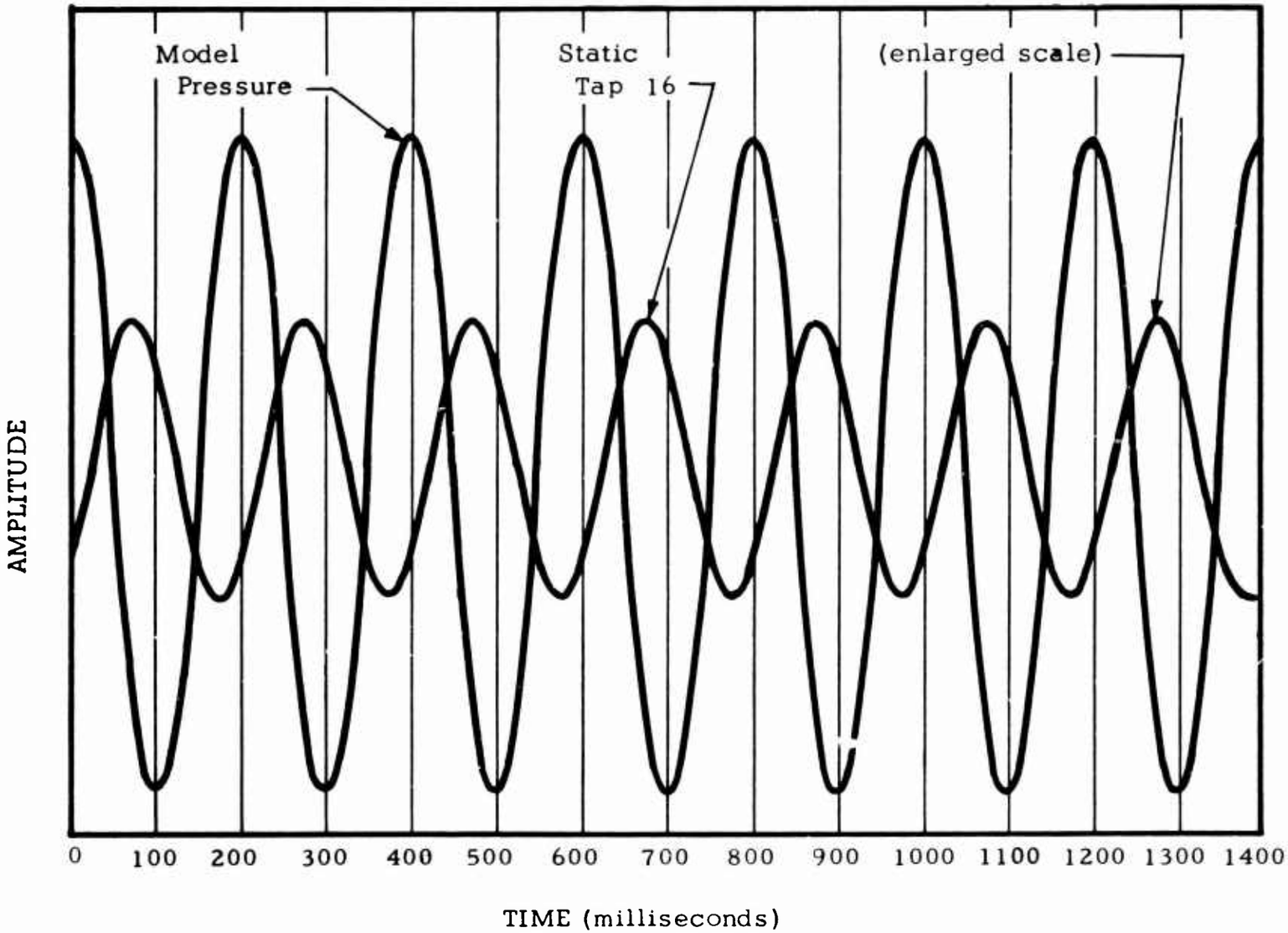

FIG. 52. PULSATING STATIC PRESSURE AND MODEL PRESSURE FOR ELLIPTICAL AIRFOIL OF 12-PERCENT-THICKNESS RATIO (VALVE SPEED = 150 r. p. m.).

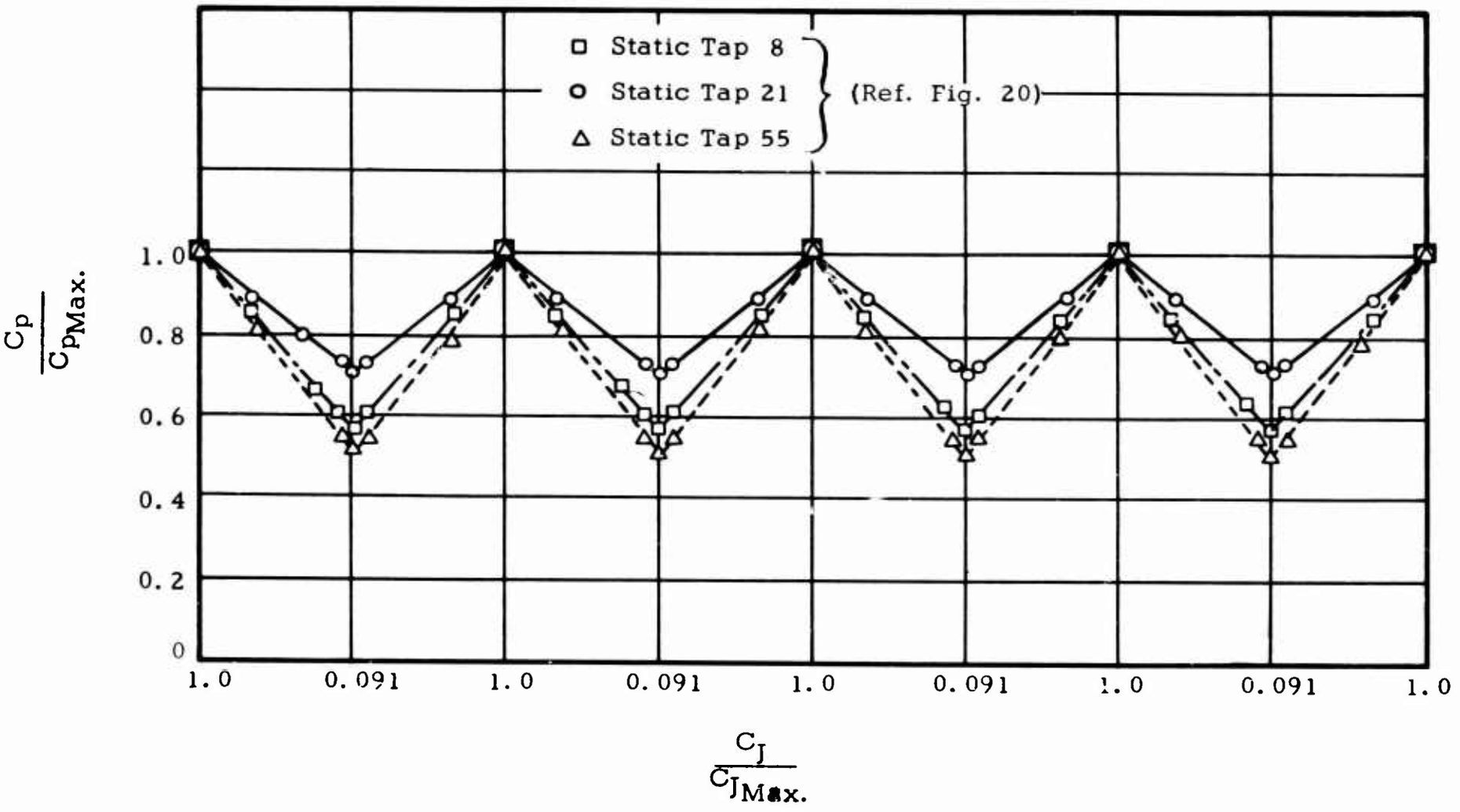

FIG. 53. PULSATING PRESSURE COEFFICIENT VERSUS PULSATING JET COEFFICIENT FOR 12-PERCENT MODEL AT VALVE SPEED 300 r. p. m.

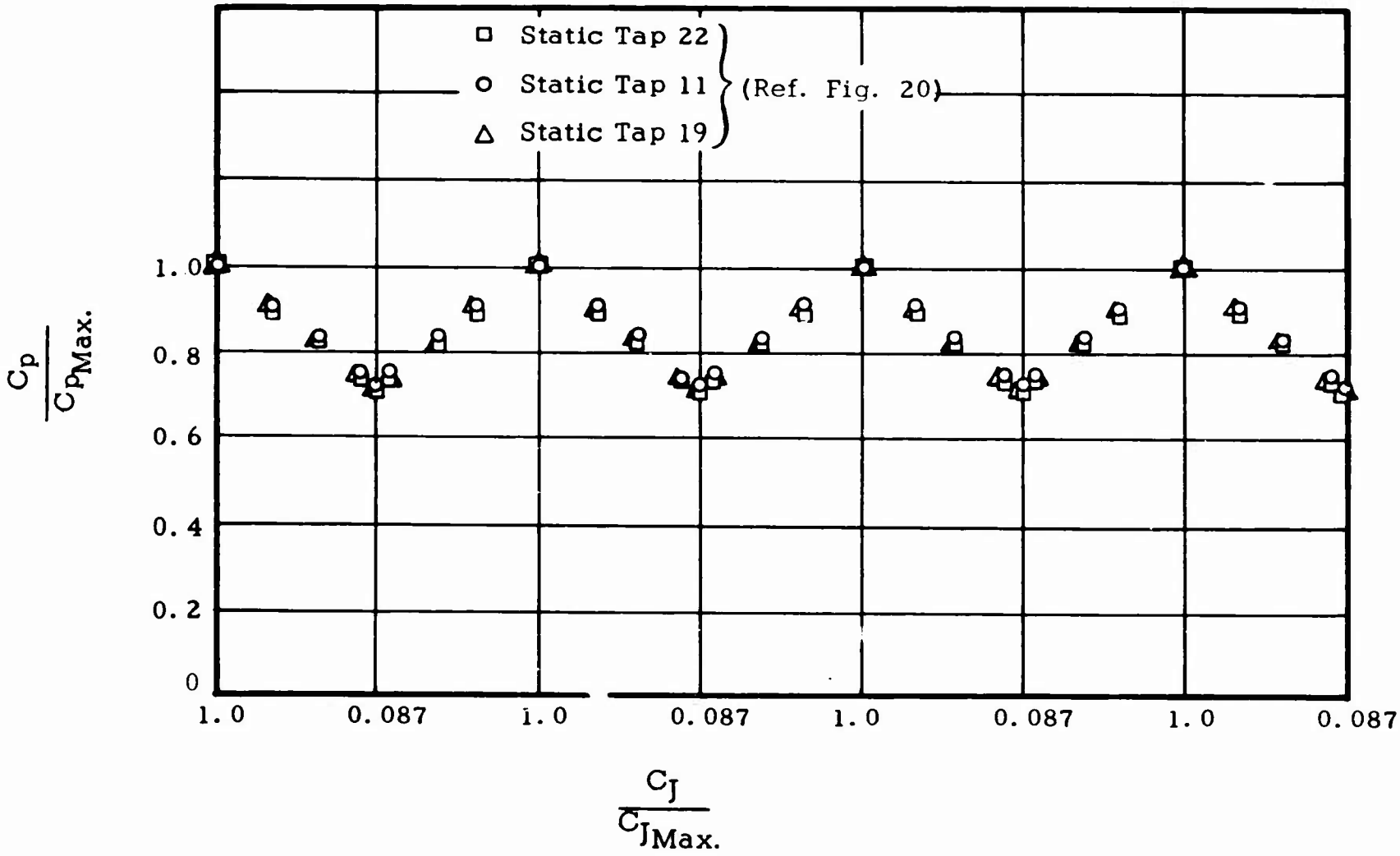

FIG. 54. PULSATING PRESSURE COEFFICIENT VERSUS PULSATING JET COEFFICIENT FOR 12-PERCENT MODEL AT VALVE SPEED 300 r. p. m.

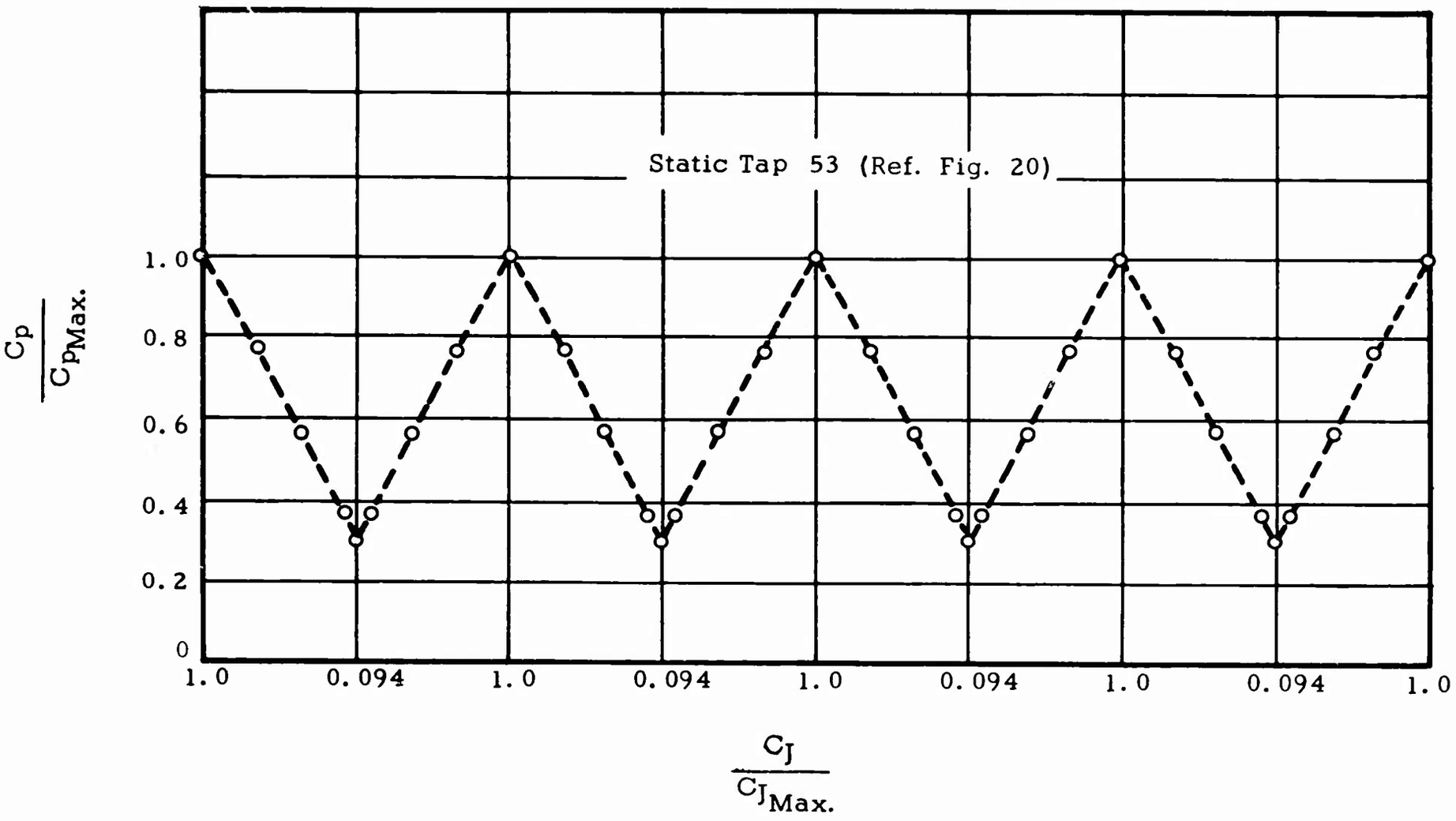

FIG. 55. PULSATING PRESSURE COEFFICIENT VERSUS PULSATING JET COEFFICIENT FOR 12-PERCENT MODEL AT VALVE SPEED 300 r. p. m.

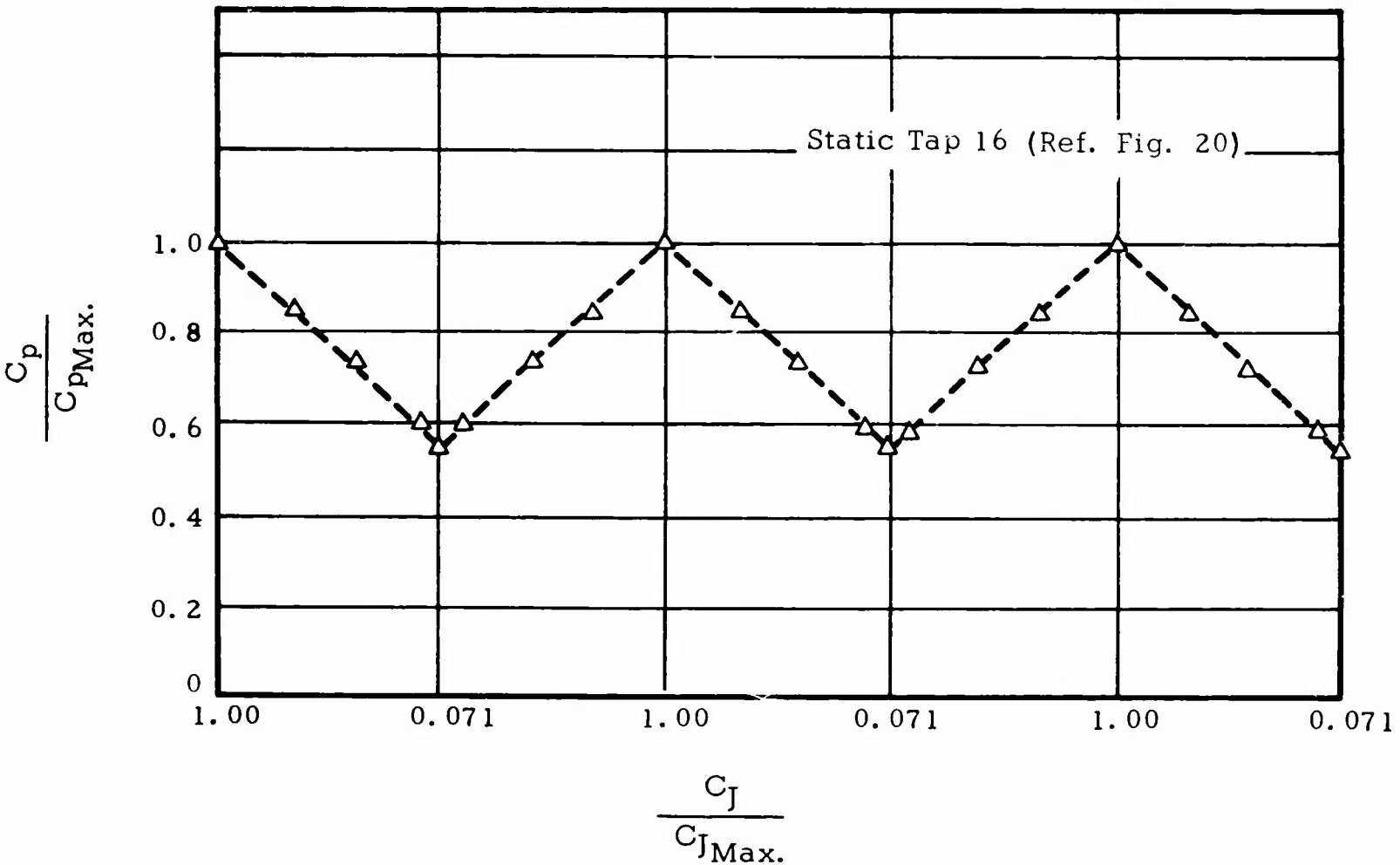

FIG. 56. PULSATING PRESSURE COEFFICIENT VERSUS PULSATING JET COEFFICIENT FOR 12-PERCENT MODEL AT VALVE SPEED 150 r. p. m.

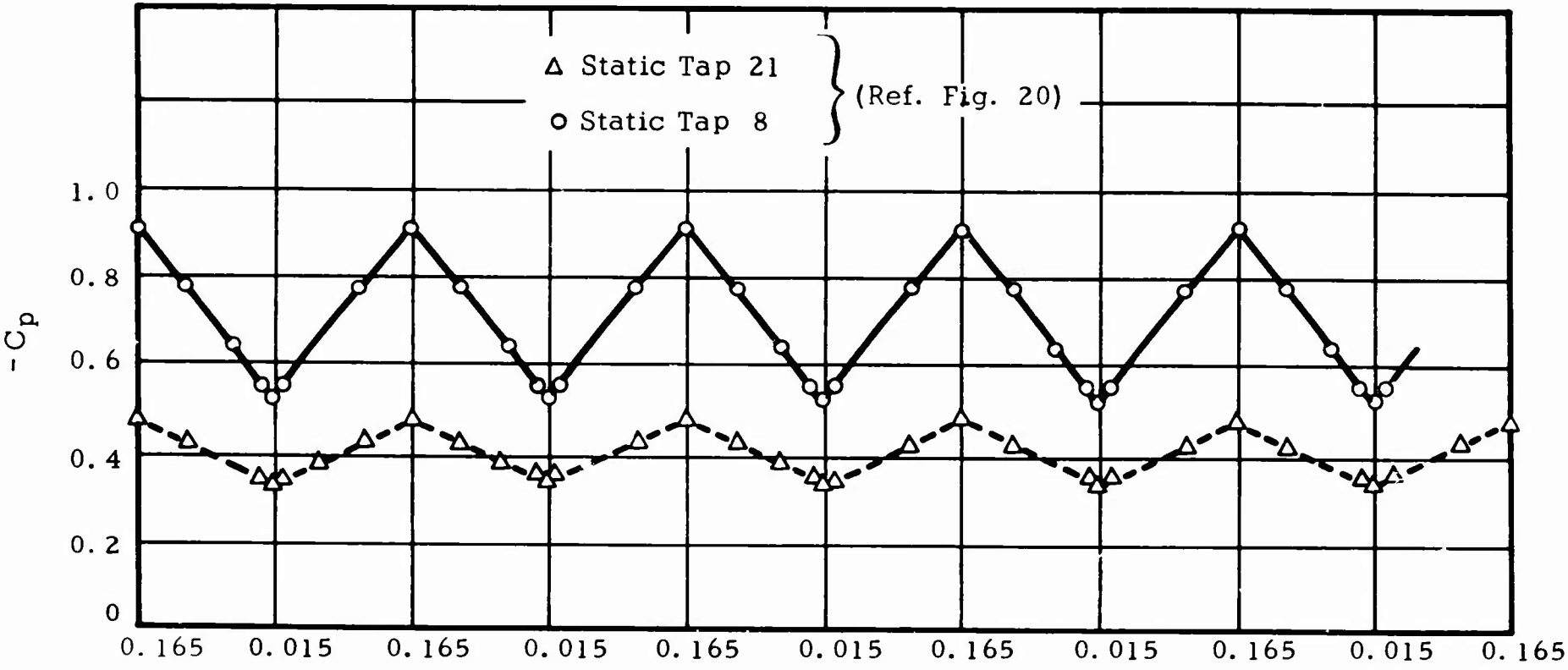

FIG. 57. PULSATING PRESSURE COEFFICIENT VERSUS PULSATING JET COEFFICIENT FOR 12-PERCENT MODEL AT VALVE SPEED 300 r. p. m.

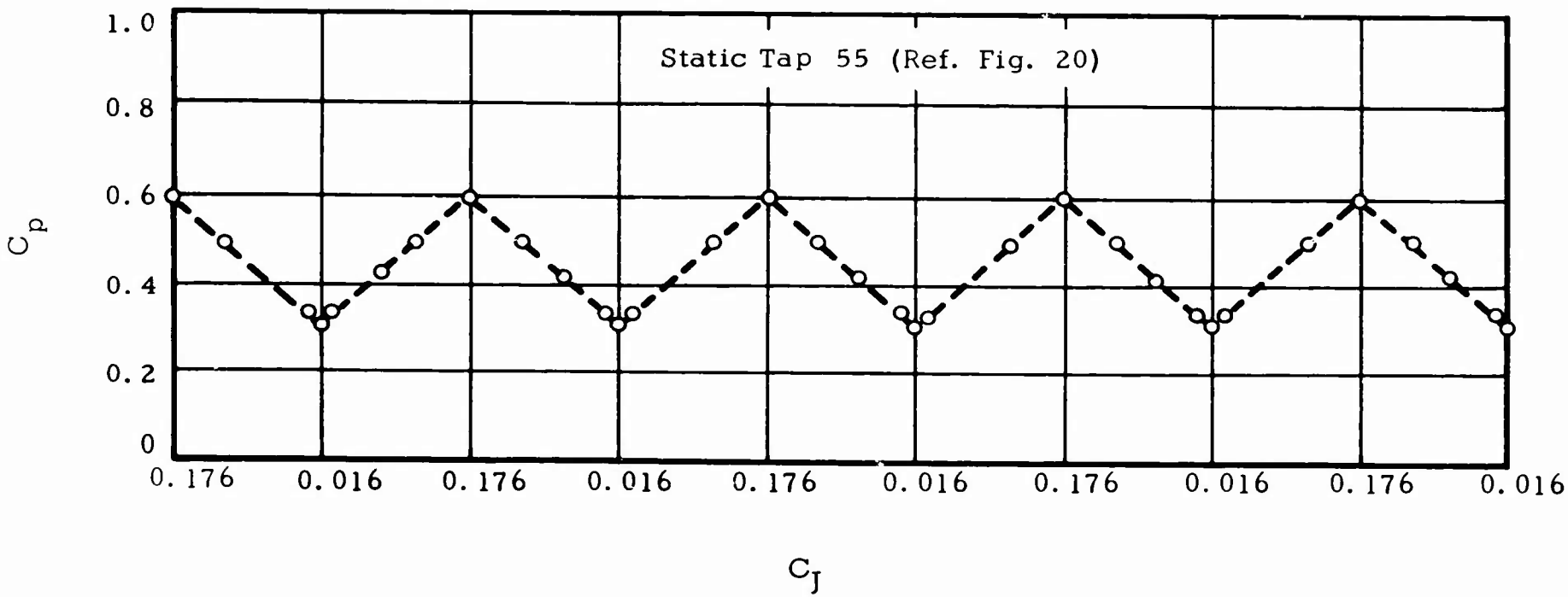

FIG. 58. PULSATING PRESSURE COEFFICIENT VERSUS PULSATING JET COEFFICIENT FOR 12-PERCENT MODEL AT VALVE SPEED 300 r. p. m.

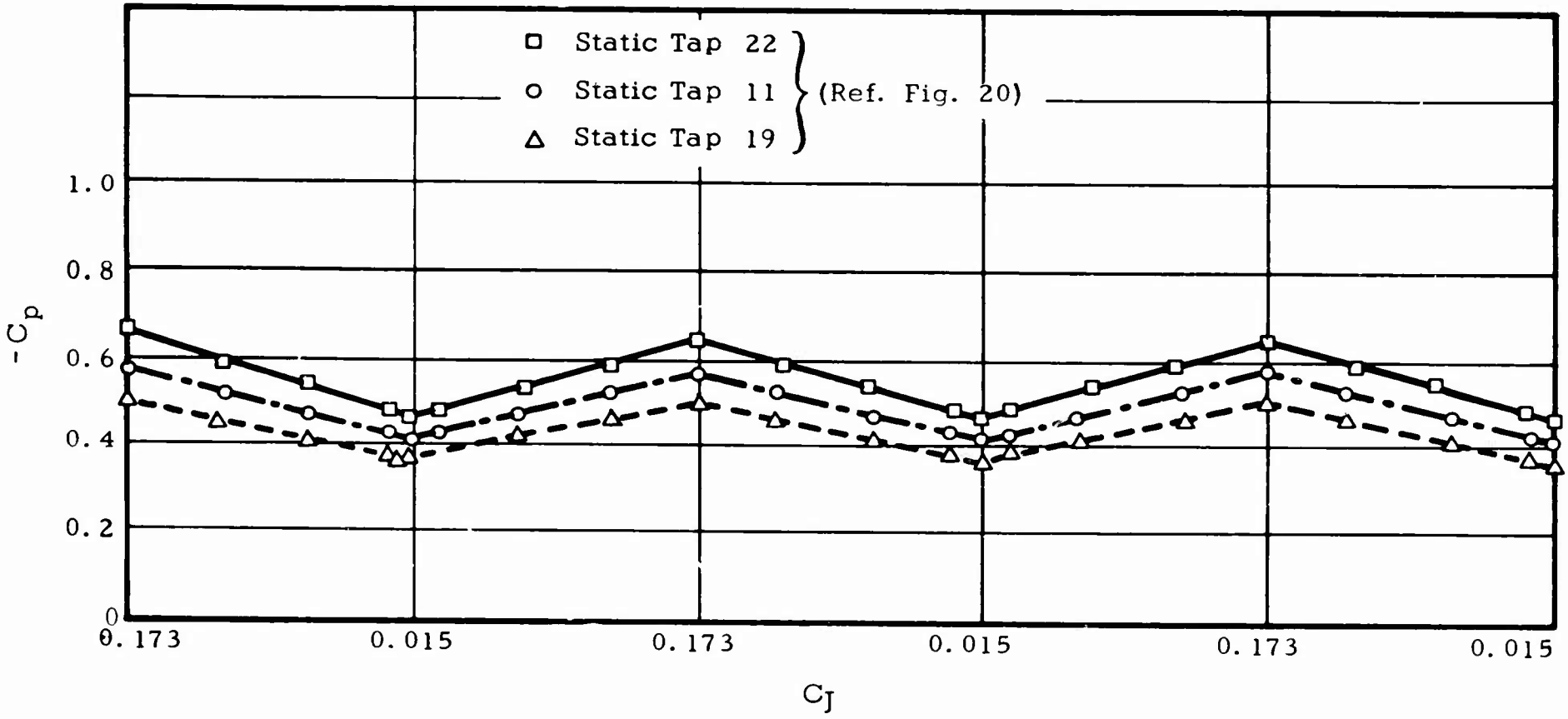

FIG. 59. PULSATING PRESSURE COEFFICIENT VERSUS PULSATING JET COEFFICIENT FOR 12-PERCENT MODEL AT VALVE SPEED 300 r. p. m.

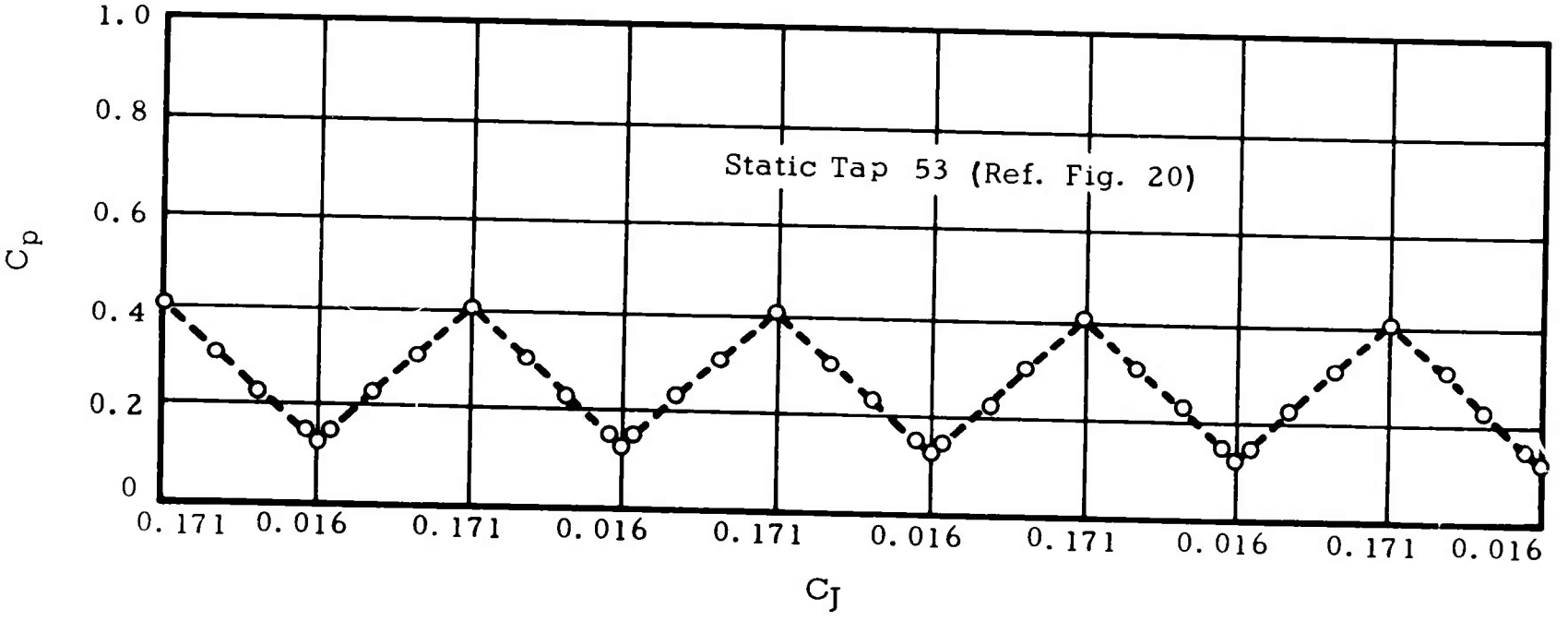

FIG. 60. PULSATING PRESSURE COEFFICIENT VERSUS PULSATING JET COEFFICIENT FOR 12-PERCENT MODEL AT VALVE SPEED 300 r. p. m.

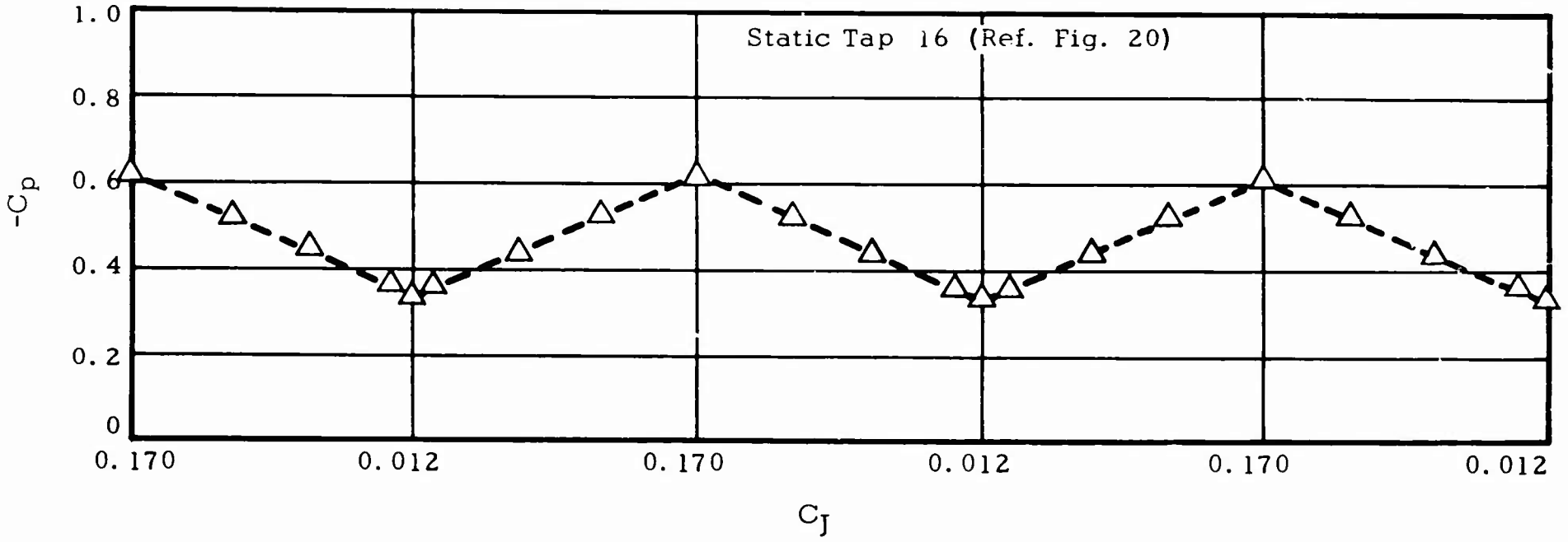

FIG. 61. PULSATING PRESSURE COEFFICIENT VERSUS PULSATING JET COEFFICIENT FOR 12-PERCENT MODEL AT VALVE SPEED 150 r. p. m.

Unclassified

Security Classification

DOCUMENT CONTROL DATA - R&D

(Security classification of title, body of abstract and indexing annotation must be entered when the overall report is classified)

1 ORIGINATING ACTIVITY *(Corporate author)*

The University of Texas

2a REPORT SECURITY CLASSIFICATION

Unclassified

2b GROUP

3 REPORT TITLE

Investigation of Circulation Control Airfoils by Means of Jets

4 DESCRIPTIVE NOTES *(Type of report and inclusive dates)*

Final report (1 July 1964 to 15 August 1965 and 1 February 1966 to 30 June 1966)

5 AUTHOR(S) *(Last name, first name, initial)*

Yuan, S. W. Kemp, L. D.
Westkaemper, J. C. Richter, W. L.

6 REPORT DATE	7a TOTAL NO. OF PAGES	7b NO. OF REFS
November 1966	105	14

8a CONTRACT OR GRANT NO.

DA 44-177-AMC-200 (T)

b PROJECT NO.

Task 1D121401A14203

c.

d.

9a ORIGINATOR'S REPORT NUMBER(S)

USAAVLABS Technical Report 66-72

9b OTHER REPORT NO(S) *(Any other numbers that may be assigned this report)*

NONE

10 AVAILABILITY/LIMITATION NOTICES

Distribution of this document is unlimited.

11 SUPPLEMENTARY NOTES

12 SPONSORING MILITARY ACTIVITY

U. S. Army Aviation Materiel Laboratories, Fort Eustis, Virginia

13 ABSTRACT

Based on the potential flow theory calculation, the capacity of the air supply, the limitation of the internal pressure of the model and the limitation due to the compressibility effect of the jet stream at high velocities, the elliptical airfoils of 18-and 12-percent-thickness ratios were designed and constructed. Experimental investigations for both models with trailing edge jets include force (lift and drag) and pitching moment measurements. In addition, static pressure measurements were made in both spanwise and chordwise directions. These results were used to compare with available theories.

Circulation control with dual jets for the elliptical airfoil of 18-percent-thickness ratio was tested with very satisfactory results. Tests were also made to determine the practicality of circulation control using a jet issuing from the leading edge region of the airfoil.

The determination of the aerodynamic response of the airfoil model to cyclic changes in jet mass flow was also made. The cyclic results were very satisfactory and are presented in the form of pulsating lift coefficient, drag coefficient, and pressure coefficient as a function of pulsating jet coefficient.

DD FORM 1 JAN 64 1473

Unclassified

Security Classification

Unclassified

Security Clas. ification

14. KEY WORDS	LINK A		LINK B		LINK C	
	ROLE	WT	ROLE	WT	ROLE	WT
1. Circulation Control Airfoils with Jets						
2. Cyclic Blowing Control Airfoil						
3. Jet-controlled-circulation Airfoil						

INSTRUCTIONS

1. ORIGINATING ACTIVITY: Enter the name and address of the contractor, subcontractor, grantee, Department of Defense activity or other organization *(corporate author)* issuing the report.

2*a*. REPORT SECURITY CLASSIFICATION: Enter the overall security classification of the report. Indicate whether "Restricted Data" is included. Marking is to be in accordance with appropriate security regulations.

2*b*. GROUP: Automatic downgrading is specified in DoD Directive 5200.10 and Armed Forces Industrial Manual. Enter the group number. Also, when applicable, show that optional markings have been used for Group 3 and Group 4 as authorized.

3. REPORT TITLE: Enter the complete report title in all capital letters. Titles in all cases should be unclassified. If a meaningful title cannot be selected without classification, show title classification in all capitals in parenthesis immediately following the title.

4. DESCRIPTIVE NOTES: If appropriate, enter the type of report, e.g., interim, progress, summary, annual, or final. Give the inclusive dates when a specific reporting period is covered.

5. AUTHOR(S): Enter the name(s) of author(s) as shown on or in the report. Enter last name, first name, middle initial. If military, show rank and branch of service. The name of the principal author is an absolute minimum requirement.

6. REPORT DATE: Enter the date of the report as day, month, year; or month, year. If more than one date appears on the report, use date of publication.

7*a*. TOTAL NUMBER OF PAGES: The total page count should follow normal pagination procedures, i.e., enter the number of pages containing information.

7*b*. NUMBER OF REFERENCES: Enter the total number of references cited in the report.

8*a*. CONTRACT OR GRANT NUMBER: If appropriate, enter the applicable number of the contract or grant under which the report was written.

8*b*, 8*c*, & 8*d*. PROJECT NUMBER: Enter the appropriate military department identification, such as project number, subproject number, system numbers, task number, etc.

9*a*. ORIGINATOR'S REPORT NUMBER(S): Enter the official report number by which the document will be identified and controlled by the originating activity. This number must be unique to this report.

9*b*. OTHER REPORT NUMBER(S): If the report has been assigned any other report numbers *(either by the originator or by the sponsor)*, also enter this number(s).

10. AVAILABILITY/LIMITATION NOTICES: Enter any limitations on further dissemination of the report, other than those imposed by security classification, using standard statements such as:

(1) "Qualified requesters may obtain copies of this report from DDC."

(2) "Foreign announcement and dissemination of this report by DDC is not authorized."

(3) "U. S. Government agencies may obtain copies of this report directly from DDC. Other qualified DDC users shall request through _____."

(4) "U. S. military agencies may obtain copies of this report directly from DDC. Other qualified users shall request through _____."

(5) "All distribution of this report is controlled. Qualified DDC users shall request through _____."

If the report has been furnished to the Office of Technical Services, Department of Commerce, for sale to the public, indicate this fact and enter the price, if known.

11. SUPPLEMENTARY NOTES: Use for additional explanatory notes.

12. SPONSORING MILITARY ACTIVITY: Enter the name of the departmental project office or laboratory sponsoring *(paying for)* the research and development. Include address.

13. ABSTRACT: Enter an abstract giving a brief and factual summary of the document indicative of the report, even though it may also appear elsewhere in the body of the technical report. If additional space is required, a continuation sheet shall be attached.

It is highly desirable that the abstract of classified reports be unclassified. Each paragraph of the abstract shall end with an indication of the military security classification of the information in the paragraph, represented as *(TS)*, *(S)*, *(C)*, or *(U)*.

There is no limitation on the length of the abstract. However, the suggested length is from 150 to 225 words.

14. KEY WORDS: Key words are technically meaningful terms or short phrases that characterize a report and may be used as index entries for cataloging the report. Key words must be selected so that no security classification is required. Idenfiers, such as equipment model designation, trade name, military project code name, geographic location, may be used as key words but will be followed by an indication of technical context. The assignment of links, rules, and weights is optional

Unclassified

Security Classification

7452-66